NOTICE

CERTAIN DATA
CONTAINED IN THIS
DOCUMENT MAY BE
DIFFICULT TO READ
IN MICROFICHE
PRODUCTS.

DOE/ER/12813--1

DE93 011734

MULTIPARTICLE IMAGING TECHNIQUE FOR TWO-PHASE FLUID FLOWS USING PULSED LASER SPECKLE VELOCIMETRY

Final Report

September 1988 - November 1992

T. A. Hassan

Department of Nuclear Engineering

Texas A&M University

College Station, TX 77843

December 1992

PREPARED FOR THE U.S. DEPARTMENT OF ENERGY
UNDER GRANT NUMBER DE-FG07-88ER12813

DISCLAIMER

This report was prepared as an account of work sponsored by an agency of the United States Government. Neither the United States Government nor any agency thereof, nor any of their employees, makes any warranty, express or implied, or assumes any legal liability or responsibility for the accuracy, completeness, or usefulness of any information, apparatus, product, or process disclosed, or represents that its use would not infringe privately owned rights. Reference herein to any specific commercial product, process, or service by trade name, trademark, manufacturer, or otherwise does not necessarily constitute or imply its endorsement, recommendation, or favoring by the United States Government or any agency thereof. The views and opinions of authors expressed herein do not necessarily state or reflect those of the United States Government or any agency thereof.

MASTER

DISTRIBUTION OF THIS DOCUMENT IS UNLIMITED

ABSTRACT

Development of Pulsed Laser Velocimetry Techniques for Measurement of
Two-Phase Interfacial Drag in a Horizontal Stratified Flow. (December 1991)
Thomas Kevin Blanchat, B.S., M.S., Texas A&M University
Chair of Advisory Committee: Dr. Yassin Hassan

The practical use of Pulsed Laser Velocimetry (PLV) requires the use of fast, reliable, computer-based methods for tracking numerous particles suspended in a fluid flow. Two methods for performing tracking are presented. One method tracks a particle through multiple, sequential, images (minimum of four required) by prediction and verification of particle displacement and direction. The other method, requiring only two sequential images, uses a dynamic, binary, spatial, cross-correlation technique. The algorithms are tested on computer-generated synthetic data and experimental data which was obtained with traditional PLV methods. This allowed error analysis and testing of the algorithms on real engineering flows.

A novel method is proposed which eliminates tedious, undesirable, manual, operator assistance in removing erroneous vectors. This method uses an iterative process involving an interpolated field produced from the most reliable vectors.

Methods are developed to allow fast analysis and presentation of sets of PLV image data.

Experimental investigation of a two-phase, horizontal, stratified, flow regime was performed to determine the interface drag force, and correspondingly, the drag coefficient. A horizontal, stratified flow test facility using water and air was constructed to allow interface shear measurements with PLV techniques.

The experimentally obtained local drag measurements were compared with theoretical results given by conventional interfacial drag theory. Close agreement was shown when local conditions near the interface were similar to space-averaged conditions. However, theory based on macroscopic, space-averaged flow behavior was shown to give incorrect results if the local gas velocity near the interface was unstable, transient, and dissimilar from the average gas velocity through the test facility.

TABLE OF CONTENTS

LIST OF FIGURES

Figure Page

Figure Page

CHAPTER I

INTRODUCTION

1.1 Background

The fundamental difficulty in the measurement and analysis of two-phase flow may be attributed to the large variety of flow patterns and flow conditions that can exist. A local (microscopic) probe measuring a parameter may see one phase continuously (such as that occurring in a stratified flow), or two phases intermittently (as in a bubbly or mist regime). The space-averaged (macroscopic) behavior of the two phases, commonly the parameter of choice in practice, cannot identify the local condition at some particular point. Unfortunately, the interaction between the two phases (or fluids) is dependent upon the microscopic behavior. The basic problem is how to predict the microscopic phenomena with practical and measurable macroscopic behavior. Interphase surfaces are encountered with two-phase flows that lead to jump conditions between the two phases. Only after the jump conditions are accounted for (which describe mass, momentum, and energy exchange between the phases), can a volume with two phases be treated as a single fluid.

Stratified two-phase flow in pipes may occur in various industrial processes. Examples include the flow of steam and water in horizontal pipe networks during certain postulated loss-of-coolant accidents (LOCA's) in a pressurized water reactor (PWR).

This thesis follows a style based on the ASME Transactions Journal of Heat Transfer.

and the flow of oil and natural gas (two-phase, two-component system) in pipelines. Theories for the creation of a particular interface or the various interactions occurring at the interface are not yet developed. Development of correlations to predict various flow patterns and identify interfacial actions, such as interfacial waviness and the resultant drag, is slowly progressing, and sometimes without satisfactorily results. The objective of this study was to extend Pulsed Laser Velocimetry (PLV) flow visualization techniques to allow analysis of a two-phase, horizontal, stratified, fluid flow. A current stratified flow drag correlation was compared with measured data to determine if a new correlation should be developed.

During a LOCA in a PWR, stratified flow of steam and water may take place in a horizontal channel when the emergency core cooling water is injected into the pipe. This type of flow also occurs in the auxiliary feedwater system of the steam generator in a PWR after stopping the main feedwater pumps. The flow stability in the two cases is very important to the safety analysis of the water reactor. It is necessary to explicate the mechanism of the transition from stratified flow to slug flow in horizontal, stratified, gas-liquid flow. Knowledge of interfacial shear stress and drag is required for the above applications.

Analytical solutions do not exist for most complex geometry flows, turbulent flows, and multiphase flows. Turbulent flow is described by the Navier-Stokes equations, since the size of the smallest eddy is generally much greater than the mean free path of the molecules of the system. The Navier-Stokes equations are nonlinear, partial differential equations that are difficult to solve in their rigorous form, and it is often necessary to make simplifications in order to reduce their complexity. Because of the three-dimensional nature of turbulent flow, even today's supercomputers cannot resolve all the scales needed for a high Reynolds number simulation. Thus, the analysis is limited to the low number range. Attempts have been made to successfully describe complex flow profiles by the use of empirical formulae which are derived from experimental data and numerical correlations obtained by solving simplified forms of the conservation equations. Reliable and accurate data from similar flow patterns must be obtained for these techniques to accurately predict a given flow's behavior.

Pulsed Laser Velocimetry is a powerful tool which performs both qualitative and quantitative fluid flow visualization by tracking seed particles suspended in the fluid. The resultant full-field flow visualization is capable of providing both time-varying and or instantaneous maps of fluid flow parameters, such as velocity, vorticity, and turbulence, over extended areas. This quantitative flow information is necessary to verify analytical solutions, and to formulate new correlations. Tens of thousands of simultaneous, individual (local), measurements with typical point flow probes would have to be performed to provide the same data given by one PLV "snapshot". The full-field nature of fluid flow parameters provided by PLV measurements will provide the "big picture". Fluid flow researchers and experimentalists have a powerful technique which should provide new insights to explain and predict fluid flow phenomena.

I.2 Literature review

Pulsed Laser Velocimetry (PLV) is a method to quantitatively extract information from complicated flows by tracking particles suspended in the flow. PLV is constantly being improved with new algorithms and experimental techniques in the laboratory.

Summaries of particle image velocimetry (PIV), one form of PLV, can be found in a number of papers (Adrian and Yao, 1983; Adrian, 1988a; Lourenco and Krothapalli, 1988; Grant and Smith, 1988; Adrian, 1991). The accuracy of PLV research has advanced to where thousands of data points can be accurately determined (Adrian and Yao, 1984). This accuracy is needed to insure the validity of the quantitative results. Studies of two phase flow are now possible with these new techniques (Delahunte and Hassan, 1990; Hassan and Blanchat, 1991; Hassan and Canaan, 1991).

Flow visualization with PLV involves seeding the fluid with "neutral density" particles (which are assumed to follow the flow pathlines), and then measuring their movement over a known period of time. PLV is performed by illuminating the fluid with a thin sheet of pulsed laser light, and then capturing images of the particles moving in the flow either with photographic film or digital cameras. After data acquisition has occurred, tracer seed identification and tracking is performed.

The dimensionality of the flow, type of fluid, and speed of the flow should be considered prior to performing a PLV investigation. Turbulent flows are of interest to many investigators. Turbulent flows are by their nature three dimensional. Care must be taken to produce two dimensional flow, unless the data can be taken in all three dimensions. If two dimensional data is being acquired, the effect of the third dimension can cause particle tracking algorithms to produce incorrect vectors (Sinha, 1988). The index of refraction of the fluid medium should also be noted. The scattered light from the seeds will be refracted to some extent, possibly introducing another possible source of error (Sinha, 1988). Flow speed can cause difficulties in tracking particles. If the flow speed is too fast, in reference to camera acquisition time, the camera will not capture seeds in successive frames.

An algorithms ability to track complicated flows must be verified. It is extremely difficult to produce a flow that can be accurately predicted to within several percent (Meynart, 1983). Therefore, error analysis in a PLV tracer tracking program should be performed using synthetic data. (Meynart, 1983; Agui and Jimenez, 1987; Sheng, 1988; Guezennec and Kiritsis, 1990).

Many studies have been done on tracer seed suitability (Agarwal and Johnson, 1981; Adrian, 1984; Lourenco and Krothapalli, 1987) and a variety of vendors produce seeds with desirable features. The main features, in determining the suitability of the seed, are the seed density, size, color (or fluorescence), and concentration, as well as the fluid medium that will be seeded. The density and size effect the seed's ability to accurately follow the flow. The seed must have a neutral buoyancy in the fluid medium. The ability of the seeds to follow the flow is dependent upon the seed momentum (Yano and Umeda, 1986). The momentum equations allow estimating the time required for a seed to achieve the flow speed (Braun et al., 1990). These equations show that the time required for the seed to match the flow speed is dependent upon fluid viscosity, as well as seed density and size. This is particularly important if studying turbulent flow, because of the small time and length scales involved. Further, the size of the seed affects the ability to scatter light. (Lourenco and Krothapalli, 1988). Very small seeds will scatter light according to Mie scattering theory, whereas large seeds undergoes Rayleigh scattering and reflection (Adrian and Yao, 1985). The color of the seed, for some experiments, is also of importance. Many studies have been done on the effect of color (Lakshmanan, 1986; Economikos, 1988; Russ, 1988). The particle color (in conjunction with a color recording device) can be used to discriminate between tracer seeds and bubbles in the fluid. Some seeds are fluorescent, and thus make discrimination easy with the use of bandpass light filters. The concentration, or source density, of the tracer seeds is also of concern. The source density must be small enough so that the recording instrumentation can record individual seeds. This is dependent on the resolution of the equipment and the size of the particle. However, the concentration must be large enough to insure data is available to accurately construct the full-field flow velocities.

The production of a thin sheet of pulsed laser light is a key element in PLV research. This flash of light provides the ability to determine the instantaneous positions of the seeds in the flow. In a two dimensional study, the laser light should be shaped into a thin light sheet. Note that errors can still be introduced even with very thin light sheets, because of out of plane motion (Lourenco, 1986; Sinha, 1988).

A pulsed laser can be used to produce the light sheet. The four major aspects of lasers, in regards to PLV research, are the peak power, the laser wavelength, the pulse frequency, and the pulse width. The peak power and laser wavelength are important parameters to be considered in the scattering of light by tracer seeds. Scattered light will increase with higher laser powers, allowing smaller seeds to be used. However, too much light can overexpose camera tubes or CCD arrays, producing permanent damage. The light wavelength affects the Mie scattering characteristics. Also, depending upon the fluid media, certain wavelengths are inappropriate. For example, infrared wavelengths would not probe water very well due to a large absorption coefficient. The pulse frequency determines the maximum possible flow speed which can be measured. It is often necessary to use the highest pulse frequency to study the details of turbulent flows. In addition, the smallest pulse width is desired to obtain an instantaneous "snapshot" of the flow.

The two major means of image recording are photographic film and digital cameras. There are many film and exposure parameters that affect the recording (Lourenco and Krothapalli, 1987; Lourenco and Krothapalli, 1988; Adrian, 1991). Both recording devices have a maximum frame acquisition speed, which determines the maximum pulse frequency. Double pulsing experiments typically have very fast pulse frequencies, causing image acquisition difficulties, and many methods have been suggested to overcome them (Archbold and Ennos, 1972; Adrian, 1986; Collicott and Hesselink, 1986; Adrian, 1988b; Dudderar et al., 1988; Landreth et al., 1988; Adrian et al., 1990). One such method is called laser speckle velocimetry. In this method, a double-exposed specklegram is illuminated by a laser beam and analyzed using Young's fringe patterns (Burch and Tokarski, 1968; Grousson and Mallick, 1977; Meynart, 1980; Meynart, 1982; Robinson, 1983; Meynart, 1985; Arnold et al., 1986; Huntley, 1986; Coupland and Pickering, 1988; Huntley, 1989; Chen and Chiang, 1990; Adrian, 1991).

After the imaging system has recorded the scattered light, it is necessary to derive individual seed or spot data. Digital cameras record the scattered light in the form of gray levels. Spot data can be found through thresholding and edge detection techniques (Hueckel, 1971; Otsu, 1979; Haralick, 1980; Chu, 1987; Hanzevack and Ju, 1988; Hild, 1989). The threshold choice can introduce a major source of error. If the threshold value is too high, then many faint spots may not be identified, and the spots that are identified may have misplaced centroids. If the thresholding value is set too low, then background may be identified as being part of spots. This can lead to errors when using tracking algorithms, which require accurate pixel locations when determining spot correlation. The use of a single threshold value is inappropriate for many images. Regional threshold values should be used if the laser sheet is not perfectly uniform, or when there are unequal scattering properties in the media, such as encountered with special two-phase flows (Canaan, 1990).

The local flow velocity can be determined from the seed movement between two sequential images. The flow velocity (assumed to be the seed velocity) is the distance the seed traveled divided by the pulse time. Some algorithms that determine velocity require many different images taken in sequential time steps. Other programs require only two time steps. Some double pulsing experiments produce one double-exposed image. This results in a directional ambiguity problem for the tracking programs (Adrian, 1986; Coupland et al., 1988). The goal of PLV is to quantitatively measure large numbers of vectors over the full-field, which will require fast, relatively error-free particle tracking algorithms.

At the present time, no methods currently exist for direct measurement of interfacial shear, and consequently, interfacial drag. Previously proposed criteria for predicting interfacial stress did not represent high gas density experimental data (Kowalski, 1987). Theory does not exist which predicts interfacial effects, and development of correlations to model interface interactions are progressing slowly, and sometimes with unsatisfactory results (Oh and Mahalingam, 1987). Knowledge of interfacial effects is of utmost importance in many applications, such as PWR accident safety analyses, and investigators are finding that interfacial shear stress contributions are important in determining stratified flow transition regimes (Wang and Kondo, 1990). PLV techniques have been used to measure horizontal flow velocities, but only with single-phase flow (Utami and Ueno, 1987)

1.3 Methodology

The following steps were taken to advance PLV techniques to allow PLV measurement of interfacial drag in a horizontal, stratified, two-phase flow field:

1) Literature searches of PLV and associated measurement techniques were performed.
2) Literature searches of two-phase interaction phenomena were performed, especially relating to interfacial drag experiments and correlations.
3) A computer program was developed to analyze high-speed, full-field, spatial, flow data obtained with PLV methods. This program utilizes cross-correlation techniques on binary data with correlating regions chosen dynamically to improve speed and reduce computer cost. Methods were utilized to double-check the vectors computed by the program.
4) The new two-frame, spatial tracking method was verified with synthetic production of typical fluid flows. The production incorporated random generation of seeds in a typical camera view, and flow-field equations to "move" the seeds to simulate data obtained with PLV methods.

5) Methods were developed to allow interpolation of sparse vector data into full-field maps, and extract flow parameters, such as streamline and vorticity. The interpolation used the Hardy multiquadratic equations (Hardy, 1971). A method to automatically remove erroneous vectors was implemented.

6) A facility to allow investigation of a two-phase, horizontal, stratified fluid flow with PLV techniques was designed, built, and tested.

7) Interphase drag data obtained with the stratified flow facility was compared with current correlations to determine if it was necessary to develop new criteria for predicting interfacial drag.

1.4 Summary

A new PLV tracking algorithm was developed which performs particle tracking on two, sequential, images obtained with either a slow, single-pulsed mode of laser operations, or a high-speed, double-pulsed, mode of laser operation. The algorithm was tested with synthetic data to provide error estimates, and to demonstrate method reliability. A method to interpolate and remove erroneous vectors from the flow field was developed, and methods to extract flow parameters such as streamline and vorticity determined. Two-phase, horizontal, stratified, interfacial drag measurements were performed. A new PLV flow channel was constructed to facilitate this goal. Tracking of experimental data with the tracking algorithm highlighted the practical aspect of applying the new method to real engineering flows. Current interphase drag correlations used in industry and research were reviewed to see if new criteria for predicting interphase drag would be needed.

CHAPTER II

MULTIFRAME AND CROSS-CORRELATION TRACKING CODE DESCRIPTION

II.1 Introduction

The practical use of Pulsed Laser Velocimetry (PLV), also known as Particle Image Velocimetry (PIV), requires the use of fast, reliable, computer-based methods for tracking numerous particles suspended in a fluid flow. Two methods for performing tracking are presented. One method tracks a particle through multiple, sequential, images (minimum of four required) by prediction and verification of particle displacement and direction. The other method, requiring only two sequential images, uses a dynamic, binary, spatial, cross-correlation technique.

II.2 Multiframe Tracking Algorithm

The purpose of the multiframe particle tracking code was to track images through multiple (ten) time steps (Hassan et al., 1990). A minimum of four sequential images are required for this method. The input into the code, which performs a direct point-by-point matching of particles from one frame to the next, is usually the output from an image analysis program operating on data obtained with a PLV system. The output from the particle tracking code is a listing of a track (composed of sequential frame numbers and particle centroid) for each particle tracked. These tracks are plotted as velocity vectors.

The 10 files that are created as the output of the image analysis (particle determination) program or synthetic data production program contain all the data necessary for any tracking scheme. The tracking scheme tracked particles through four sequential frames at a time. A track was based on the minimum variance of length and angle (referred to as the sigma total value σ_{total}) of all possible tracks from some starting particle centroid. The tracking was accomplished by the prediction of the displacement and the direction of the particle through four consecutive time steps.

Figure 1 illustrates the tracking procedure. A particle in frame 1 was selected to start the track. A search area in frame 2 was centered at a position determined by the frame 1 particle centroid. The search area in the second frame for a particle starting in the first frame was determined by a rough estimate of the maximum flow velocity. The search areas in the third and fourth frames were based on a fraction of the second frame's search area. The center of the search area in frame 3 was found by straight-line projection of a possible track for a particle found in frame 2. For each particle then found in frame 3, the center of a search area in frame 4 was determined using the length of the track from frames 2 to 3 and the deviation of the track's angle between frames 2 and 3. A statistical method was used to determine and dispose incorrect tracks if more than one track shared the same particle. The following relations are used to calculate σ_{total}:

$$\sigma_l = \sqrt{\frac{\left(l_{1-2} - \bar{l}\right)^2 + \left(l_{2-3} - \bar{l}\right)^2 + \left(l_{3-4} - \bar{l}\right)^2}{3}} \tag{1}$$

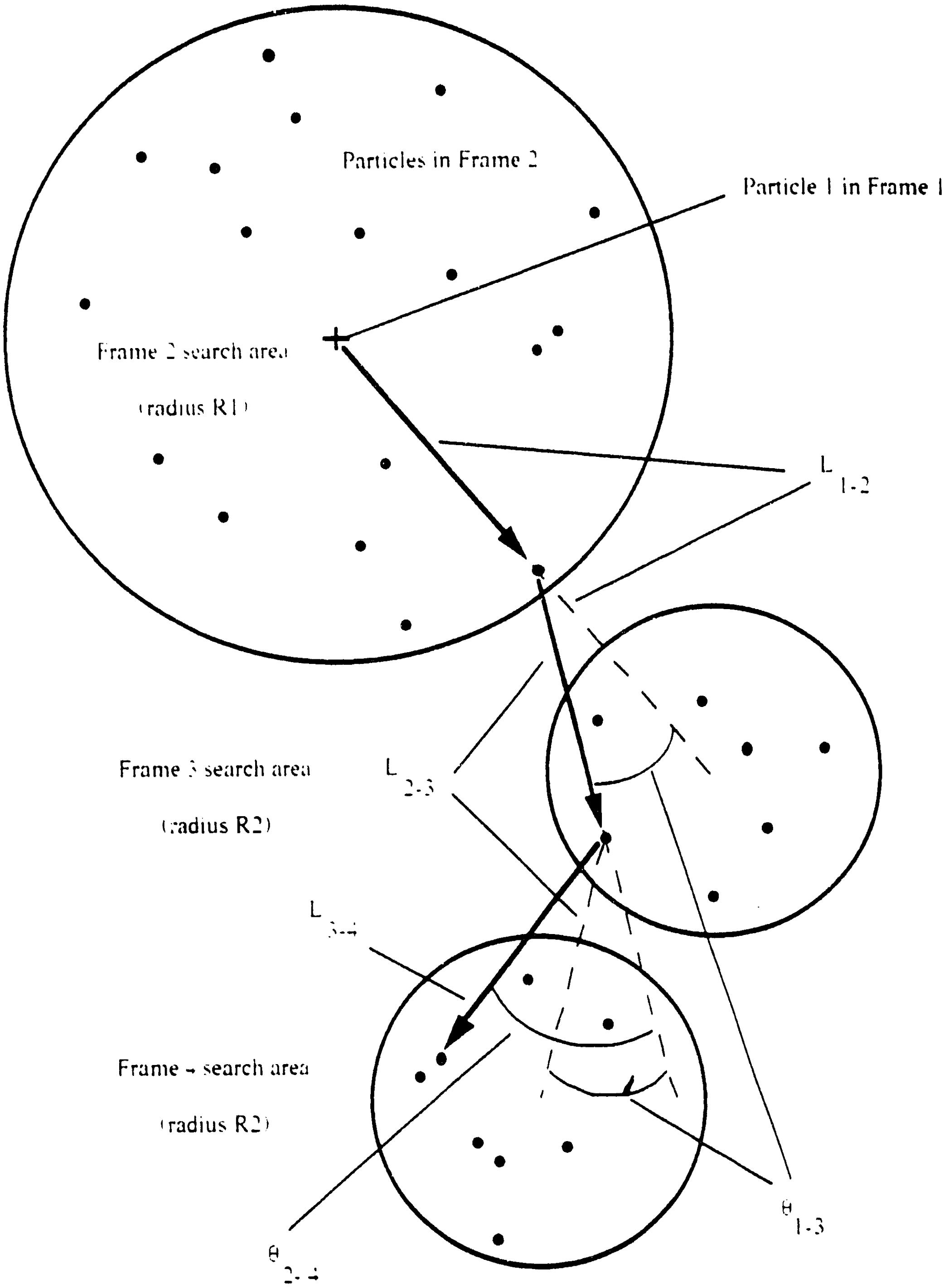

Figure 1. Multiframe Tracking Description

$$\sigma_\theta = \sqrt{\frac{\left(\theta_{1-3} - \bar{\theta}\right)^2 + \left(\theta_{2-4} - \bar{\theta}\right)^2}{2}} \tag{2}$$

$$\sigma_{total} = \sqrt{\frac{\sigma_l^2}{\bar{l}^2} + \sigma_\theta^2} \tag{3}$$

where

l_{1-2} = length between particles in the 1st and 2nd frames.

l_{2-3} = length between particles in the 2nd and 3rd frames.

l_{3-4} = length between particles in the 3rd and 4th frames.

θ_{1-3} = angle between l_{1-2} and l_{2-3}.

θ_{2-4} = angle between l_{2-3} and l_{3-4}.

$\bar{l}$ = average length between particles = $\frac{l_{1-2}+l_{2-3}+l_{3-4}}{3}$

$\bar{\theta}$ = average angle between vectors = $\frac{\theta_{1-3}+\theta_{2-4}}{2}$

σ_l = standard deviation for the lengths of the vectors.

σ_θ = standard deviation for the angles between the vectors.

Note that the perfect track would have a σ_{total} value of 0.0. The division by $\bar{l}^2$ in equation (3) is used to nondimensionalize the σ_{total} value. Tracks originate in frames 1 through 7, and conclude in frames 7 through 10. After these seven sets of four-frame tracks are calculated, any tracks which start in different frames, but use the same particle in their common frames, are added together to form long tracks up to 10 frames in length. For example, consider two four-frame tracks, originating in frames 1, 2, 3, 4 and frames 2, 3, 4, 5, respectively. If both tracks share common particles in frames 2, 3, 4, and each track has a σ_{total} value less than some selected minimum value, the two sets of four-frame tracks are combined into one five-frame track. A new σ_{total} value is then computed by linear averaging of the original four-track σ_{total} values. For example, assume the previously mentioned two four-tracks that were combined into a five-track had σ_{total} values of 0.001 and 0.5 (e.g. a good track and a poor track). The new (if allowed), combined track σ_{total} value would be 0.2505, and provides an opportunity for later removal of "bad" tracks.

After track combining is performed, the tracks are then cross referenced against each other to assure that all tracks are unique, i.e., no two separate tracks use the same particle. This occurrence is called track crossing and occurs infrequently, but often enough that it must be treated. If a track crossing has been determined, the track with the largest σ_{total} value is assumed to be the incorrect track, and is discarded.

II.3 Cross-correlation Tracking Algorithm

A dynamic, particle tracking method can be quickly performed between two sequential, high resolution (1024 x 1024 x 8 bit) images, if the particle tracer information is first converted to binary data. The binary data conversion is a method where all the 8-bit (0-255 gray level) pixels defining a particle have been converted to 2-bit (value 0 or 1) pixels through image processing techniques, e.g. thresholding and connectivity algorithms. The particle velocity is found by determining the correspondence between particles in two sequential video frames. This correspondence is obtained through the calculation of a correlation coefficient between a referenced pattern in the first binary image and a possible candidate pattern in the second binary image, where the latter is shifted so that the centroids of the possible particle pair coincide (Yamamoto et al., 1988). Every particle belongs to a characteristic group which has a specific local distribution pattern. One particle in the first image will correspond to the particle in the second image which keeps the most similar pattern, providing the local pattern of the distributed particles changes little between sequential video frames.

This method is especially useful when only two sequential images are available, and when the multiframe particle tracking method (requiring at least four sequential video images) cannot be performed. The video technology currently available to us can capture multiple, high resolution, images at intervals of approximately 60 frames/sec. However, images of faster phenomena can be acquired through the use of two or more cameras, or by double exposure of a single image with a pulsed light source. The method described below (modified for single frame data) has been successful in analyzing particle velocities on a double exposed image obtained with a pulsed laser light source (150 microseconds between pulses), yielding an effective frame acquisition rate of 6666 frames/sec (Delahunte and Hassan, 1990).

The algorithm is illustrated in Fig. 2. Acquisition of two video frames has occurred, and image processing of gray level information (noise removal, thresholding, tracer particle labeling, and binary conversion) completed (Hassan et al., 1990). Two separate frame arrays are "filled" with 0's and 1's. The fill pattern is an outward spiral centered at each particle centroid, with the spiral stopping when the total number of pixels in the particular particle being "filled" is reached. The arrows denote the expected flow field direction and magnitude.

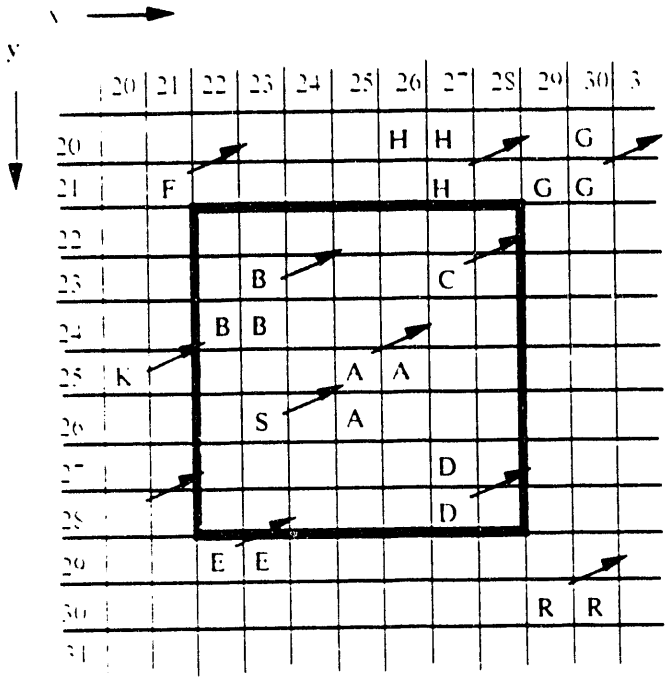

Dynamic region in frame 1 centered at particle A

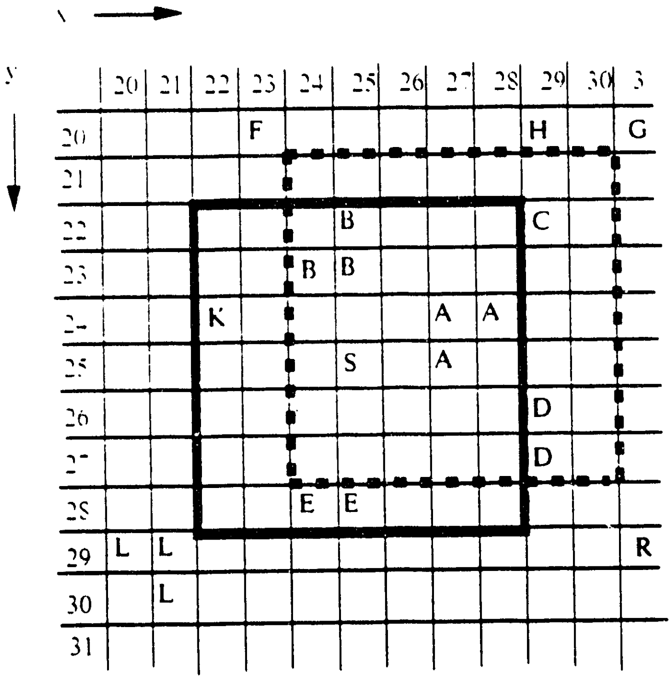

Dynamic regions in frame 2 centered at particles S and A

Figure 2. Cross-correlation Tracking Description

A rectangular *candidate* region (shown by the solid line) is centered in frame 2 at pixel location (25,25), based on the centroid of particle A (pixel location 25,25) in frame 1. The size and shape of this search region is based on the maximum possible particle velocity expected. All particles that lie within this *candidate* region in frame 2 are then determined. Five possible candidates have been found, consisting of varying number of pixels. They are denoted by the letters K, BBB, S, EE, and AAA. All these particles now become candidates for pairing with particle A in frame 1.

Next, a *dynamic* region is placed in frame 2 so that it is centered at each of the possible pair candidates previously determined. Then, this *dynamic* region size is adjusted to obtain a minimum of five particles. Correlations are performed between the *dynamic* region centered on particle A in frame 1 and the *dynamic* region centered on each of the candidates in frame 2. The cross-correlation coefficient on binary images, C_{ij}, between *dynamic* regions in frames 1 and 2 is calculated from

$$C_{ij} = \frac{\sum_{y=1}^{H} \sum_{x=1}^{L} F1_{xy} \cdot F2_{xy}}{\sqrt{B1 \cdot B2}} \tag{4}$$

where

$F1_{xy}$ = binary pixel value at position x,y in frame 1.

$F2_{xy}$ = binary pixel value at position x,y in frame 2.

$B1$ = total number of pixels with value 1 in frame 1.

$B2$ = total number of pixels with value 1 in frame 2.

L = length of dynamic region in pixels.

H = height of dynamic region in pixels.

The numerator gives the sum of the logical products of the binary data between the *dynamic* regions in the two images. The logical product is a test which is only true if the corresponding pixels in the *dynamic* regions are both of value 1. Note that $B1$ and $B2$ determine the total number of pixels for all the particles in their respective *dynamic* regions. Remember that a pixel with a value of 1 denotes that it is part of a particle, and a pixel with value 0 implies no particle at that location.

Referring to Fig. 2, the sum of the logical products between the *dynamic* region in frame 1 (solid line) and the *dynamic* region in frame 2 (also shown by the solid line centered on particle S) is 2.0, the value of $B1$ is 10.0, and $B2$ is 10.0. This gives a C_{ij} value, as calculated with equation (4), equal to 0.200 (note the total number of pixels in the *dynamic* region is 49). However, the C_{ij} value for the *dynamic* region in frame 2 (dashed line centered on particle A) is 1.000, a perfect correlation.

The velocity for a particle is determined by the particle movement divided by the image acquisition time. The candidate pair with the largest C_{ij} value is identified as the correct particle pair match. Given an irrotational flow, large values of C_{ij} (close to 1.0) are obtained for the correct particle correspondence. In regions of high vorticity, the C_{ij} values can be much smaller, and the identified matches are not always correct. Another means of checking is required to remove erroneous vectors. Two checks are performed. The first check calculates the sum of the distances between all overlaying particle centroids. For example, in Fig. 2, during the correlation between the frame 1 dynamic region (solid line) and the frame 2 dynamic region (solid line), two particles in frame 2 are overlaid with particles from frame 1, B-K (particle B in frame 1 and particle K in frame 2) and A-S. The sum of the distances between the overlaid centroids is approximately 2 pixels. For the correlation between the frame 1 dynamic region (solid line) and the second frame 2 dynamic region (dashed line), all five particles in frame 2 are perfectly overlaid with particles from frame 1, yielding zero for the sum of the distances between the overlaid centroids.

The second check determines a reliability index, R_{ij}, for a possible candidate pair. This check is based on the number of particles which overlap, N_{ij}, and the number of overlapped pixels with a logical product of 1, A_{ij}, which occur when checking a correspondence for possible pair i-j. Again, Fig. 2 shows two correspondence checks: that between candidate pair A-S (frame 1 dynamic region (solid line) and frame 2 dynamic region (solid line)), and A-A (frame 1 dynamic region (solid line) and frame 2 dynamic region (dashed line)). For the A-S candidate pair, two particles have overlapped (B-K and A-S), with a total number of two overlaid pixels. The N_{ij} counters for both pairs B-K and A-S are incremented by 1 (since the pair being checked will always overlap, it is not used in the N_{ij} calculation) and the A_{ij} counters for both pairs is incremented by 2. For the A-A pair check, 5 pairs overlap (A-A, B-B, C-C, D-D, and S-S) with a total of 10 overlapped pixels. Therefore, the N_{ij} counters for each of the 5 pairs are incremented by 4, and each A_{ij} pair counters by 10.

As other particles in frame 1 are corresponded to possible pair matches in frame 2, the counters for the A-S and A-A pairs may also increase, since each particle usually belongs to some local group. When all correspondences are completed, the reliability index R_{ij} is calculated using

$$R_{ij} = N_{ij} \times A_{ij} \tag{5}$$

where

N_{ij} = number of overlapped particles.

A_{ij} = number of overlapped pixels.

The possible pair with the largest C_{ij} value, the largest R_{ij} value, and the smallest sum of the distances between centroids, is generally found to be the correct match. Note that this algorithm will find a correspondence (not necessarily correct) for a particle in frame 1 to a particle in frame 2. Some means must be devised to assess the accuracy of calculated vectors, and is the subject of the following chapter.

CHAPTER III

TRACKING CODE TESTING AND ERROR ANALYSIS

III.1 Introduction

The practical use of Pulsed Laser Velocimetry (PLV) requires the use of fast, reliable, computer-based methods for tracking numerous particles suspended in a fluid flow. It is extremely difficult to experimentally produce a flow that can be accurately predicted to within several percent (Meynart, 1983). Since an algorithm's ability to track complicated flows must be verified, error analysis on a PLV tracer tracking program should be performed using synthetic data (Meynart, 1983; Agui and Jiménez, 1987; Sheng, 1988; Guezennec and Kiritsis, 1990). The multiframe tracking (MFT) algorithm and the cross-correlation tracking (CCT) algorithm were tested with synthetic data and experimental data. The synthetic data was computer generated and the experimental data was obtained with traditional PLV methods. This allowed error analysis and testing of the algorithms on real engineering flows.

III.2 Synthetic Data Production

The production of synthetic data is necessary for the validation of tracking methods. There must be a standard set of particles with known positions moved through several frames. This produces a known particle track. The tracking method can then be performed using these frames of data to produce particle tracks. Comparisons are then made between the tracks produced in the method and the known particle tracks.

The synthetic data set, used for testing, simulates inviscid flow about a cylinder (Sheng, 1988). Particles are randomly placed on a 1024 x 1024 pixel image to simulate an image acquired with the high resolution camera. These particles are then moved in subsequent frames by using the following equations. First, a transformation from a rectangular to polar coordinate system is necessary to use the equation of uniform, stream flow around a stationary, circular cylinder. The cartesian coordinate centroid x_c, y_c of a particle was shifted to x_o, y_o (due to the center-based polar coordinate system). This effectively moves the origin to the center of the picture. Next, this was converted to a cylindrical coordinate r_o, θ_o. The radial and circumferential velocity components u_r, v_θ were then determined. The particle was then moved with a time step Δt to a new cylindrical coordinate r_n, θ_n. Finally, this coordinate was transformed to x_n, y_n to correspond with the original cartesian system.

$$x_o = x_c - 512 \tag{6}$$

$$y_o = y_c - 512 \tag{7}$$

$$r_o = \sqrt{\left(x_o^2 - y_o^2\right)} \tag{8}$$

$$\theta_o = \arctan\left(\frac{y_o}{x_o}\right) \tag{9}$$

$$u_r = U\left(\frac{R^2}{r_o^2} - 1\right)\cos\theta_o \tag{10}$$

$$v_\theta = U\left(\frac{R^2}{r_o^2} - 1\right)\sin\theta_o \qquad (11)$$

$$r_n = r_o - u_r\Delta t \qquad (12)$$

$$\theta_n = \theta_o - \left(\frac{v_\theta}{r_o}\right)\Delta t \qquad (13)$$

$$x_n = r_n\cos\theta_n - 512 \qquad (14)$$

$$y_n = r_n\sin\theta_n - 512 \qquad (15)$$

where

x_o = old cartesian coordinate in x .

y_o = old cartesian coordinate in y.

x_o = shifted old cartesian coordinate in x.

y_o = shifted old cartesian coordinate in y.

r_o = old cylindrical coordinate in r.

θ_o = old cylindrical coordinate in θ.

u_r = radial velocity component.

v_θ = circumferential velocity component.

U = freestream velocity.

R = cylinder radius.

Δt = time step parameter.

r_n = new cylindrical coordinate in r.

θ_n = new cylindrical coordinate in θ.

x_n = new cartesian coordinate in x.

y_n = new cartesian coordinate in y

Five hundred particles were randomly placed in the first image to simulate a flow field seeded with tracer particles. Particle densities ranged from 10 to 3000 particles per image. Each particle was assigned a random average pixel gray level (50-150) and area (5-25 pixels). Particle movement in the following "sequential time" images was accomplished by setting the time step parameter Δt and the freestream velocity U. The analysis with synthetic data set R equal to 150 pixels, U equal to 1, and Δt ranged from 5 to 125. This provided a particle movement between images of approximately 5 to 125 pixels. Figure 3 shows the 500 synthetic particles being moved in time ($\Delta t = 10$) through ten frames. This figure overlays the ten synthetic data files, to allow flow visualization. Note that the flow moves from right to left.

III.3 Interpolating Scattered Vectors into a Full Vector Field

A method for interpolating sparse, scattered, velocity data was needed to produce a vector at any given point in the flow field. The interpolation method that was developed is based on the Hardy multiquadratic equations (Hardy, 1971) as discussed by Narcowich and Ward (1991). The basic equations are

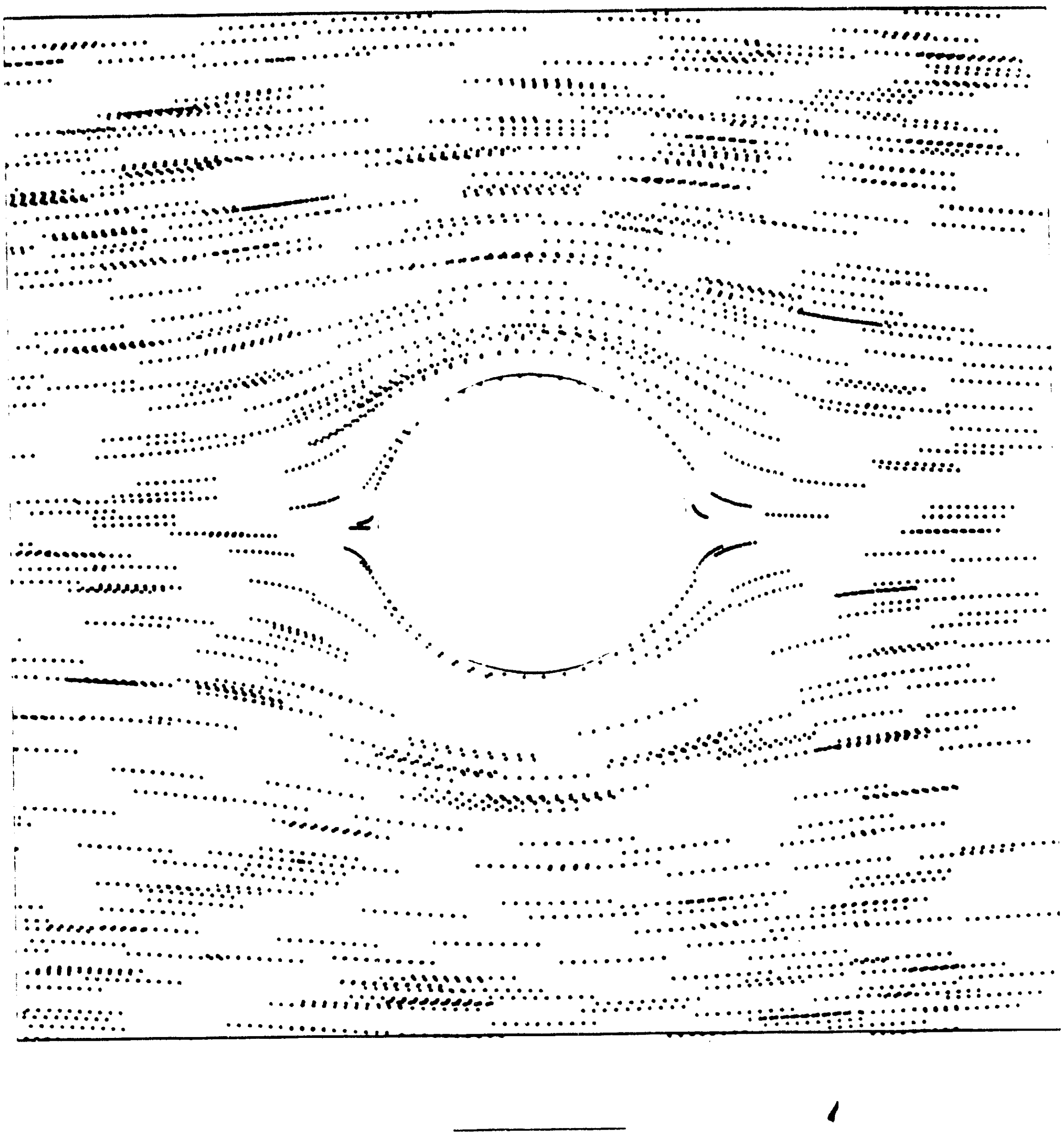

Simulated flow from right to left

Camera view: 1024 x 1024 pixels

Figure 3. Synthetic Data Overlay, Frames 1-10

$$\vec{V}_i = (u_i, v_i) \tag{16}$$

$$u_i(x_i, y_i) = \sum_{j=1}^{N} a_j \sqrt{1 + (x_i - x_j)^2 + (y_i - y_j)^2} \tag{17}$$

$$v_i(x_i, y_i) = \sum_{j=1}^{N} b_j \sqrt{1 + (x_i - x_j)^2 + (y_i - y_j)^2} \tag{18}$$

where

$\vec{V}_i$ = velocity vector at coordinates x_i, y_i.

u_i = x component of $\vec{V}_i$.

v_i = y component of $\vec{V}_i$.

N = number of vectors used in interpolation.

x_j = x coordinate of $\vec{V}_j$.

y_j = y coordinate of $\vec{V}_j$.

a_j = x component constants

b_j = y component constants

For each vector component, the Hardy equations involve a set of N simultaneous equations, with N unknowns (the constants a_j and b_j). Solutions to these equations can be found by a variety of matrix operation techniques, such as Gaussian elimination or Gauss-Siedel methods. A Gaussian-elimination matrix solver was written utilizing full scaling and implicit partial pivoting to find the constants a_j and b_j. Using these constants, and their associated x_j and y_j position coordinates, the velocity can be determined *at any point* in the flow field by replacing x_i and y_i in equations (17) and (18) with the x and y coordinate of interest. Vorticity and flow streamlines can then be derived using the equations for the interpolated vector field.

An example using equations (16) through (18) follows. Assume two, horizontal vectors of length 10 are known, the first originating at $x, y = 10, 10$ (traveling left to right) and the second originating at $x, y = 20, 20$ (above the first traveling right to left). This simulates two plates sliding in opposite directions across each other. Therefore, $u_1(10, 10) = 10$, $v_1(10, 10) = 0$, and $u_2(20, 20) = -10$, $v_2(20, 20) = 0$. Solving the Hardy equations using these two vectors gives $a_1 = -0.7588$, $a_2 = 0.0$, $b_1 = 0.7588$, and $b_2 = 0.0$. With these constants, a velocity of zero (as expected) is determined at $x, y = 15, 15$, again using the Hardy equations.

III.4 Tracking Synthetic Data

Referring to Fig. 3, although 500 spots were placed in frame 1, only 495 remain in frame 2, 482 spots remain through frame 4, and 455 spots remain in the view area through all 10 frames. This is due to motion of spots out of the imaginary viewing area by the flow field. Further scrutiny will show that there are high density regions (upper right side) and low density regions (directly below the cylinder) of particles, along with a mix of straight and curving flow regions. The multiframe tracking technique uses all ten frames of data (only the first four frames are used for analysis purposes), while the cross-correlation algorithm is performed on the first two frames of data.

Figure 4 and Fig. 5 are produced with the multiframe tracking program. Figure 4 shows the particle trajectory tracks through all 10 frames, essentially 'connecting the dots' from some starting particle. Figure 5 plots 'instantaneous' vectors, by pulling out the piece of a track which started in frame 1 and stopped in frame 2. The vector magnitudes have been multiplied by 3. The tail of a vector "arrow" marks the point of the velocity coordinate. A velocity scale is provided, and can be used in the following manner: If the length of a velocity vector is 1.5 times the scale length, the velocity magnitude of that vector is 15 pixels/frame. Neither of these figures discards any tracks due to high σ_{total} values. When there are two particles adjacent to one another in a flow with changing vorticity, the program may track across different spots through the turn. This creates difficulty in combining sets of four-tracks, and also in deleting tracks which incorrectly share a common spot. This is evident with the small incorrect track starting with the little circle near the lower left hand portion of the cylinder shown in Fig. 4. The small circle indicates that this track started in frame 5, obviously incorrect since all tracks started in frame 1, and therefore not shown in Fig. 5.

Figure 6 was produced by plotting the output of the cross-correlation program. The cross-correlation program shows more vectors leaving the view area at the left side of Fig. 6, as compared to Fig. 5. This is due to the less stringent requirement of only two sequential frames, vice four frames for the multiframe tracking program. Also, Fig. 6 shows that the cross-correlation program correctly determined the two vectors missed (previously mentioned) by the multiframe tracking method. However, there are two vectors (near the bottom and top right portion of the cylinder) missing. Cross-correlation uses the overlaying of neighboring particles between frames. The

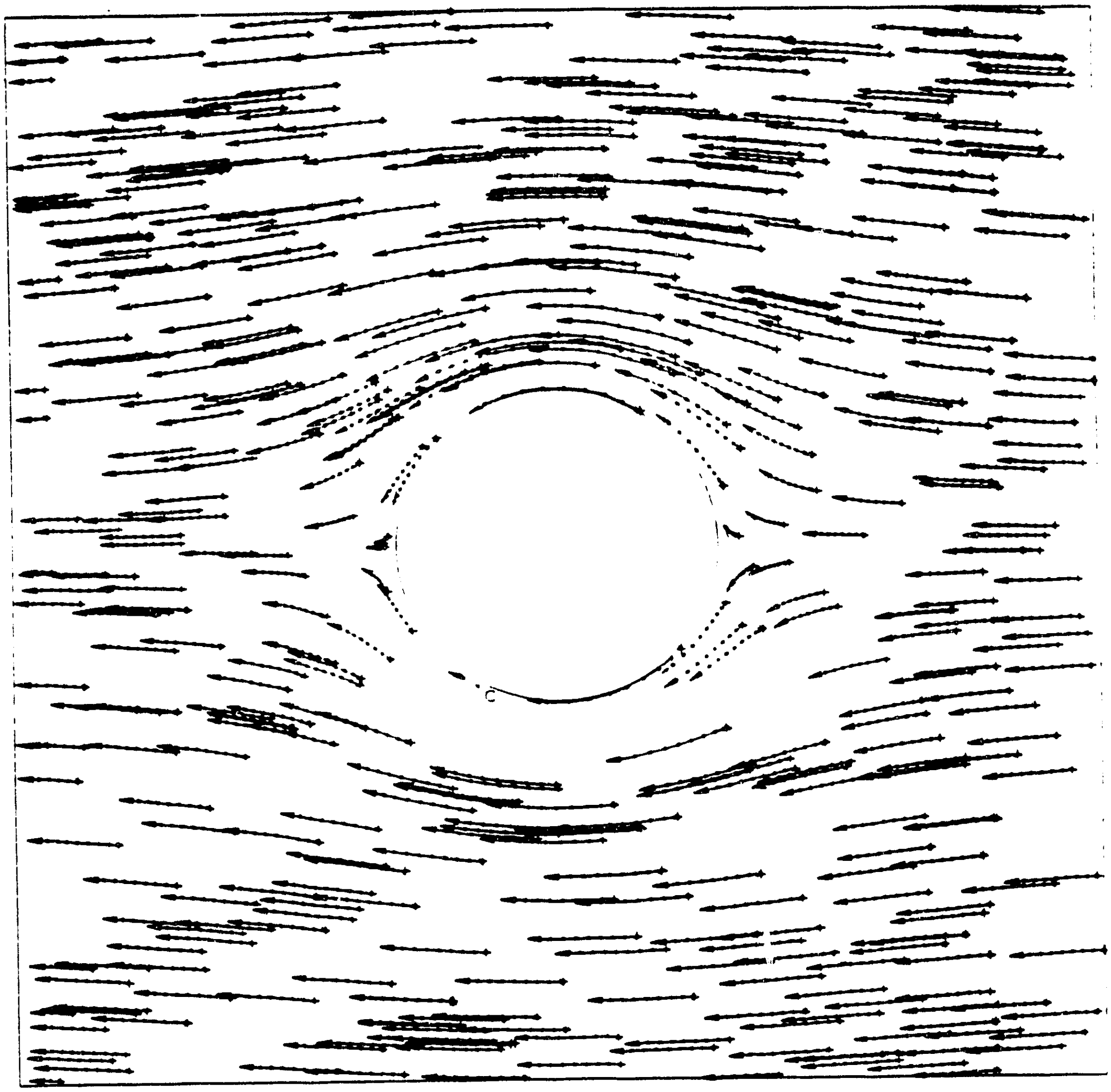

Camera view: 1024 x 1024 pixels

Figure 4. MFT Method on Synthetic Data, Frames 1-10

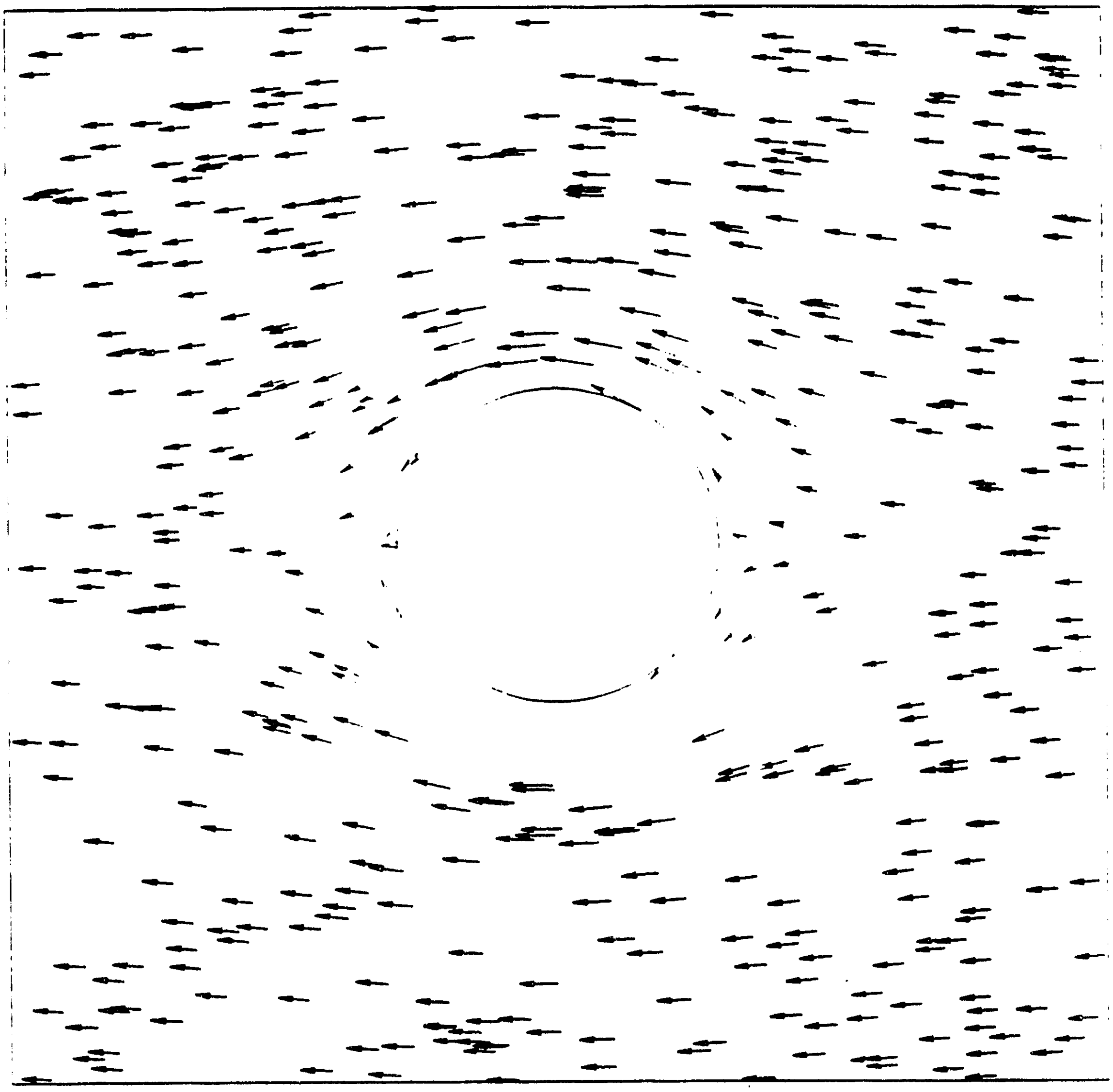

Camera view: 1024 x 1024 pixels
Velocity scale: — 10 pixels/frame
Vector multiplier: 3

Figure 5. MFT Method on Synthetic Data, Frames 1-2

dynamic correlation region will expand to ensure at least 5 particles are included in the correlation for a specific particle match. The program did find these vectors, but the reliability index for these particle pairs were 0.0, due to no close neighbors, and consequently not plotted.

There are many parameters that can affect the functioning and computer speed of the tracking routines. The first parameter, that will be discussed, is the Number of Spots per Image (NSI). As would be expected, if there are more spots, it will take the tracking programs longer to track all of them.

The second parameter is number density. Number density is the number of spots per area. For the tracking program analysis, area was defined in square pixels because the digital imager used to obtain experimental data had a resolution of 1024 x 1024 pixels. It is irrelevant, to the tracking programs, whether the camera was viewing a 50 cm^2 area or a 25 cm^2 area. The number of square pixels remained the same. Number density is a concentration measurement, whereas, NSI is a measurement of the total seeds captured. Number density was defined in terms of number of spots per 1024 x 1024 image. Thus, if 500 spots were evenly distributed on a 1024 x 1024 image, the number density and NSI are equal to 500. If the 500 spots were present only on the right half of the image, the number density (for the right half of the image) would be 1000, and the NSI would remain 500. The number density is an important parameter to the tracking programs. The cross-correlation algorithm requires adjacent spots for its tracking, and the local number density could significantly affect the results.

A third parameter is the spot movement between sequential camera frames (or images). This is the distance, in pixels, that a single particle travels between two

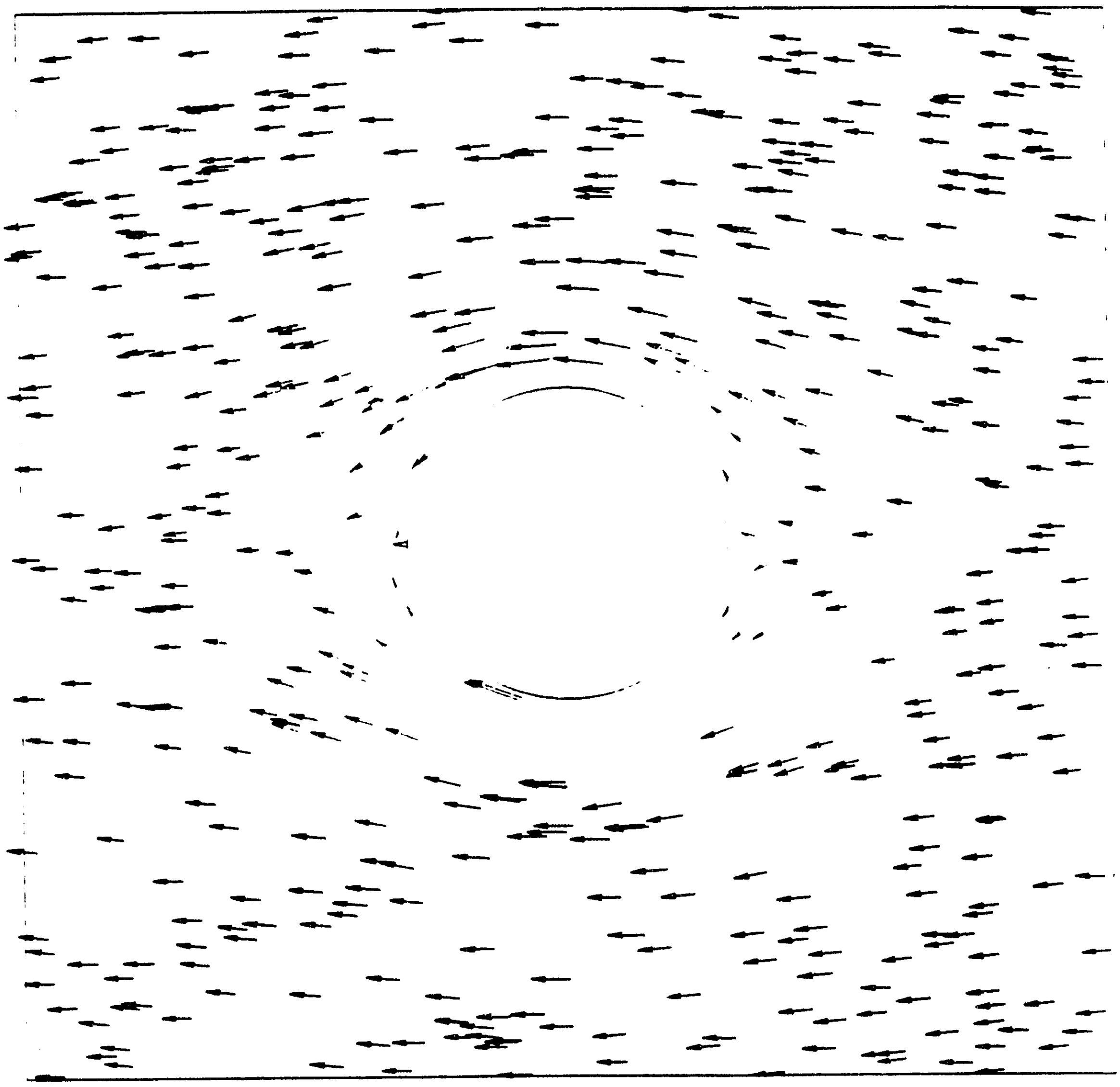

Camera view: 1024 x 1024 pixels
Velocity scale: — 10 pixels/frame
Vector multiplier: 3

Figure 6. CCT Method on Synthetic Data. Frames 1-2

consecutive images. This is particularly important if the flow has significant *local* vorticity. This implies that local pattern distributions will change greatly between frames, especially with large particle movement between frames, yielding poor particle group correlations.

Both tracking methods were analyzed for yield and reliability. *Yield* was defined to be the ratio of the number of total vectors determined by a tracking method to the number of actual vectors available. *Reliability* is the measure of the accuracy of the vectors. This was defined as the number of correct vectors determined by a tracking method divided by the total number of vectors determined by the tracking method. Multiplying the number of vectors in an image by the reliability will give the number of accurate vectors produced by the tracking program.

Figure 7 compares the effects of spot movement for the two tracking methods, cross-correlation tracking (CCT) and multiframe tracking (MFT), on the cylindrical flow field. Spot movement defines various freestream velocities, i.e., a spot movement of 10 simulates a particle freestream velocity of 10 pixels/frame (in the x direction). In order to accurately compare the tracking methods, particles were randomly placed (simulating a tracer seed release) near the cylinder (bounded by $511 < x < 1023$ and $256 < y < 757$). This allowed the seeds to remain in the picture through at least four sequential frames, even with large pixel movement, which is a requirement of the multiframe tracking method. Analysis was made with movements of 5, 10, 15, 20, 25, 50, 75, 100, and 125 pixels between frames. NSI was a constant 125 particles, and number density was held constant at 500. Reliability and yield for

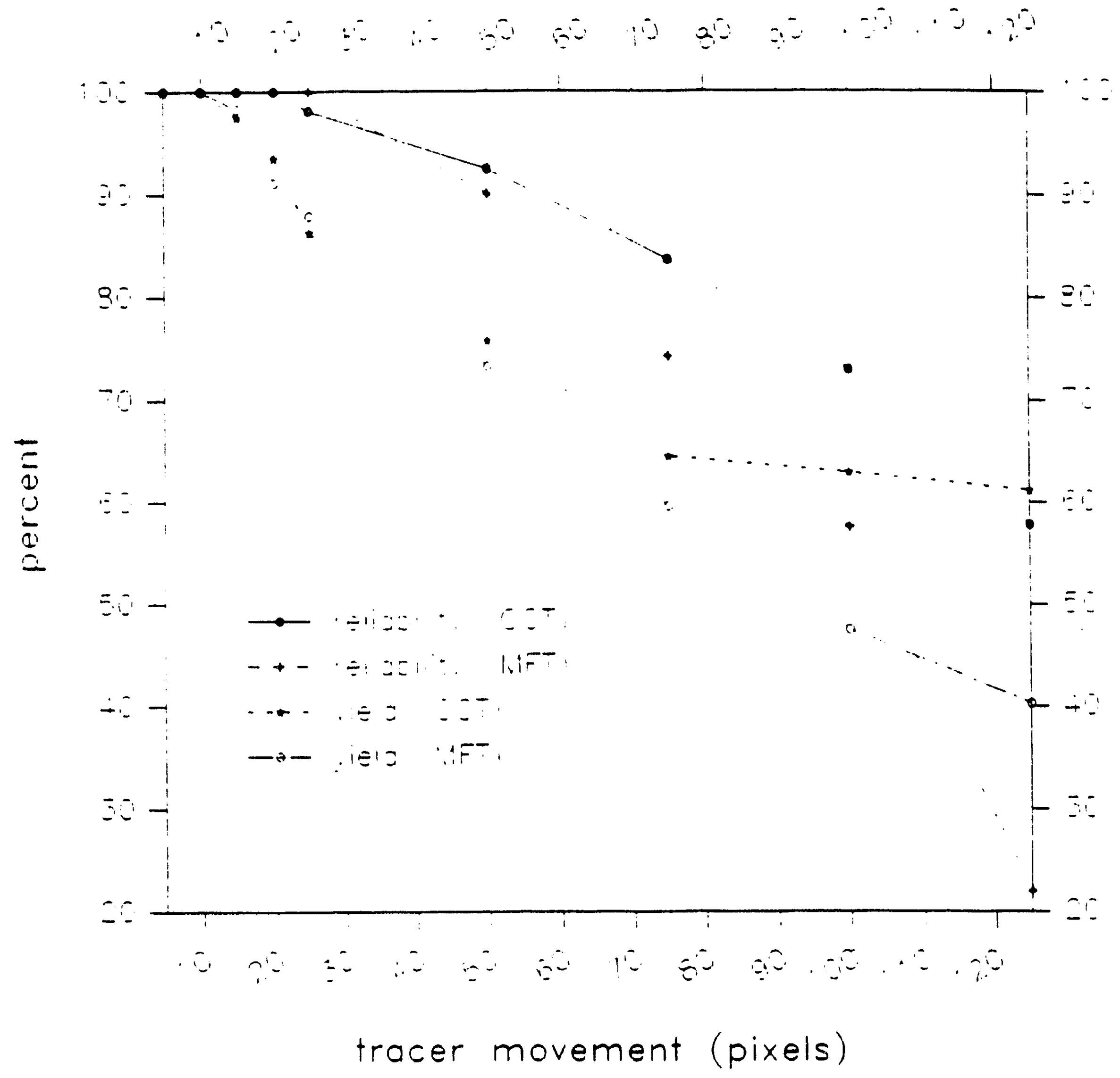

Number density constant at 500 tracer particles

Figure 7. Movement Analysis of Synthetic Data

both tracking techniques were greater than 70% for movements as large as 50 pixels between frames. The multiframe tracking method was outperformed by the cross-correlation technique for particle movements greater than 35 pixels. This was due to the tracer seeds moving in somewhat "S-shaped" patterns around the cylinder, versus simple "C-shaped" patterns for smaller spot movements. This would yield a large value for the deviation from the mean of the vector angles (equation (2)), and subsequently a poor value for the total track deviation (equation (3)).

Figure 8 compares the affects of number density for the two tracking methods, on the cylindrical flow. The spot movement was kept constant at 10 pixels per frame. As this figure shows, number density does not affect the accuracy of the tracking methods to any significant degree, except that the cross-correlation method cannot track properly if there are very few spots on an image. This was because there are no adjacent spots to correlate, which then gives a reliability index R_i value equal to 0.0, and subsequently not tracked.

Figure 9 shows the CPU cost analysis for the tracking methods using a VAX 8600 computer. Even though the binary cross-correlation tracking method is generally more reliable than the multiframe tracking method, it can cost considerably more CPU time. It should be noted, however, that the binary correlation uses far less CPU time as compared to an 8-bit gray level correlation, where the number of floating point operations can be significantly higher (Yamamoto et al., 1988). This figure demonstrates the expected effect that increasing movement and number density increases the time for analysis.

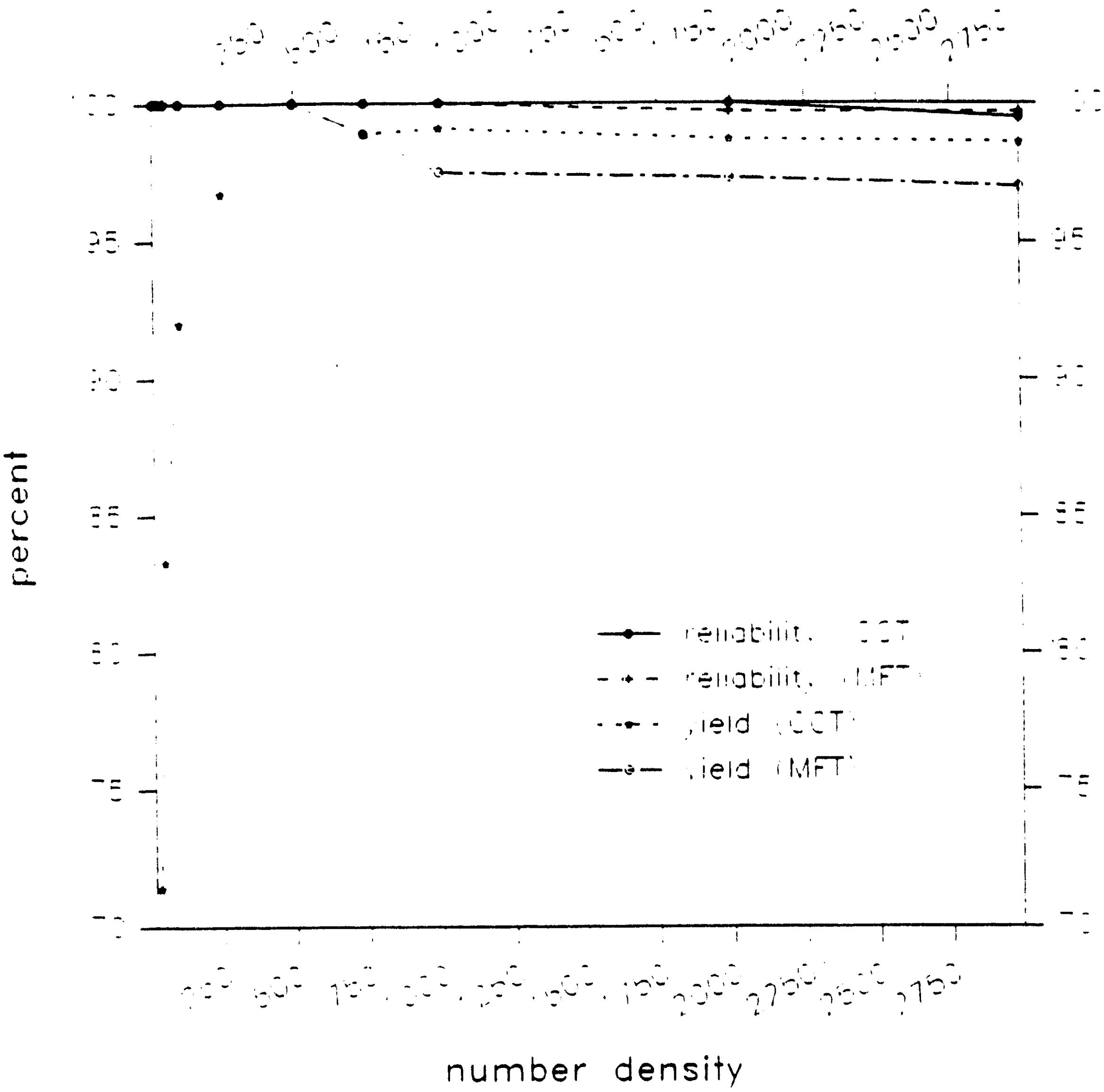

Spot movement constant at 10 pixels/frame

Figure 8. Density Analysis of Synthetic Data

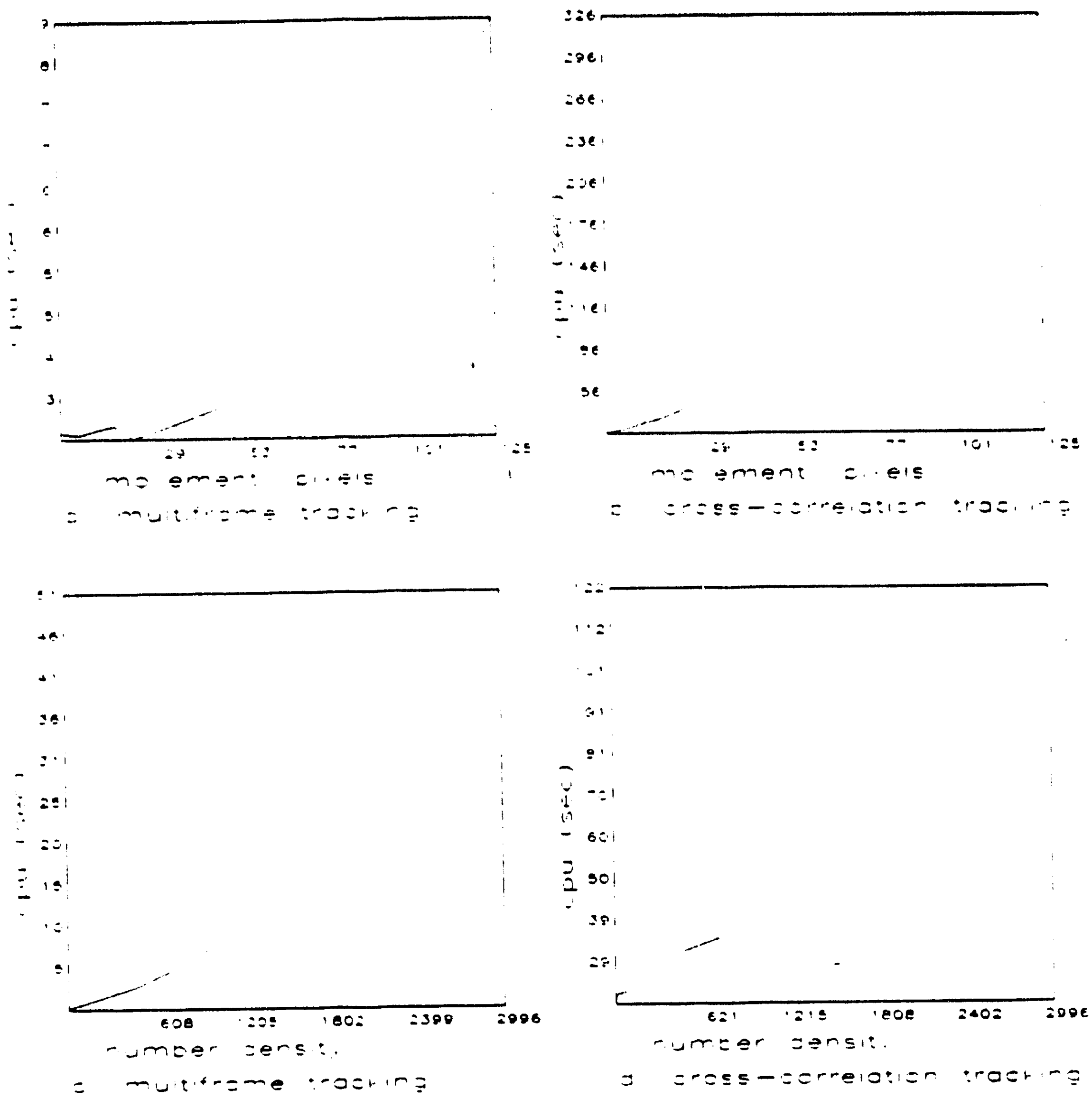

a) Number density constant at 500 spots
b) Number density constant at 500 spots
c) Spot movement constant at 10 pixels/frame
d) Spot movement constant at 10 pixels/frame

Figure 9. CPU Cost Analysis of Synthetic Data

Table 1 summarizes the analysis for the two tracking methods. The simulations have shown that each tracking method has unique advantages and disadvantages. The main advantage for the MFT method is speed. Another advantage, due to the requirement of 4 sequential frames, is that the additional data helps confirm a track. The requirement of 4 sequential frames is also the biggest disadvantage, especially with high velocity flows where 4 frames cannot be captured. In addition, the statistical algorithm which computes the 'best track' breaks down with complicated, turbulent, flows. Also, a little thought on the question 'What if the allowed search radius's for the MFT method are too large?', will give the answer that perfect (and completely wrong!) tracks can be found. This is due to the statistical probability that particle positions can be found, given large search areas, which gives a good σ_{total} value (especially for high seed concentration).

The main advantages for the CCT method are that only 2 sequential frames are required, and that the method is more tolerant to large particle movement between frames than the MFT method. The major disadvantage is slower run times. Another possible disadvantage is that a vector will almost always be found for each particle in the first frame (inherent in the method). This vector may not be correct, shown later by the tracking of experimental data. Lastly, a good vector can be found by the CCT method and wrongly discarded, if the reliability index for that vector is poor due to a low local seed concentration.

Since both tracking methods have demonstrated an ability to track 'clean' synthetic data (a noise-free, extremely smooth flow field) accurately and efficiently, it becomes necessary to test them on experimental data.

Table 1. Analysis Summary for Tracking Methods

Cross-correlation tracking number density analysis

= density	NSI	total vectors	good vectors	yield	reliability	cpu
12	3	—	—	—	—	—
28	7	5	5	0.714	1.000	19.02
48	12	10	10	0.833	1.000	21.52
100	25	23	23	0.920	1.000	21.89
248	62	60	60	0.967	1.000	26.45
496	124	124	124	1.000	1.000	32.08
740	185	183	183	0.989	1.000	35.35
996	249	247	247	0.991	1.000	41.06
1996	499	493	493	0.987	1.000	76.47
2996	749	739	736	0.986	0.995	122.62

Multiframe tracking number density analysis

= density	NSI	total vectors	good vectors	yield	reliability	cpu
12	3	3	3	1.000	1.000	0.71
28	7	7	7	1.000	1.000	0.97
48	12	12	12	1.000	1.000	1.06
100	25	25	25	1.000	1.000	1.30
248	62	62	62	1.000	1.000	2.09
496	124	124	124	1.000	1.000	3.51
740	185	182	182	0.989	1.000	5.61
996	249	243	243	0.975	1.000	8.18
1996	499	486	485	0.973	0.997	22.96
2996	749	727	725	0.970	0.997	51.24

Table 1. Continued

Cross-correlation tracking spot movement analysis

pixel movement	NSI	total vectors	good vectors	yield	reliability	cpu
5	124	124	124	1.000	1.000	26.62
10	124	124	124	1.000	1.000	29.74
15	124	121	121	0.975	1.000	34.12
20	124	116	116	0.935	1.000	37.29
25	124	107	105	0.863	0.981	42.80
50	124	94	87	0.758	0.925	83.48
75	124	80	67	0.645	0.837	149.32
100	124	78	57	0.629	0.730	239.56
125	124	76	44	0.612	0.578	326.91

Multiframe tracking spot movement analysis

pixel movement	NSI	total vectors	good vectors	yield	reliability	cpu
5	124	124	124	1.000	1.000	3.38
10	124	124	124	1.000	1.000	3.35
15	124	122	122	0.983	1.000	3.42
20	124	113	113	0.911	1.000	3.48
25	124	109	109	0.879	1.000	3.29
50	124	91	82	0.733	0.901	3.75
75	124	74	55	0.596	0.743	5.04
100	124	59	34	0.475	0.576	6.64
125	124	50	11	0.403	0.220	9.10

III.5 Tracking Experimental Data

The synthetic data produced for this report was very clean (i.e. one particle moved smoothly from one frame to the next, particles did not appear or disappear in the middle of the picture, and none of the given data was actually noise that could be called a particle by the imaging systems). Experimental data, no matter how carefully the experiment is performed, will usually have these sources of error. Unfortunately, the actual vectors are not known and quantified error analysis cannot be performed. However, by visually comparing the calculated vectors determined by the tracking programs with the experimental data overlay pictures, a qualitative evaluation of the general pattern of flow can be extracted.

The experimental data was obtained with a Pulsed Laser Velocimetry setup (Hassan and Blanchat, 1991) shown in Figure 10. A pulsed laser light sheet was obtained using a Spectra-Physics Nd:YAG high energy laser and a series of four cylindrical lens; and directed to the flow region of study by five mirrors. The laser can produce a 1 J pulse with a 8 ns pulse width. This experiment imaged flow produced by a jet located 5 cm above the bottom of a large tank; thereby creating a step flow. The camera viewpoint was 19 cm above the flow step and 15 cm from the tank inlet. The tank was 44 cm wide, 92 cm long, and 32 cm high. Water, pumped at 5 gpm, entered the jet inlet region, where a series of screens produced a distributed flow at the step. The principal flow path was out of the step, up and to the right, where the water would flow over a wall to a pump suction plenum. However, three recirculation regions were found to exist. The first, directly below the step, was small and had a clockwise rotation.

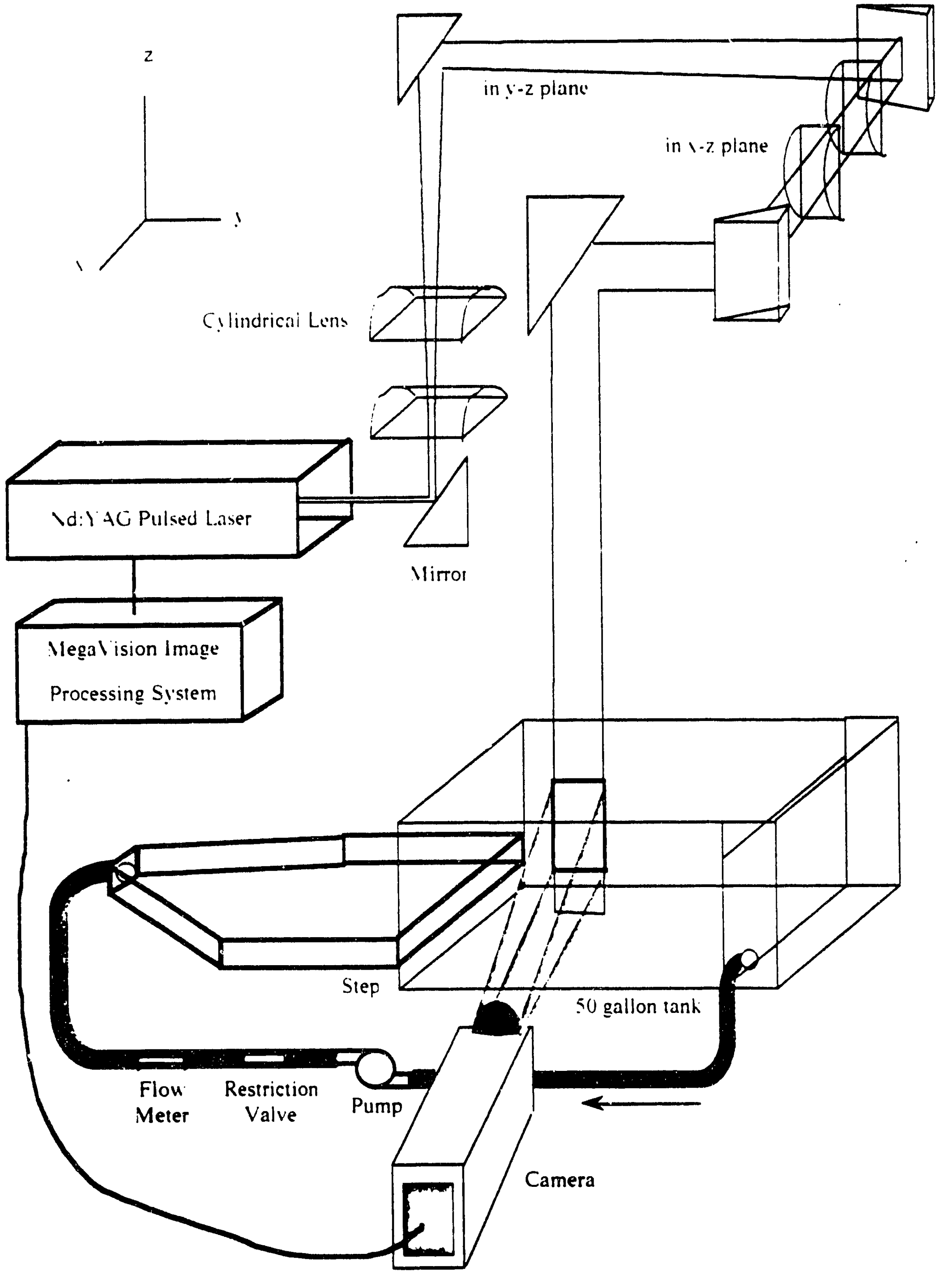

Figure 10. Pulsed Laser Velocimetry Step Flow Setup

The second, directly above the step, was much larger, and had a counter-clockwise rotation. The *back* of this second recirculation region, where the water flowed left and down, was where the light sheet was directed, coplanar to the two-dimensional pathlines. The water flow was seeded with 6 μm diameter, neutral density, polystyrene particle tracers (1.02 specific gravity). The images were recorded with a MegaVision imaging system using a high resolution (1024 x 1024 x 8 bits) Vidicon camera with its principal axis normal to the laser sheet. The camera viewing area of the light sheet was 5 x 5 cm. The MegaVision imaging system provides realtime acquisition and pipeline processing of 1024 x 1024 images, and performs many standard image processing functions. Multiple time frame digitization was achieved using a 150 ms time separation between laser pulses, and obtained by allowing a vertical drive camera signal to externally fire the laser.

Distributions of the track values are presented in Fig. 11, which compares the multiframe σ_{total} values of tracks between the synthetic data simulating flow around a cylinder and experimental data obtained from the step flow facility. This figure also compares the cross-correlation method C_{ij} values of tracks using synthetic data and experimental data. Given synthetic data (i.e. no noise), the majority of the σ_{total} track values should be approximately zero, and the majority of the C_{ij} correlation values should be near one, as shown in Fig. 11. It is readily apparent from Fig. 11 that the sources of error in the experimental data will shift the distributions: σ_{total} values move away from zero and C_{ij} values move toward zero. The consequence of these shifts makes it harder to differentiate between 'good' and 'bad' vectors. Remember that perfect vectors have 0.0 σ_{total} values and 1.0 C_{ij} values.

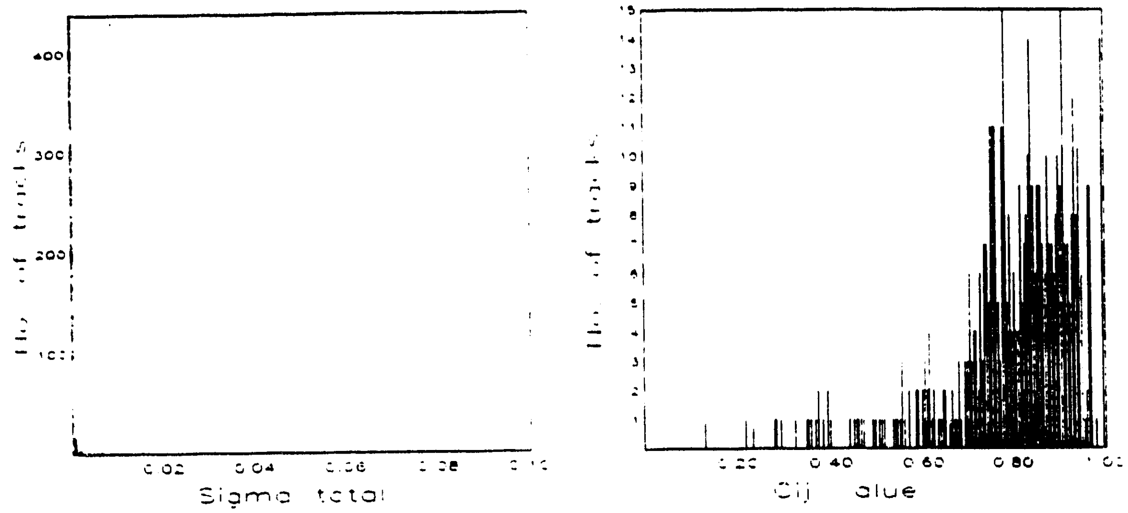

a) synthetic data

b) synthetic data

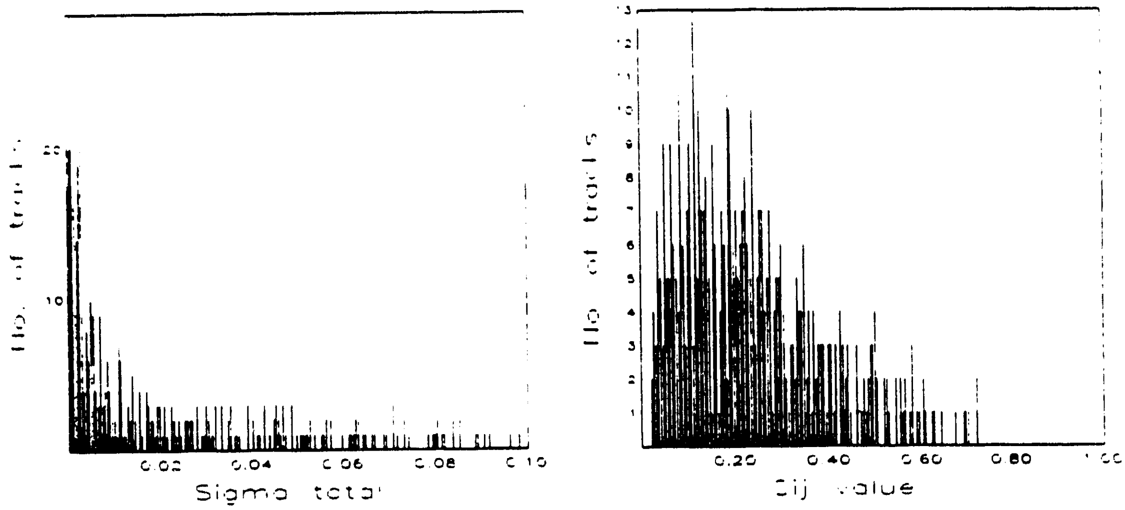

c) experimental data

d) experimental data

Figure 11. Multiframe and Cross-correlation Track Distributions

Distributions of track pair reliability index values are presented in Fig. 12. This figure compares the synthetic vs. experimental data R_I values for each track obtained with the cross-correlation tracking method, dramatically showing the effect noise has on the CCT method. Each data set had approximately 500 tracks, and they were sorted and plotted in order of reliability index. The R_I's for the noise-free synthetic data typically are very large, providing a measure of confidence for these track pairs. The smaller R_I's for the experimental data introduce an uncertainty into the confidence of their tracks.

In Fig. 13, ten consecutive experimental frames are overlaid to produce a "multiple exposure" picture. Note the noise at the image top, bottom, and right boundaries. This was due to the camera tube beginning to fail due to a small crack, releasing the vacuum. As mentioned previously, flow issuing from the jet was from left to right, which produces a recirculation pattern flowing down and to the left, in the camera view area located above the jet. Streamlines of the flow, predicted by the 3-D computational fluid hydraulics code FLUENT, along with the position of the image plane of the camera, are also shown in Fig. 13. It was relatively easy to visually track most of the seed with little ambiguity, except at the edges where noise was located and the flow was nearly stagnant. Figure 14 shows the particles that were tracked through all 10 frames. Figure 15 and Fig. 16 show instantaneous vectors (magnified by 3 for clarity) for particles found between frames 1 and 2. Figure 15 has 132 vectors on it, although it appears through visual comparison with the flow pattern shown in Fig. 13 that maybe 15-20% of these are probably incorrect. Figure 16 shows the effect

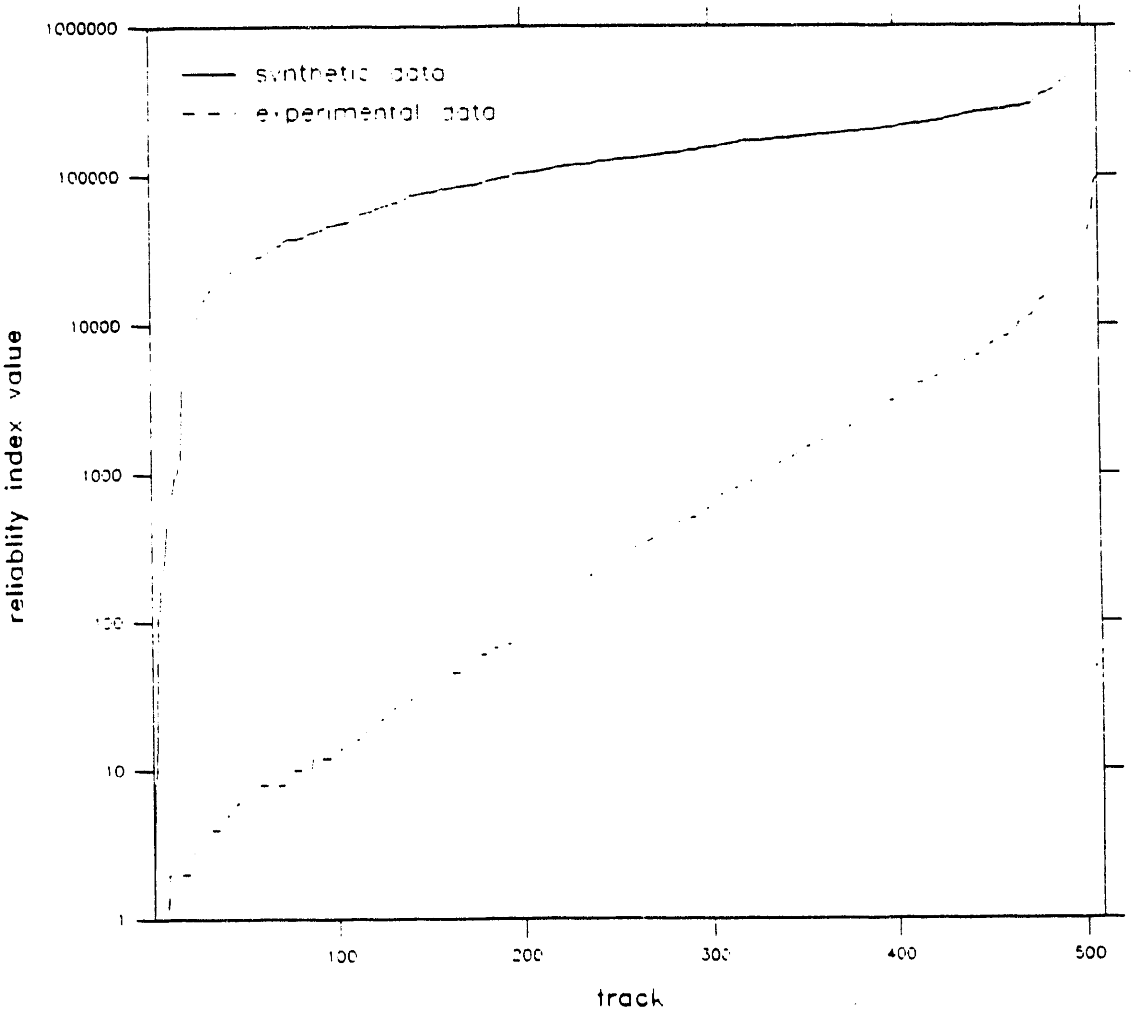

Figure 12. Comparison of CCT Method R_{ij} Values for Synthetic and Experimental Data

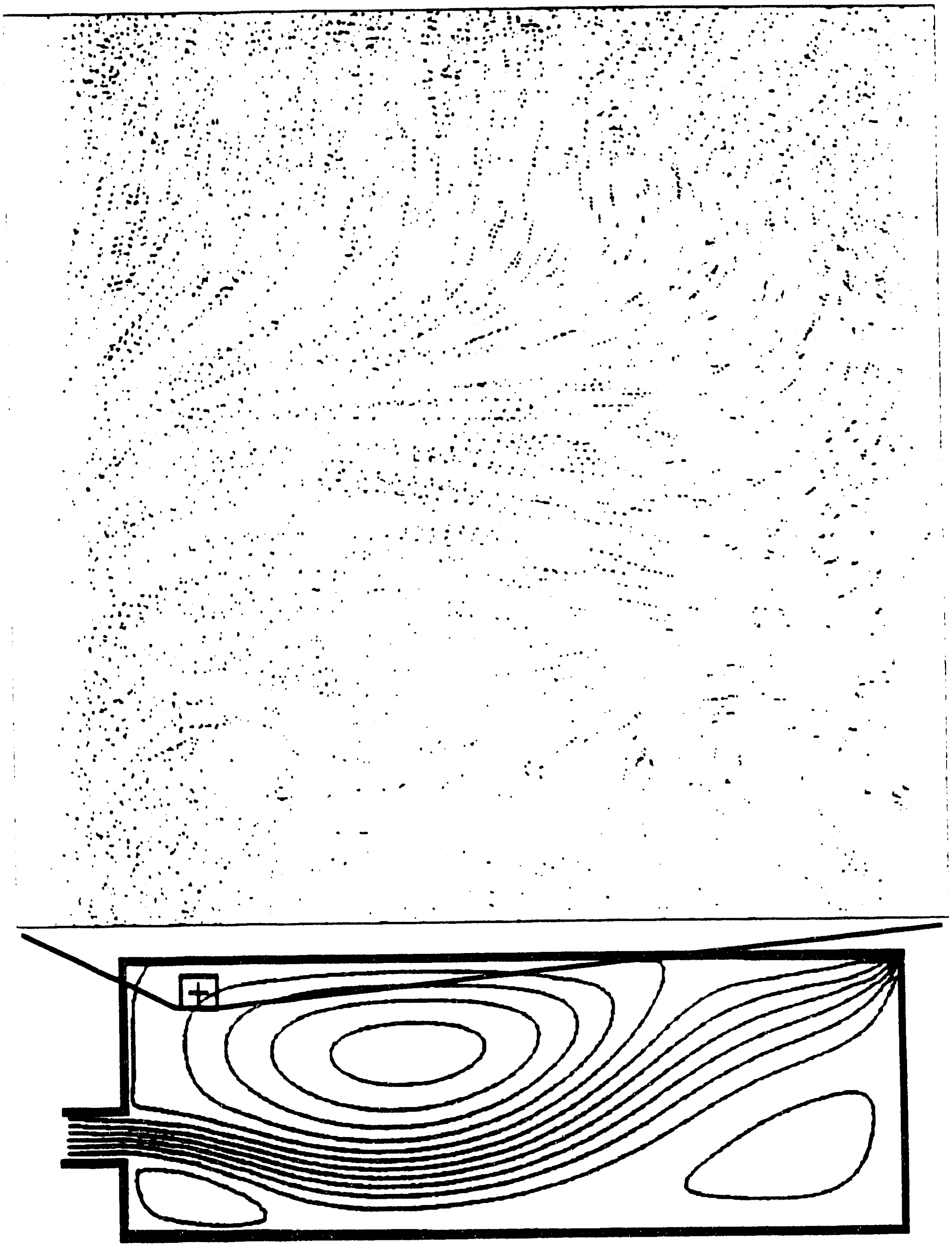

Flow direction in camera view (50 x 50 mm) is right to left and top to bottom

Figure 13. Experimental Data Overlay, Frames 1-10

of using a σ_{total} cutoff of 0.004 on Fig. 15, leaving 50 vectors. Figures 14– 16 show the results of the multiframe tracking (MFT) algorithm on the experimental data.

Figure 17 is an overlay of frames 1 and 2 of the experimental data. Figure 18 shows 469 vectors (magnified by 3), with maybe 20-25% appearing incorrect. There were 31 vectors which had a C_{ij} value greater than 0.5 (refer to Fig. 11). These were plotted in Fig. 19, and all of them (magnified by 3) appear to be correct. Note that Figs. 17– 19 present data used by, and results from, the cross-correlation tracking (CCT) method.

Operator assistance in analyzing and cleaning the data (subjectively removing erroneous vectors) is tedious and undesirable. The above numbers suggest that the cutoff values (σ_{total}, C_{ij}) can be used to initially 'clean' the data. However, they also eliminate many accurate vectors. Looking at Fig. 15 and Fig. 18, many vectors appear to be wrong. Thus, a computational means for cleaning the data was developed using suggestions from Landreth and Adrian (1988).

III.6 Interpolating, Cleaning, and Presentation of Experimental Data

To determine the accuracy of the Hardy equations (equations (16–18)), they were first applied to the vectors from frames 1 to 2 of the synthetic data. A vector map of the interpolated vector field was produced. Verification of this field was performed by applying the flow equations (equations (6–15)) to the same locations as the vectors in the vector map. A comparison between what the flow field should have been, and what the interpolated field produced, was then performed. The mean of the errors in the x and y directions were 0.0112 and 0.0104, respectively, and the standard deviation

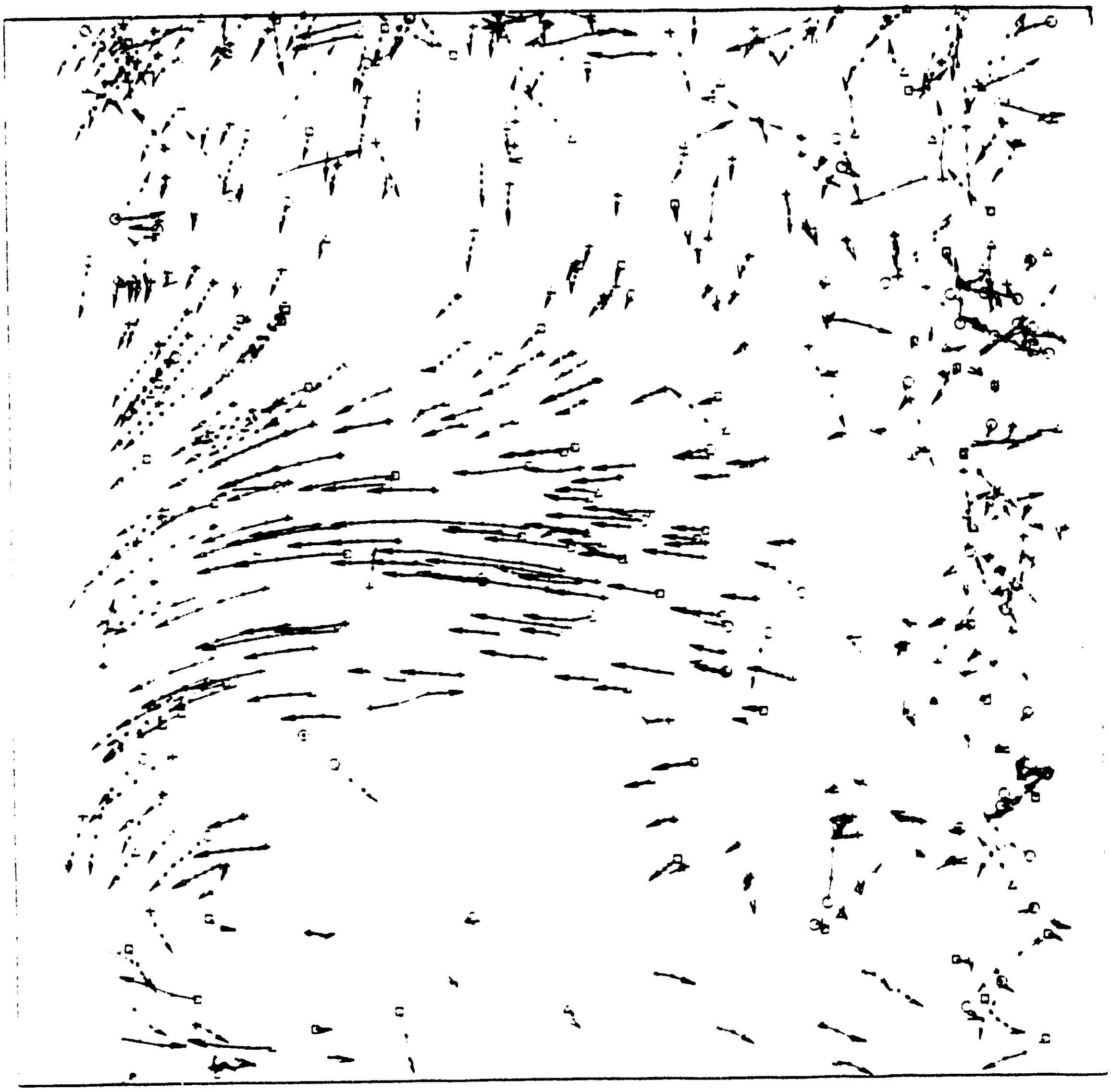

Camera view: 50 x 50 mm

Figure 14. MFT Method on Experimental Data. Frames 1-10

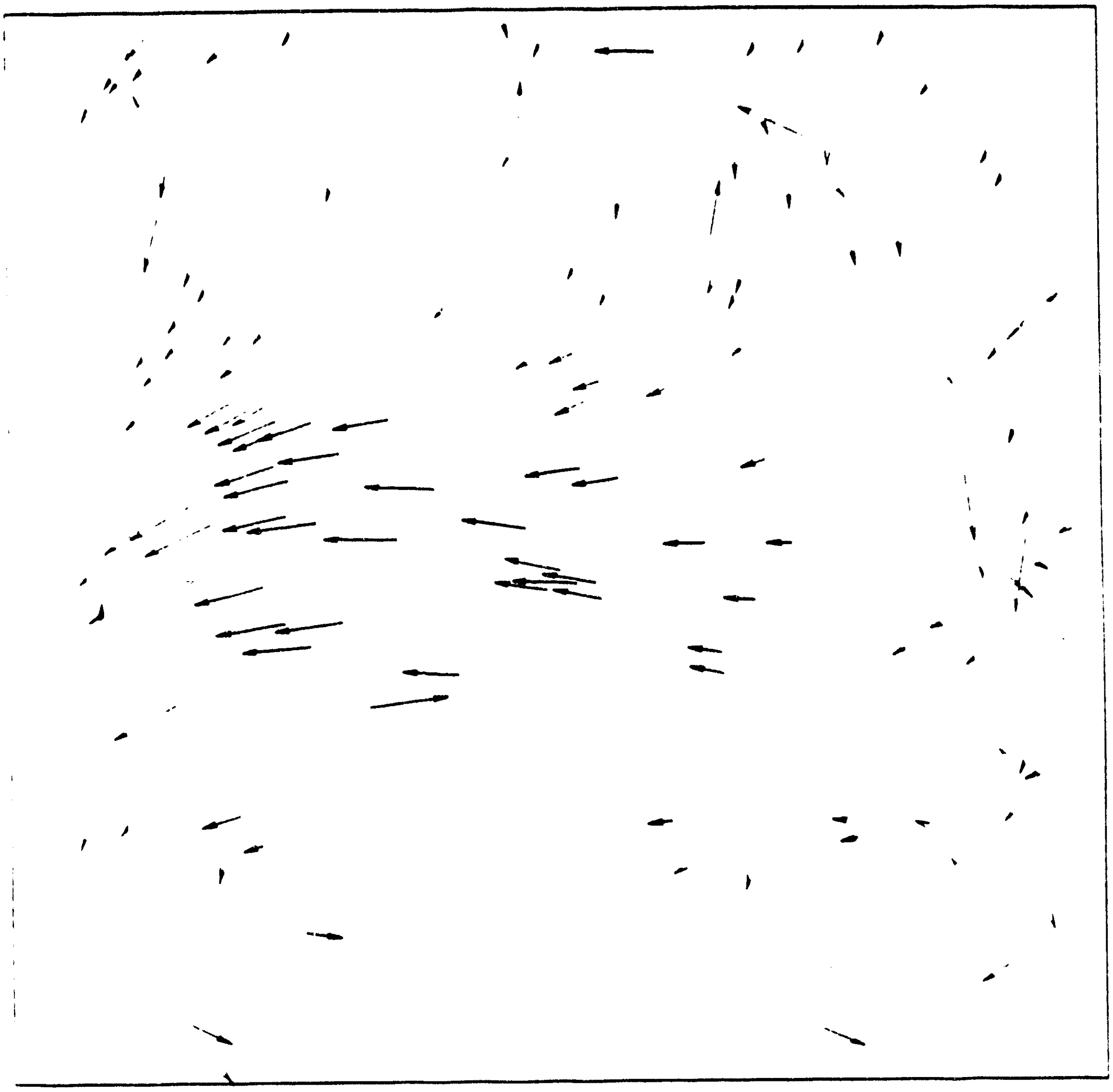

Camera view: 50 x 50 mm
Velocity scale: ——— 10 mm/s
Vector multiplier: 3

Figure 15. MFT Method on of Experimental Data. Frames 1-2

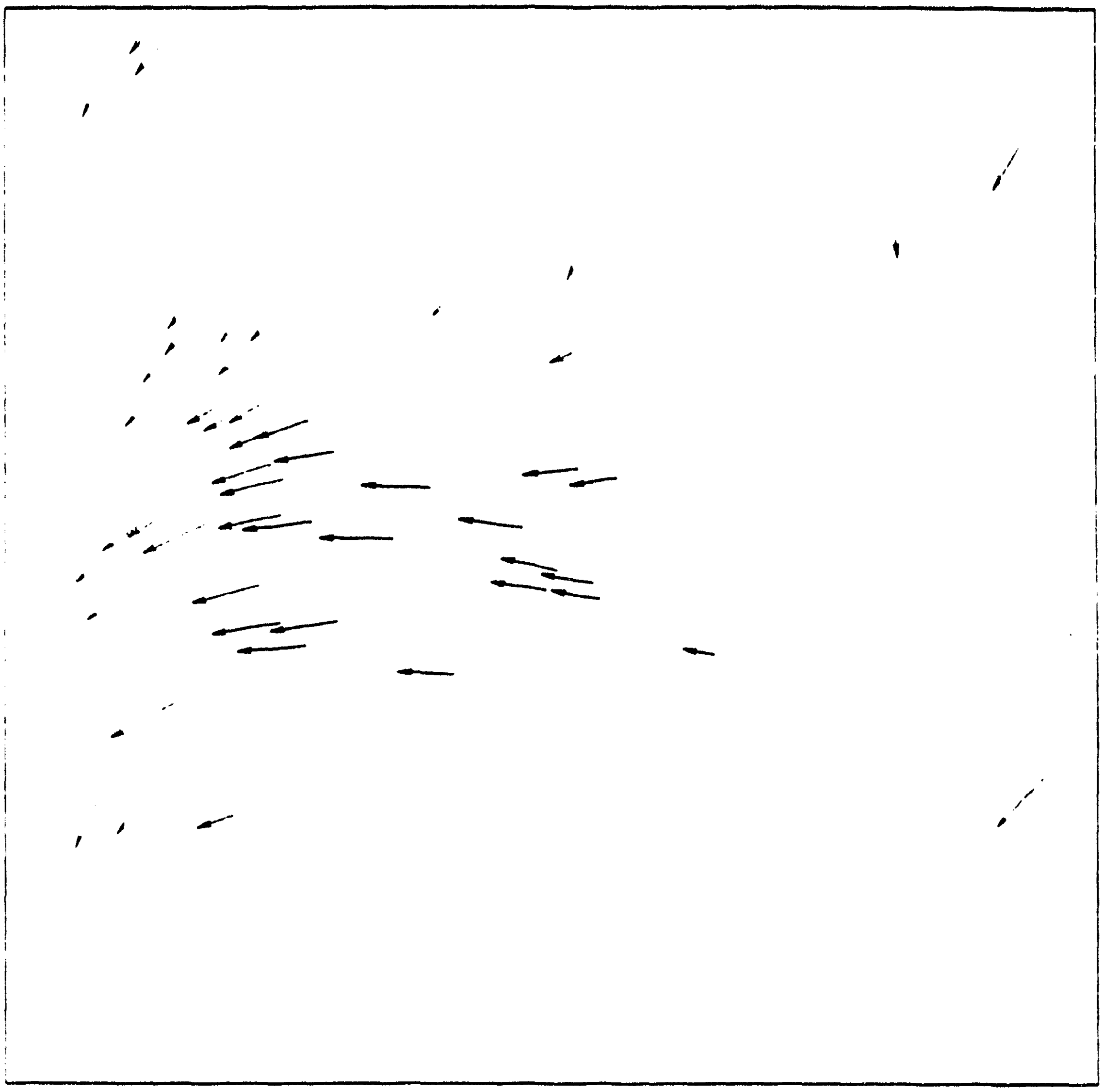

Camera view: 50 x 50 mm
Velocity scale: ——— 10 mm/s
Vector multiplier: 3

Figure 16. MFT Method on Experimental Data, Frames 1-2 (with Cutoff)

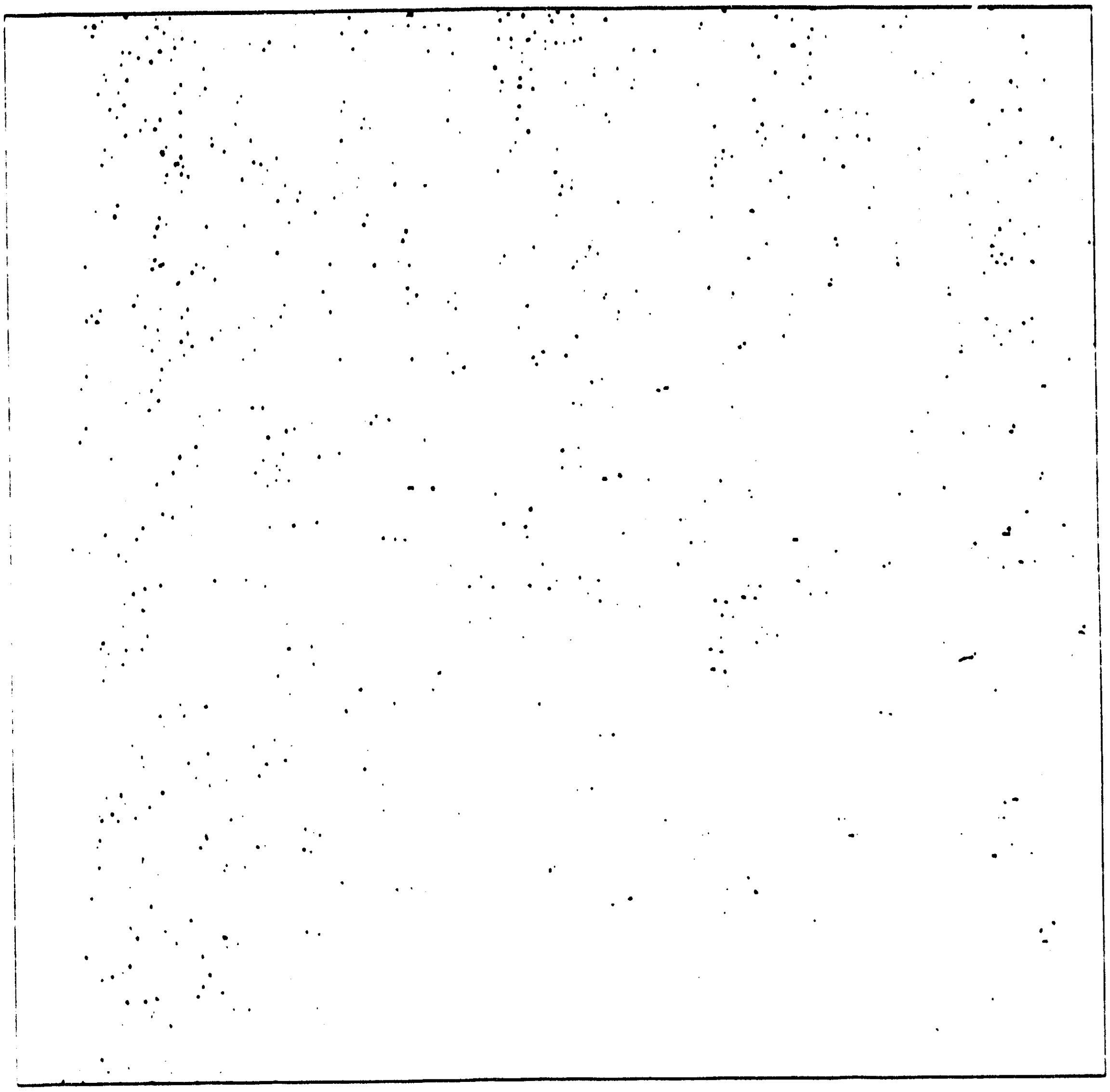

Camera view: 50 x 50 mm

Figure 17. Experimental Data Overlay, Frames 1-2

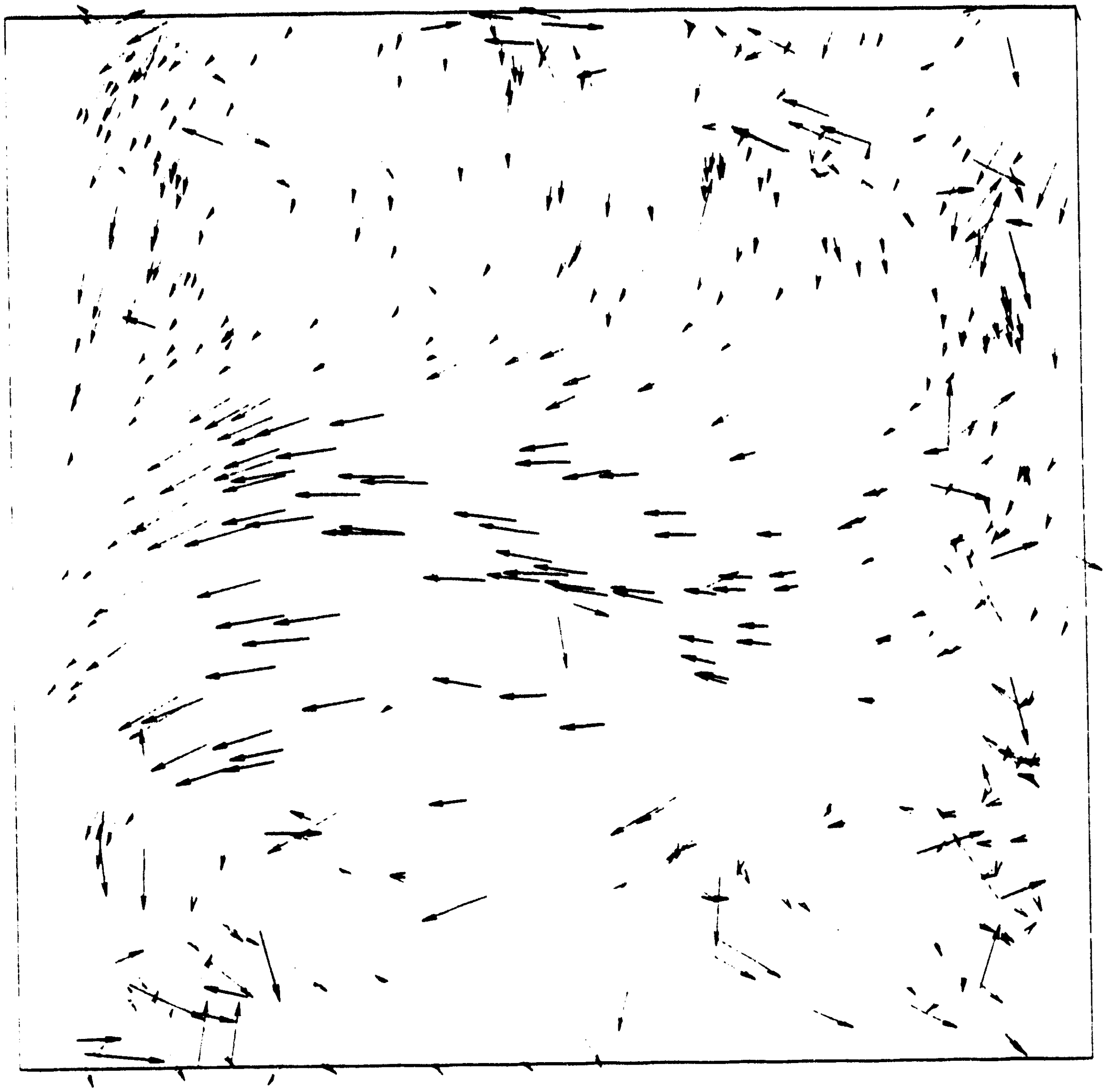

Camera view: 50 x 50 mm
Velocity scale: ——→ 10 mm/s
Vector multiplier: 3

Figure 18. CCT Method on Experimental Data, Frames 1-2

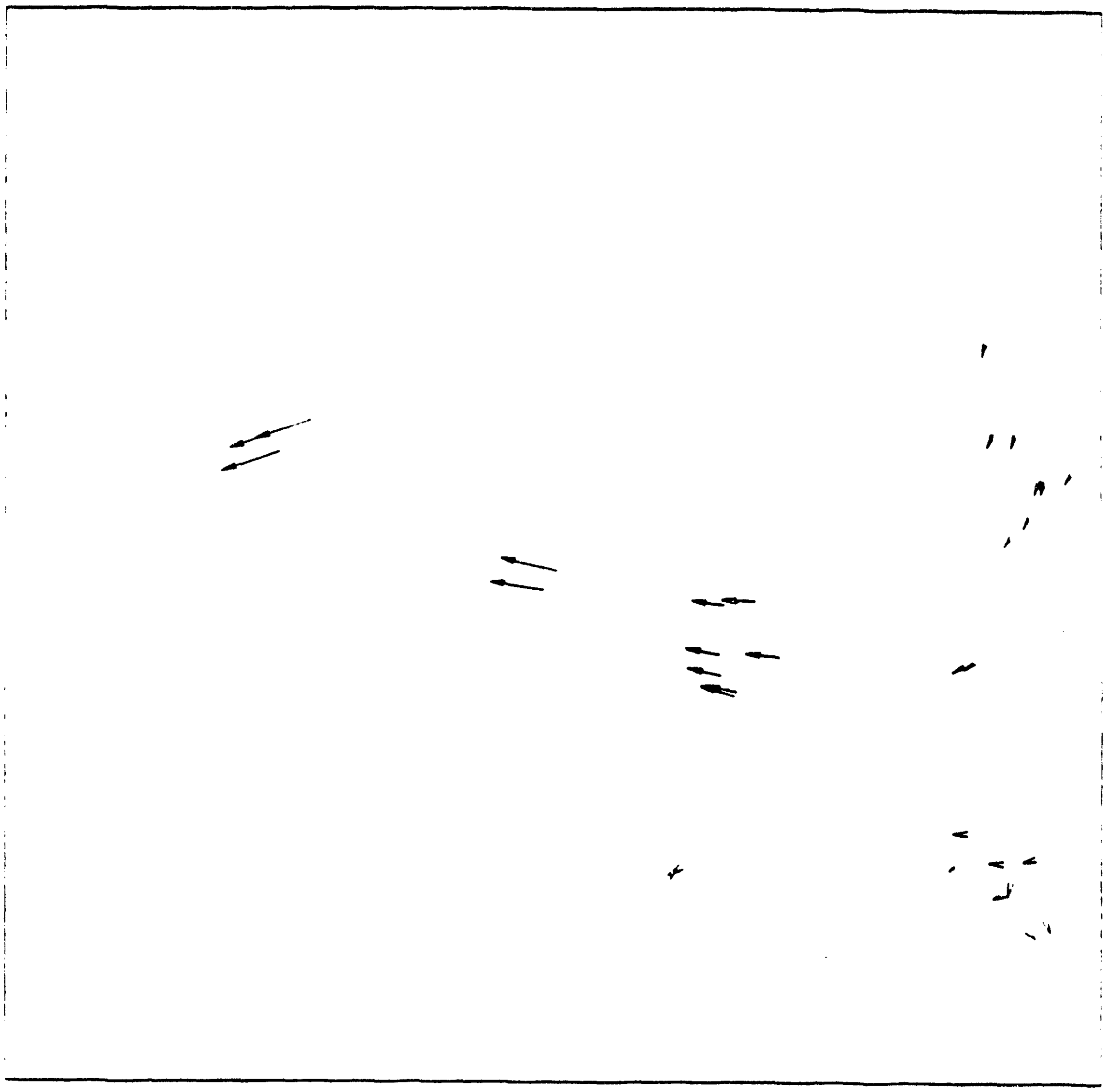

Camera view: 50 x 50 mm
Velocity scale: ——— 10 mm/s
Vector multiplier: 3

Figure 19. CCT Method on Experimental Data Frames, 1-2 (with Cutoff)

in the x and y directions were 0.0468 and 0.0400, respectively. These results are very good and, suggest that the interpolation scheme is accurate.

The Hardy equations were then applied to the experimental data from the cross-correlation tracking method using the initial cutoff value, Fig. 19, to produce the interpolated velocity field (multiplied by 3), shown in Fig. 20. Once the initial interpolated flow field has been made, and the constants used with the Hardy equations stored, the cleaning process can be performed. This involves checking every vector from the initial output of the tracking program against the interpolated vector field at that same point. If the magnitude of the difference of these two vectors is within a few pixels, it is considered an accurate vector. These vectors are then used to produce another, more refined, interpolated field, which is used to 'clean' the original picture. This iteration process is continued until no new vectors are added. Fig. 21 and Fig. 22 present the final 'cleaned' instantaneous velocity plot and the refined interpolated plot (both plots multiplied by 3) of the experimental data by the cross-correlation method. A final number of 372 vectors was produced. A flow field streamline plot, Fig. 23, was produced using the refined interpolated plot. Note that there is no proof that these final flow fields are correct, and that only a qualitative evaluation with the general pattern of flow as presented by the experimental data frame overlays can be performed.

While performing this analysis, it was discovered that the cross-correlation method performed significantly better (i.e. had a higher yield, compare Fig. 15 and Fig. 18) than the multiframe tracking technique on noisy images. This is due to the fact that

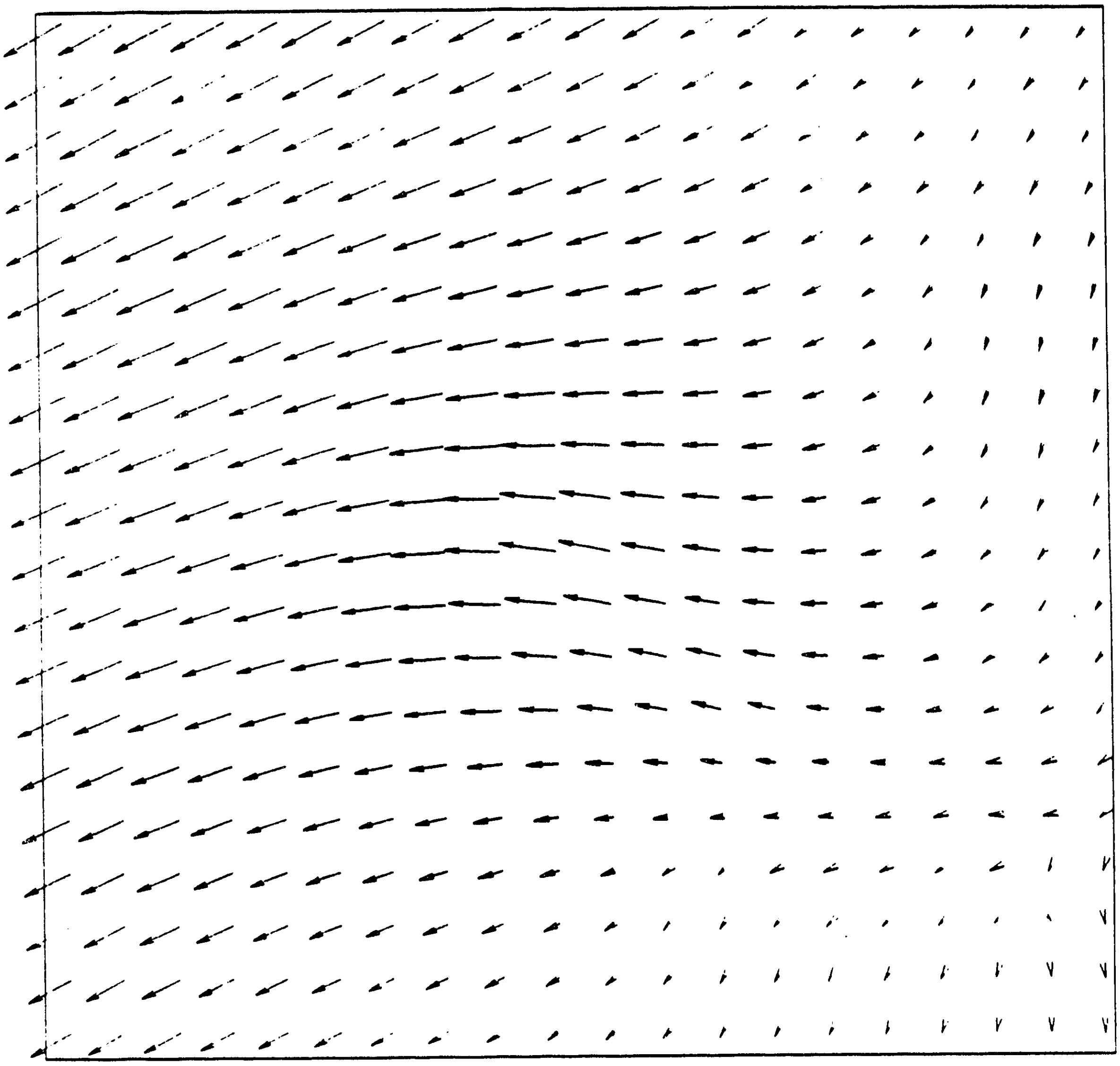

Camera view: 50 x 50 mm
Velocity scale: ——— 10 mm/s
Vector multiplier: 3

Figure 20. Initial Interpolated Vector Field of Experimental Data

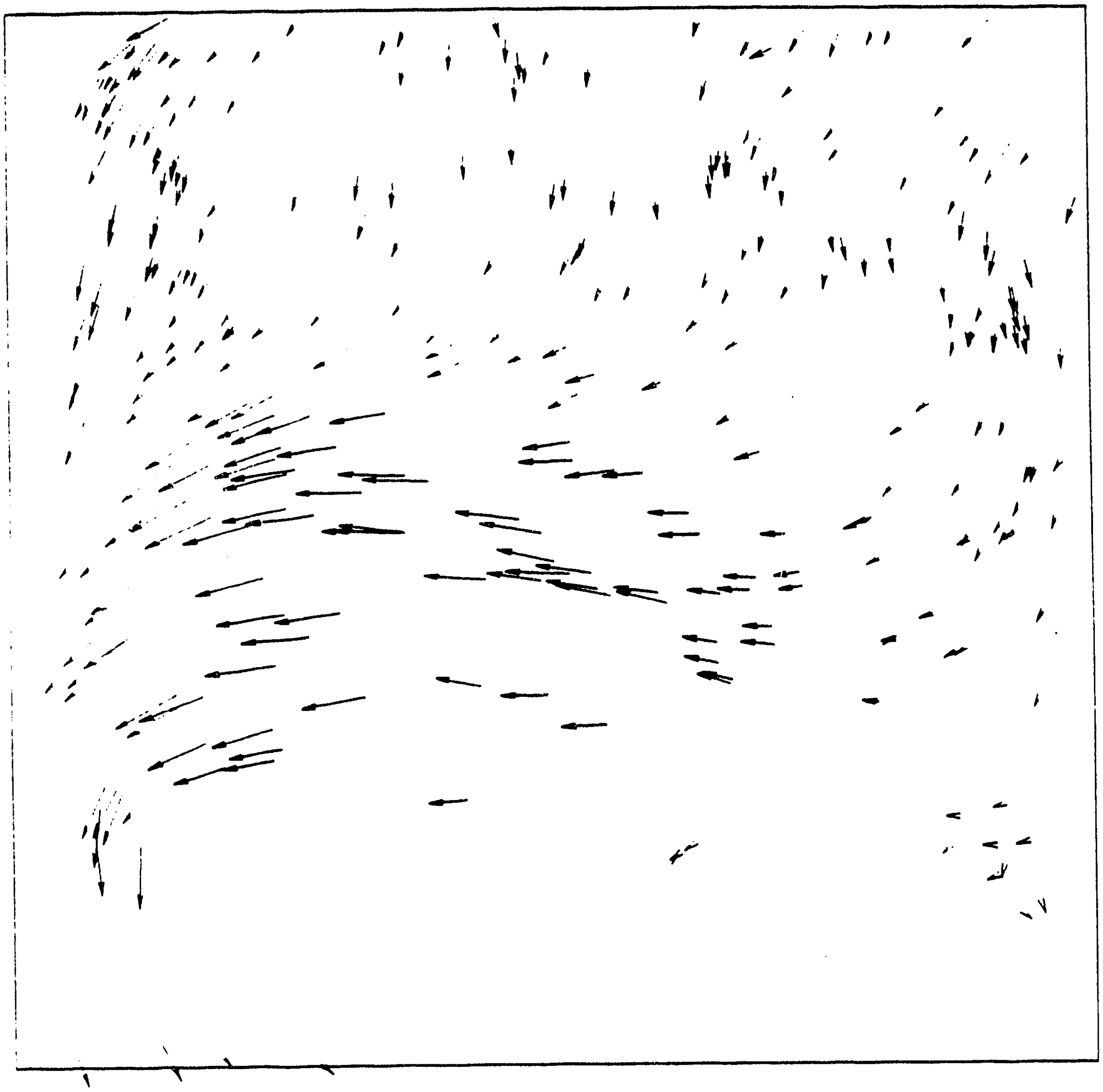

Camera view: 50 x 50 mm
Velocity scale: ——— 10 mm/s
Vector multiplier: 3

Figure 21. Final Instantaneous Vectors with Experimental Data

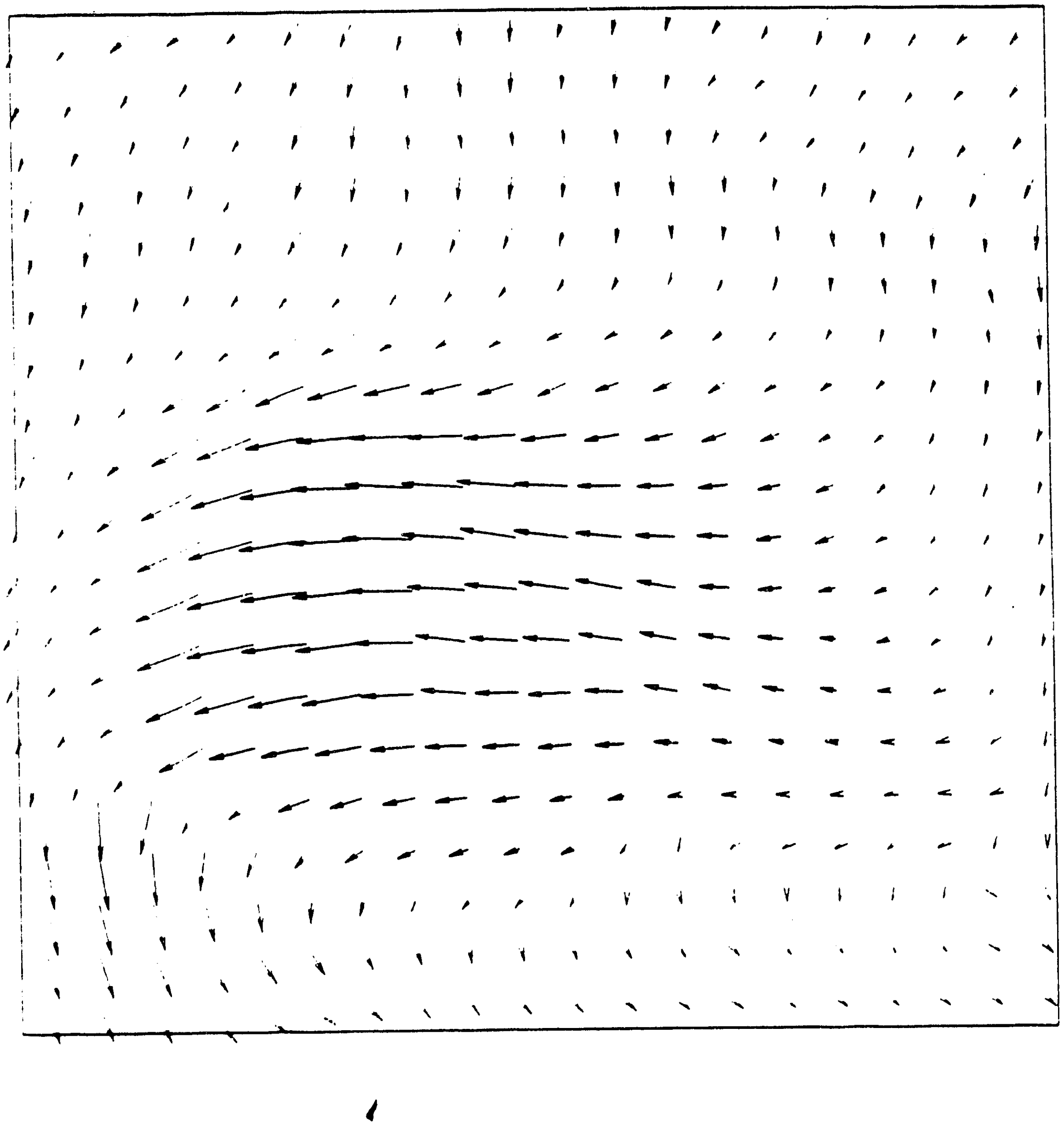

Camera view: 50 x 50 mm
Velocity scale: ——— 10 mm/s
Vector multiplier: 3

Figure 22. Final Interpolated Vector Field with Experimental Data

Camera view: 50 x 50 mm

Figure 23. Experimental Data Streamlines

large amounts of noise will provide the multiframe tracking technique with many possible particle choices. Statistically, this will increase the probability of producing an incorrect track by the multiframe tracking method. Cross-correlation techniques inherently avoid this pitfall, due to the fact that it is statistically improbable to produce the same noise patterns between sequential frames.

CHAPTER IV

STRATIFIED FLOW THEORY AND EXPERIMENT

IV.1 Introduction

Investigation of a two-phase, horizontal, stratified, flow regime is being performed to determine the interface drag force, and correspondingly, the drag coefficient. The drag force is due to the relative motion between the two fluids at the interface. This drag force cannot be solved with analytical methods, but can be experimentally determined.

Interphase drag plays an important role in two-phase fluid regimes. Study of two-phase (and similarly two-component) flow regimes is necessary to properly understand and model complex fluid flows. Many computer codes which predict two-phase fluid flow must determine interphase drag force. Typically, a drag coefficient correlation is used which was empirically determined. One such code is RELAP5/MOD2 (Ransom et al., 1985). This code is used extensively in the nuclear power industry to simulate a wide range of steady-state, transient, and accident conditions in pressurized water reactors. Some researchers have found that two-phase thermal-hydraulic codes do not model two-phase flow very well (Analytis et al., 1987; Hassan, 1987). Part of this deficiency has been attributed to an over-prediction of the drag force, which may be caused by an inappropriate drag coefficient (Putney, 1988).

Two-phase stratified flow information was determined with the pulsed laser velocimetry (PLV) method. This technique is a full-field, two-dimensional, noninvasive flow visualization technique. Many investigators have utilized this and similar imaging techniques to obtain full-field velocity measurements.

Direct digitization of the stratified flow images was accomplished with a high-resolution imaging system (1024 x 1024 pixels x 8 bit Vidicon camera). The data was analyzed with imaging system hardware and a series of new image processing and tracking analysis software being developed for two-phase flow experiments. PLV "captures" particles in the flow at one instant in time. Multiple images of the flow field were acquired by pulsing the laser and storing the digitized images. Analysis was performed later with the tracking software which was developed to match the particles from each of the consecutive image frames into tracks of the particles through time.

IV.2 Interface Shear Stress Theory

All gases and most simple fluids obey Newton's law of viscosity.

$$\tau_{yx} = -\mu \frac{dU}{dy} \tag{19}$$

This states that the shear force per unit area is proportional to the negative of the *local* velocity gradient. The shear stress (shown in Fig. 24) exerted in the x-direction on a fluid surface of constant y by an adjacent fluid surface is denoted by τ_{xy}, with U denoting the x-component of the velocity vector. Shear stress may also be interpreted as the viscous flux of x-momentum in the y-direction.

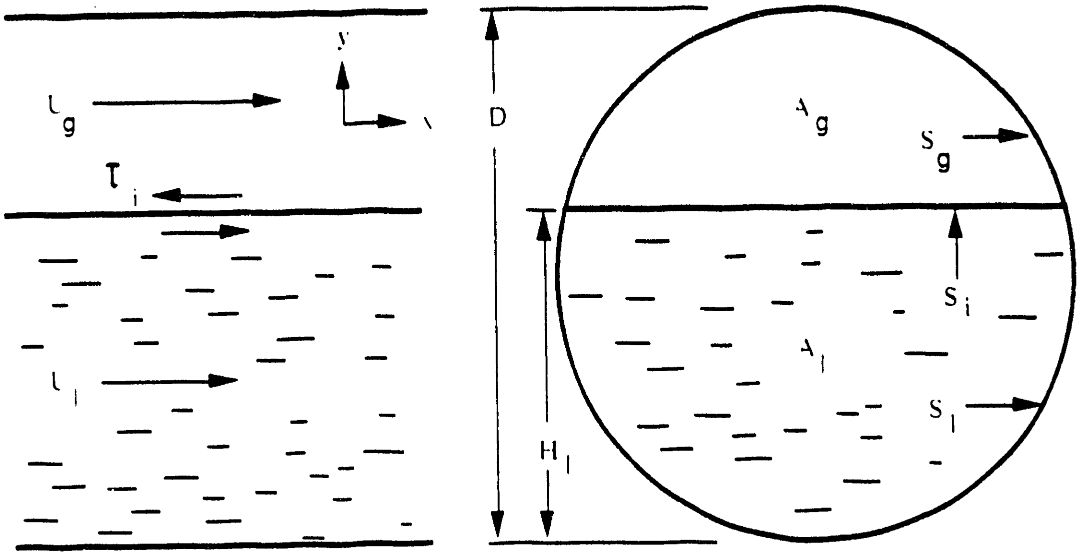

Figure 24. Cocurrent Equilibrium Stratified Flow in a Pipe

Consider a cocurrent, equilibrium, stratified flow in a pipe as shown in Fig. 24. Gas, liquid, and interface average velocities are denoted by U_g, U_l, and U_i. Gas and liquid flow areas normal to the flow direction are represented by A_g and A_l. Gas, interface, and liquid surfaces are given by S_g, S_i, and S_l. The pipe diameter is D and the liquid height is H_l. The interfacial shear stress can be evaluated in a conventional manner (Taitel and Dukler, 1975), based on the Fanning friction factor

$$\tau_i = f_i \frac{\rho_g (U_g - U_i)^2}{2} \tag{20}$$

with ρ_g denoting gas density and f_i denoting the interfacial friction factor. The gas friction factor f_g is evaluated from the Blasius equation, and given in terms of the Reynolds number Re,

$$f_g = C_g \left[\frac{\rho_g U_g D_g}{\mu_g} \right]^{-m} = C_g \left[Re_g \right]^{-m} \tag{21}$$

with D_g being the gas perimeter and μ_g being the gas viscosity. The coefficients C'_g and m are determined from theory or correlation, depending on whether the flow is laminar or turbulent.

It has been established (Gazley, 1949) (and conventionally used throughout the literature) that for smooth stratified flow, $f_i = f_g$. The gas hydraulic diameter is determined from

$$D_g = \frac{4A_g}{(S_g - S_i)} \tag{22}$$

Thus, the gas is visualized as flowing in an closed duct. From laminar *pipe* flow theory, it will be shown that appropriate coefficients are $C'_g = 16$, and $m = 1$. In order to compare experimentally determined values of shear stress with equation (20), it must be determined if these coefficients are appropriate for laminar *channel* flow.

Friction factor f is typically defined by

$$F_k = AKf \tag{23}$$

where F_k is the force exerted by a fluid on a surface due to kinetic behavior, K is the characteristic kinetic energy of the fluid per unit volume, and A is the characteristic area bounded by the wetted surface. For example, consider a gas-filled pipe of length L and diameter D (radius $R = 2D$). The area is given by $A = 2\pi RL$, and the characteristic kinetic energy per unit volume is given by $K = 1/2\rho U_g^2$. A momentum balance on the pipe gives a force caused by the pressure drop of $F_k = \pi R^2(P_o - P_L)$, where P_o is the pipe entrance pressure and P_L is the pipe exit pressure. Therefore, the pipe friction factor is given by

$$f_g = \frac{D}{2}\left(\frac{P_o - P_L}{L}\right)\frac{1}{\rho U_g^2} \tag{24}$$

An analytical solution to the pipe problem (Bird et al., 1960) for the average or bulk gas velocity is given by

$$U_g = -\frac{1}{8}\left(\frac{1}{\mu_g}\frac{\partial P}{\partial x}\right)R^2 \tag{25}$$

Substituting equation (25) into equation (24) yields

$$f_g = 16\left[\frac{\mu_g}{\rho_g U_g D_g}\right] = \frac{16}{Re_g} \tag{26}$$

which verifies the C_g constant used with the Blasius equation for laminar pipe flow with $m = 1$.

Performing the same analysis for an enclosed duct or channel filled with gas having dimensions: Height H, width W, and length L: $A = 2(H - W)L$, $K = 1/2\rho U_g^2$, and the momentum balance on the channel gives $F_k = HW(P_o - P_L)$. Therefore, the channel friction factor is given by

$$f_g = \frac{HW}{(H - W)}\left(\frac{P_o - P_L}{L}\right)\frac{1}{\rho U_g^2} \tag{27}$$

Average flow velocity for the channel can be found using the Navier-Stokes equations for continuity and x-momentum (rectangular geometry with x, y, and z vector components of velocity $\mathbf{V_g}(U_g, V_g, W_g)$). For constant density ρ_g, the continuity equation

$$\frac{\partial \rho_g}{\partial t} = -\rho_g\left(\frac{\partial U_g}{\partial x} + \frac{\partial V_g}{\partial y} + \frac{\partial W_g}{\partial z}\right) \tag{28}$$

will give (for steady-state conditions and $V_g = W_g = 0$)

$$\frac{\partial U_g}{\partial x} = 0 \tag{29}$$

Similarly, the x-momentum equation

$$\rho_g\left(\frac{\partial U_g}{\partial t}-\frac{U_g\partial U_g}{\partial x}-\frac{V_g\partial U_g}{\partial y}-\frac{W_g\partial U_g}{\partial z}\right)=\rho_g g_x-\frac{\partial P}{\partial x}-\mu_g\left(\frac{\partial^2 U_g}{\partial x^2}-\frac{\partial^2 U_g}{\partial y^2}-\frac{\partial^2 U_g}{\partial z^2}\right) \quad (30)$$

will yield Poisson's equation

$$\nabla^2 U_g=\frac{1}{\mu_g}\frac{\partial P}{\partial x} \quad (31)$$

An analytical velocity solution to the rectangular pipe problem is not easily determined since the equation of a rectangle does not have a constant Laplacian. However, through a coordinate transformation and separation of variables, an analytical solution consisting of a infinite series involving hyperbolic sine and cosine functions can be found (Langlois, 1964). This solution does not readily substitute into equation (27), and it was decided to numerically solve Poisson's equation. First, it was necessary to define an expression for average velocity for the channel similar to equation (25).

$$U_g=-\frac{1}{C_g}\left(\frac{1}{\mu_g}\frac{dP}{dx}\right)R_H^2 \quad (32)$$

The hydraulic radius R_H is equal to twice the hydraulic diameter, and using the standard definition that the hydraulic diameter is equal to four flow areas over the wetted perimeter, yields $D_H=\frac{2HW}{(H-W)}$. Inserting these expressions into equation (27) yields a equation similar to the Blasius equation for laminar pipe flow

$$f_g=2C_g\left[\frac{\mu_g}{\rho_g U_g D_H}\right]=\frac{2C_g}{Re_g} \quad (33)$$

Numerical analysis of Poisson's equation will give a gas velocity U_g for an input forcing term $(\frac{1}{\mu_g}\frac{\partial P}{\partial x})$, and the constant C_g solved for from equation (32). Note that this "constant" is only applicable for the specified geometry. A program solving

Poisson's velocity equation (Appendix H) was written. Average velocity and peak velocity were determined to be 0.325 m/s and 0.655 m/s for a forcing term of -1000. this yields a value of 7.93 for the constant C_g using the channel dimensions (H=0.0762 m, W=0.1524 m).

The PLV test facility channel velocity solution is graphically shown in Fig. 25. Substituting C_g into equation (33) yields $f_g = 15.86/Re_g$. These results indicate that it should be possible to compare experimental shear stress data obtained from a test channel (having the above dimensions) to shear stress predicted from laminar pipe flow theory.

IV.3 Design of the PLV Stratified Flow Test Facility

A flow test facility was constructed to allow full-field velocity measurements of a horizontal, two-phase, stratified flow with Pulsed Laser Velocimetry techniques. The channel flow test facility is illustrated in Fig. 26.

The enclosed transparent horizontal channel, constructed with 12.7 mm thick Plexiglas, is 3.05 m long, 150 mm wide, and 80 mm tall. The channel lid is removable to allow for cleaning and the insertion of experiments. The lid has two 1/4 inch taps (only one shown) to allow attachment of a vent valve and a 3-5 p.s.i. relief valve. Nozzles, with plastic screens and flow straighteners (plastic straws), are placed at both ends to allow quick production of a two-dimensional flow. The nozzles convert the flow from the inlet tubing cylindrical geometry to the rectangular channel geometry quickly and smoothly. The nozzle design is illustrated in Fig. 27.

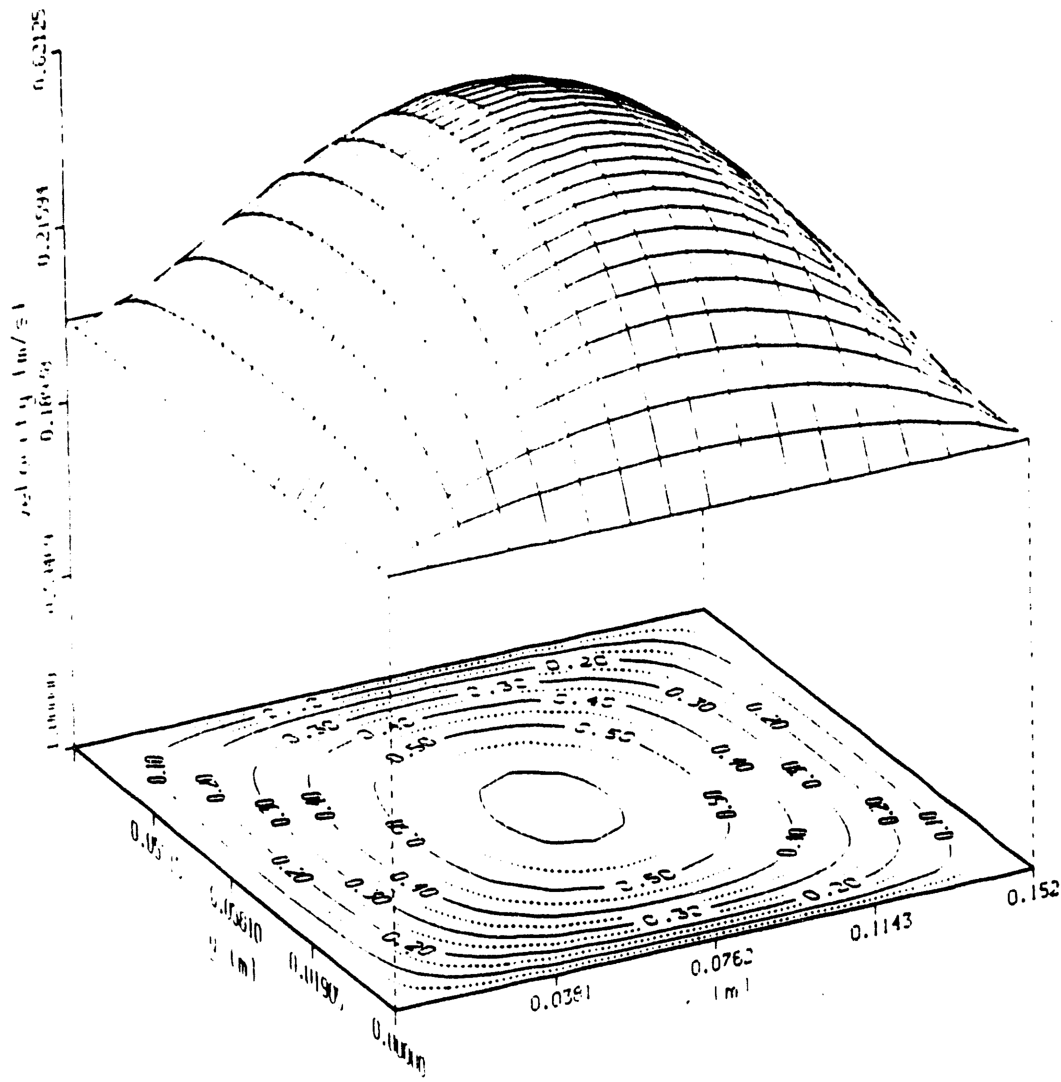

Figure 25. Numerical Velocity Solution for the Test Facility Channel

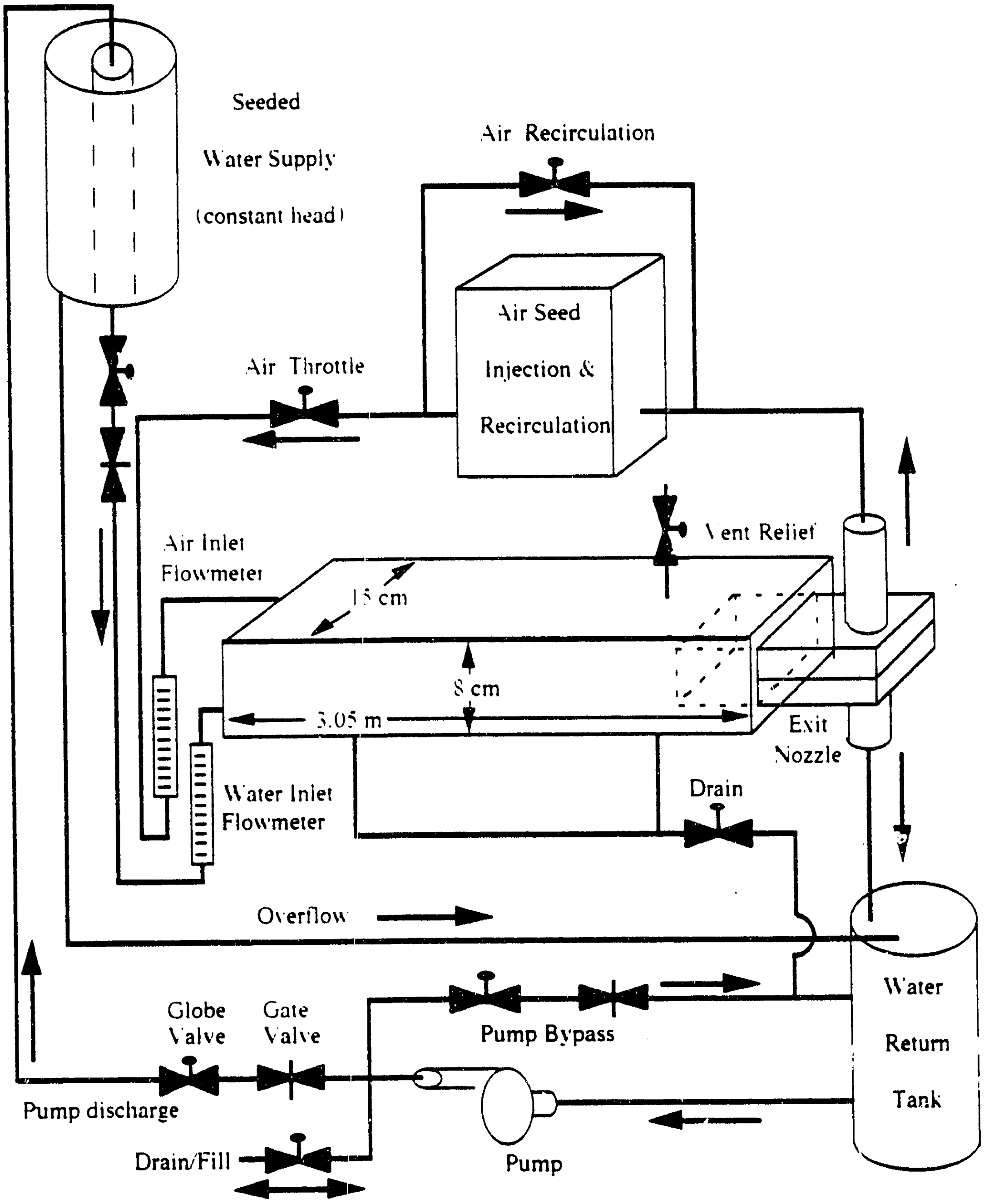

Figure 26. PLV Stratified Flow Test Facility

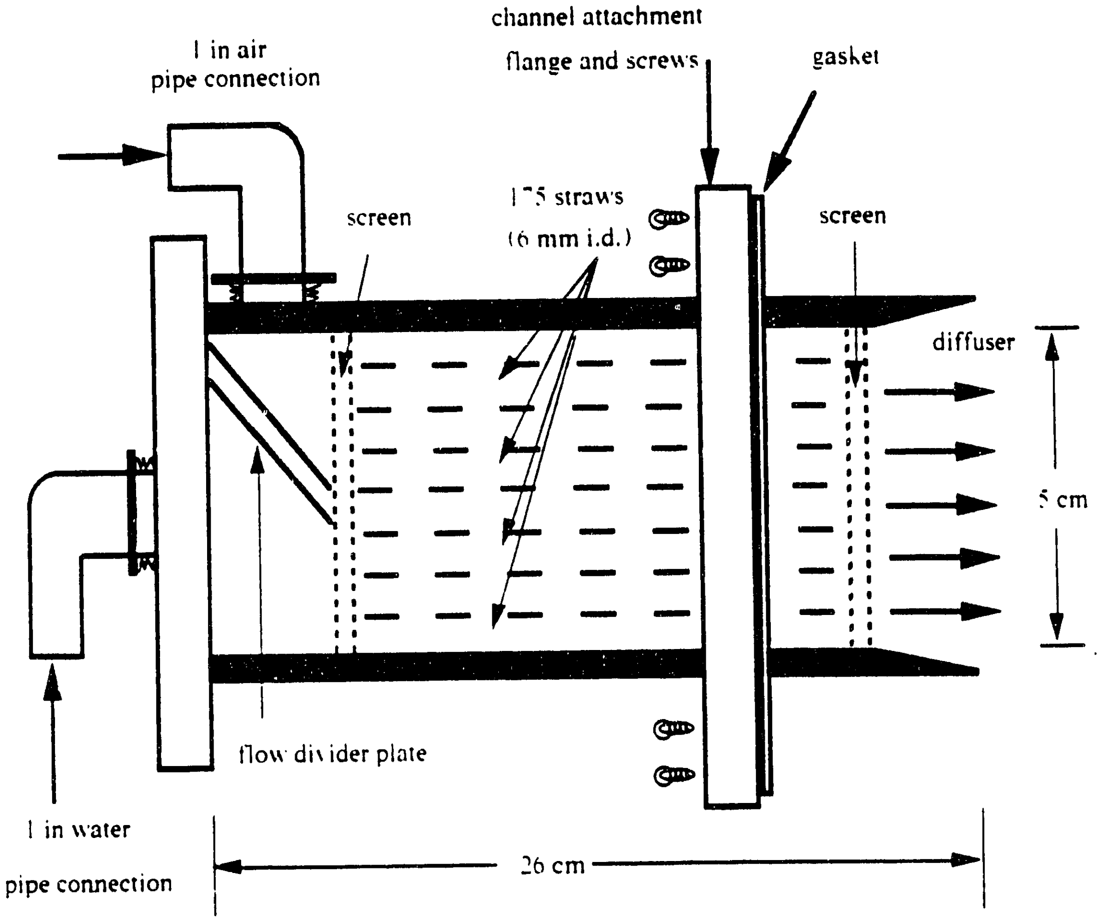

Figure 27. Nozzle Design for the PLV Stratified Flow Test Channel

Water, seeded with 6 μm diameter, polystyrene, particle tracers (1.02 specific gravity), is metered to one end of the channel from a constant pressure source provided by a constant head supply tank (55 gal capacity) located 2.36 m above the channel. This provides a constant 2.5 p.s.i. water head to the channel inlet. The constant head supply tank consists of an inner pipe surrounded by an outer annulus. A 30 gpm pump ensures that the inner pipe inside the supply tank remains full, maintaining the constant head, with the overflow into the outer annulus returning to the water return tank (90 gal capacity). The water pump also ensures a uniform seed distribution in the water by recirculation through the pump bypass. A garden hose with quick disconnect allows filling of the system from laboratory demineralized (D.I.) water supply or system drainage (expedited by the 30 gpm pump) through a valve connected to building drains. A flow control station, encompassing valves, pump controls, and air and water rotameters, was built. The gate and globe valves were used to shut off and throttle the flow, respectively.

Air, seeded with air-filled particles or "microballoons", (vinylidene chloride, 30 μm diameter, 0.036 g/ml density) can be metered to either end of the channel to allow cocurrent or counter-current flow experiments. The counter-current flow experiment is setup by reversing the air hoses at the channel inlet and outlet. A modified wet/dry shop vacuum cleaner (2 H.P., 10 gal capacity) was used to obtain both uniform seed distribution and provide the closed-loop air source. The modification consisted of attaching tees to suction and discharge ports of the vacuum cleaner to allow installation of a air bypass line. This produced a high internal recirculation which ensured seed mixing, and, at the same time, provided a low pressure bleed air flow to the channel.

The vacuum filter and the float ball and ball cage were removed. All water and air lines were constructed using 1 in i.d. clear plastic tygon tubing.

A typical experiment usually is setup by first checking that all valves are closed, and then filling the water return tank approximately three-fourths full from the D.I. water source through the drain/fill water valve. The water pump is started and the pump bypass opened to begin recirculation. The pump discharge is opened to send water to the water supply tank, and the inner pipe is checked full by checking for flowing water in the overflow line. Water flowrate to the channel is then controlled using the water rotameter and channel water inlet throttle valve. A water seed mixture is added through a nozzle connection after the water is flowing steadily through the channel. The seed is prepared by ultrasonic mixing of 1 gm of seed with 500 ml of D.I. water. Usually, half to all of the mix is added, depending upon desired seed concentration. The air flow setup begins with 1-2 cups of dry seed placed inside the vacuum cleaner. The vacuum is started with the air throttle closed and the air recirculation valve fully open. Air flow to the channel begins by fully opening the air throttle for a minute or two, and then throttling to the desired flowrate.

The laser used is a Spectra-Physics DCR-3G Nd:YAG high energy, pulsed laser. It has been calibrated at a peak throughput energy of 1.0 J/pulse for its primary wavelength of 1064 nm (infrared). The pulse width is 8 ns with a variable pulse frequency of 1-24 pulses/sec. The laser can also operate in a "double-pulse" mode, splitting the energy of a single pulse into two pulses with a variable separation from 50 to 350 microseconds. Due to a large absorptivity of water for infrared light, a frequency doubling crystal is used to produce 532 nm light (green), reducing the maximum energy to approximately 0.5 J/pulse.

The lenses and mirror setup is illustrated in Fig. 28. The 7 mm, circular, Gaussian-distributed, light pulse is directed to the point of interest (center of the channel, 96 cm from water exit nozzle) by a series of four mirrors, and shaped into a 1 mm thick, 76 mm wide, sheet of light with a series of three cylindrical lenses. All mirrors are 5 cm in diameter, with high-energy coatings. The first mirror in the beam path is a harmonic beam splitter, designed to pass the infrared to a beam stop, and reflect the green light to the lens setup. Lens dimensions are gives as length, width, and thickness; followed by a focal length f. Lens #1 is 50.8 x 50.8 x 6.17 mm, with f = 200 mm, lens #2 is 60.0 x 50.0 x 8.89 mm, with f = 100 mm, and lens #3 is 50.8 x 25.4 x 12.79 mm, with f = 25.4 mm. The sheet is produced by first removing all lenses from the beam path, and centering the beam in all mirrors to the view point of interest. Mark this reference point on a sheet of paper. It is best to keep beam power low and to use black paper for the beam target to reduce reflection. The first lens is inserted into the beam and centered; centering is insured when the distorted beam is returned to the reference point. Care must be taken to prevent damaging the optical components with the high energy laser pulse. This can be prevented by ensuring that the focal point of the first lens does not reside on the mirror, and all components are clean. This process is repeated with the second lens, and then the third lens. The final adjustment is made by fine-tuning the distance between lens #2 and lens #3, until the desired light sheet thickness is obtained.

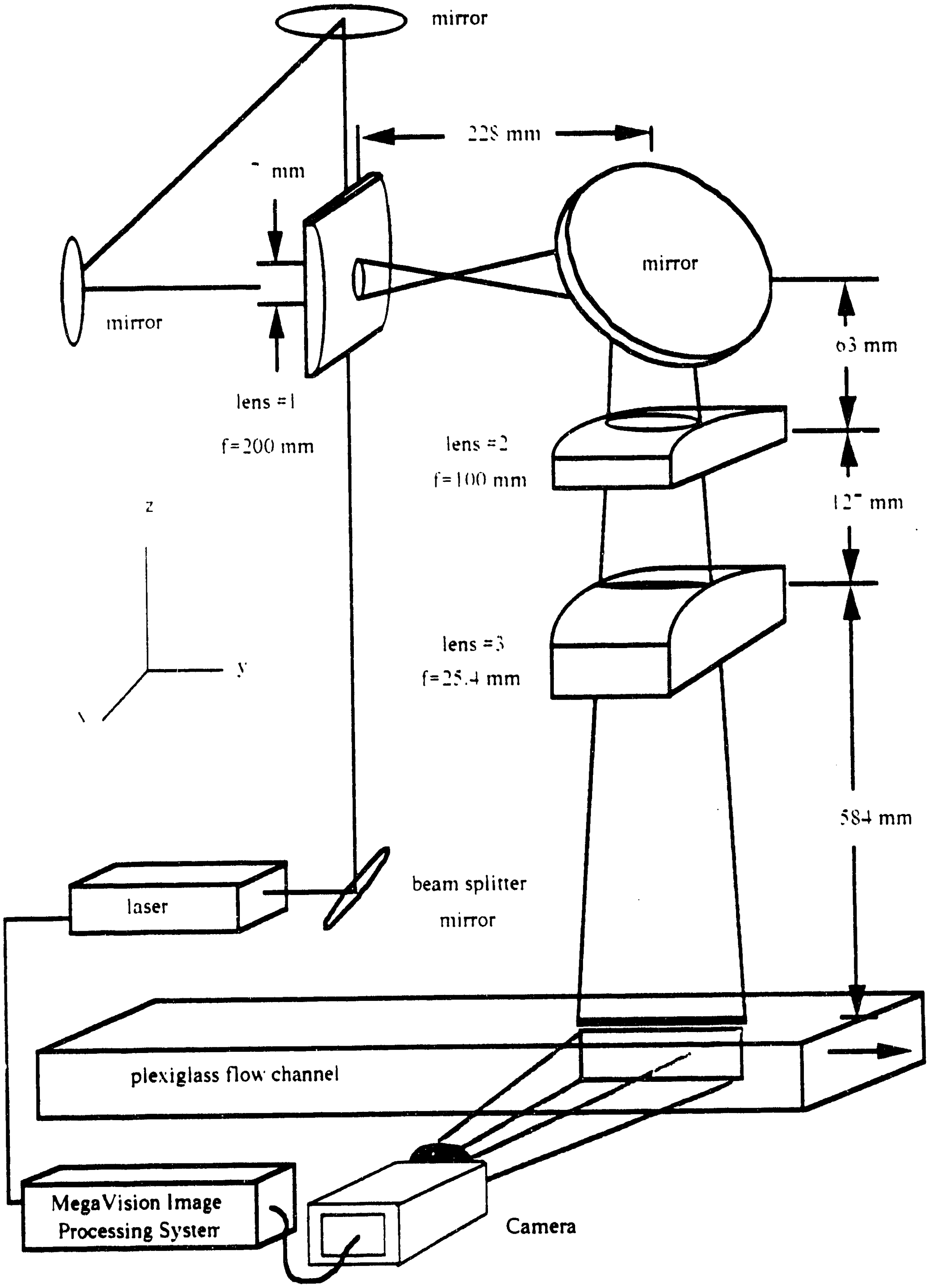

Figure 28. Lens Arrangement for Thin Sheet Production

The sheet is passed through the channel lid (normal to its surface) into the moving fluid. coplanar to the flow pathlines. at the camera's focal plane which is imaging the flow through the side of the channel. It is best to apply a nonreflective coating to all surfaces inside the channel near the beam path to reduce light scattering from surfaces. Flat black electrical tape was applied to the inside bottom. inside top (with a slot removed to allow the beam into the channel). and inside back surface (opposite to the camera) of the channel. A slot was also removed at the taped channel bottom surface. This was necessary because the energy of the sheet was concentrated enough to "burn off" tape particles. which the camera then imaged as seeds appearing to rise off the channel bottom due to the local heat production. This was a very interesting phenomena in which further study may be appropriate. Removing the slot allowed the sheet to pass through the channel bottom. finally striking a flat black painted board. which supported the channel.

The pulsed laser light is scattered from the seed. and the camera directly digitizes images ot the flow tracers. A short time later. a second laser pulse is introduced. and another flow image is required. Velocity calculations are then performed after determining particle positions. matching appropriate particles in the consecutive frames. and dividing by the time increment between recordings.

IV.4 Light Scattering by Small Particles

It is of interest to the PLV experimenter to know the scattering properties of various particles in relation to the particle image mode of PLV operations. The following theory and conclusions (Adrian and Yao, 1985) summarizes the scattering properties based on monodispersed particle populations and Mie's scattering theory for scattering from spherical particles.

The image plane intensity distribution can be determined by the following equations. The intensity of the light in the image plane $\mathbf{X}(X, Y)$ of the recording camera at time t is $\mathcal{J}(X, t)$ W/m^2, and the exposure is given by:

$$\mathcal{E}(\mathbf{X}) = \int \mathcal{J}(\mathbf{X}, t)dt \tag{34}$$

The intensity of the image of the ith particle, located at the point $x_i(t)$ in the fluid, is:

$$\mathcal{J}_i(t) = I_o(x_i, t)\mathcal{J}_o(\mathbf{X} - Mx_i) \tag{35}$$

with $I_o(x_i, t)$ = intensity of illuminating beam, and $\mathcal{J}_o(\mathbf{X} - Mx_i)$ = 2-D intensity distribution of the blurred particle image per unit illumination intensity. The function $\mathcal{J}_o$, also considered the transmissivity per unit incident intensity, normally has a maximum at the zero value of its argument. The expression for $\mathcal{J}_o$ states that a particle at x_i is mapped into an image at $\mathbf{X} = -Mx_i$, reflecting the image inversion produced by the lens of a camera having magnification M.

$\mathcal{J}_o$ is given by the magnitude squared of the convolution of the point response function of the camera lens system and the geometric image of the particle. The details of these functions determine the precise shape and diameter of the blurred image. The diameter $\mathcal{J}_o$ can be estimated from the nominal image diameter, d_e:

$$d_e = (M^2 d_p^2 + d_s^2)^{1/2} \tag{36}$$

$$d_s = 2.44(M + 1)f\#\lambda \tag{37}$$

where d_s is the diameter of the point response function of a diffraction-limited lens measured at the first dark ring of the Airy disk intensity distribution. d_e is an approximate quadrature representing the combined effects of magnification and image blurring in determining the final diameter of the image. d_p is the particle diameter. $f\#$ is the focal length of the lens divided by the aperture diameter. and λ is the light wavelength.

The mean intensity of the ith particle image. averaged over an area of diameter d_e. is defined to be:

$$\overline{\mathcal{J}_i} = \frac{4}{\pi d_e^2}\int\int \mathcal{J}_i dXdY \tag{38}$$

The integral of equation (38) is the energy flux crossing the image plane. and must be equal to the energy flux through the camera lens of the light scattered by the ith particle. given by:

$$\int\int \mathcal{J}_i dXdY = \int\int I_o(x_i,t)\mathcal{J}_o dXdY = \int_\Omega I_o(x_i,t)\frac{\sigma_i^2}{k^2}d\Omega \tag{39}$$

with σ_i = Mie scattering coefficient. k = wave number $(=\frac{2\pi}{\lambda})$. and Ω = solid angle subtended by camera lens. Thus:

$$\overline{\mathcal{J}_i}(t) = \frac{4}{\pi k^2 d_e^2} I_o(x_i,t)\int_\Omega \sigma_i^2 d\Omega \tag{40}$$

The image plane intensity distribution is found by integrating equation (40) over the image space.

Once the image plane intensity distribution is determined, the mean exposure of the imaging medium. the scattering power. and the particle requirements can be found.

Assuming the illuminating intensity I_o of a pulse with total energy W is uniform in rectangular dimensions of length Δy, thickness Δz, over a pulse duration δt, then

$$I_o = \frac{W}{\Delta y \Delta z \delta t} \tag{41}$$

and

$$W = \int I_o dy dz dt \tag{42}$$

Therefore, the equation for the mean exposure over the image plane is:

$$\bar{\varepsilon} = \frac{4}{\pi k^2 d_e^2} \frac{W}{\Delta y \Delta z} \int_\Omega \sigma^2 d\Omega \tag{43}$$

Thus, the mean exposure of a single particle image depends on three factors: illuminating intensity ($\frac{W}{\Delta y \Delta z}$), scattering power ($\int \sigma^2 d\Omega$), and image energy concentration (d_e^{-2}).

Adrian and Yao (1985) investigated these parameters as applicable to particle image PLV; a summary of their findings follows. The largest effect on mean exposure is due to changes in diameter and refractive index of the scattering particle, and changes in the refractive index of the fluid. Scattering from particles in water is significantly weaker in water than from in air. In the Rayleigh scattering regime ($d_p \ll \lambda$), scattering power is proportional to d_p^4. For ($d_p \gg \lambda$), scattering power is proportional to d_p^2, and d_e is proportional to d_p. There is an intermediate range between these limits (particles sizes from 1 to 10 μm for typical PLV experiments) where d_e is independent of d_p, the image diameter is dominated by diffraction from the photographic lens and controlled by the $f\#$ of the camera lens. The optimum particle size is a compromise between two opposing trends; the first being a large particle is desired because it is easily detected, and the second being a small particle is desired because the accuracy of velocity measurements and the spatial resolution increases with decreasing particle size. They suggest particle sizes in the 5-10 μm range are appropriate for most particle image PLV experiments.

The particles used in the stratified flow PLV experiment were in the range $d_p \gg \lambda$. This means that the mean image intensity approaches a constant, independent of the particle diameter. The air and water seed particles both showed image diameters greater than particle diameters. The intensity of the images of the air particles were greater than the water particles, due to the difference in refractive index of the two fluids. This suggests that a smaller diameter air seed can be used. However, for other reasons (availability, seed injection method, and personnel safety), the 30 μm diameter particle was used.

IV.5 Stratified Flow Data Acquisition

Seeded water was introduced into one end of the channel at three flowrates: 0 (simulating a stagnant, half-filled open duct to the air flow), 1, and 2 gallons per minute (GPM). Cocurrent seeded air flow was also introduced at three flowrates: 5, 10, and 30 standard cubic feet per hour (SCFH).

Five problems were immediately evident. It became apparent that the exit nozzle screens and/or flow straighteners were preventing water flow at the air/water interface. This was probably due to surface tension. Water under the interface was moving as expected. To correct this, the exit flow nozzle was modified by removing the screens and straighteners, and inserting a dam. The dam (a strip of plastic half the height of a screen) insured an approximately constant interface height (38 mm), regardless of the water flowrate. Prior to dam placement, it was noted that interface height would increase with increasing water flowrate. After dam installation, water velocity profiles assumed the expected shape.

The second problem that occurred was that condensation would appear on the inside channel wall in the air region whenever the water was flowing. This reduced the laser light intensity entering the top of the channel, and also obscured the camera view of the air flow. The D.I. water is delivered warm to the lab, and the "fogging" was attributed to the difference between warm water and cool, air conditioned, laboratory air. It was believed that letting the water set for a few days would allow temperature equalization, preventing the problem. However, condensation still occurred. A simple solution was to warm the channel in the area of interest prior to running the system. A few minutes with a incandescent lamp or a hair dryer prevented fogging for many hours.

The third and fourth problems, somewhat serendipitously, had a common solution. The air seed concentration would quickly decrease, coating all inside surfaces. Besides the obvious problem of losing tracer material, it would also obscure the camera view after a few runs. It is believed that the air seed or the channel acquires a static charge while air is recirculating. The use of an acryclic cleaner, polish, and "static remover" on the inside surfaces of the channel and vacuum container limited the seed deposition.

The fourth problem was that a large meniscus at the air/water/plexiglass interface would form, climbing from the water surface up the channel wall, obscuring the view of the air near the water surface. A small, inverted meniscus could be formed by careful filling of the channel with water, providing a clear view. However, the surface was unstable, and the meniscus would eventually "fall", especially if the system was bumped or shocked. It was believed that some material could be applied to the plexiglass surface to change its surface tension, and it was a surprise to learn that the plexiglass cleaner was that material.

The last problem was that the air recirculating inside the vacuum cleaner would become very warm after many hours of continuous operation, especially at low air flow bleeds. In fact, it became so hot that it destroyed a vacuum cleaner (a tygon hose collapsed, completely blocking recirculation, and the plastic bucket deformed and collapsed!). Thereafter, the vacuum cleaner was shut off after data was collected.

Nine experiments were performed, for a total of 96 flow images. Seven sets of images (with 10 consecutive images per set) were captured with a 1024 by 1024 pixel, 8-bit, Vidicon digital camera in conjunction with the MegaVision imaging system at a image rate of 6.66 frames per second (150 ms between laser pulses). These sets were named 0w5a (0 GPM water flow, 5 SCFH air flow), 0w10a, 1w5a, 1w5as (a second set with the same conditions), 1w10a, 2w5a, and 2w10a. Two set of images (with 13 consecutive frames per set) were obtained with a 640 by 480 CCD Sony digital camera at an image rate of 18.94 frames per second (52.8 ms between laser pulses). The images were stored on a 4 MByte EPIX frame grabber board. These sets were labeled 2w10am and 2w30am.

Volumetric water and air flowrate information were obtained from their respective rotameters during each experiment, along with channel water and air flow temperature. Temperatures were recorded by inserting wire thermocouples into the flow by way of the upstream channel vent valve tap.

IV.6 Image Analysis

The tracking process needs tracer information from the digital images (tracer particle centroid and area) to calculate vector information. The MegaVision hardware and software is ideal for this purpose, since it performs 1024 x 1024 pipeline processing in real time, and allows interactive threshold and filter functions.

The basic image analysis sequence is discussed below. See Appendix B for detailed processing values and programs. The first step to process images obtained with the Vidicon MegaVision camera is to recall a stored (from PC hard drive or floppy disk) raw image into a memory board. A sharpen filter is applied to enhance the density gradient and clearly define the tracers from the background. This filter sharpens a picture by subtracting an 8 x 8 pixel averaged filter from an accumulated picture. A negative or inverse of the image (necessary for the following step) is then obtained. Then, an interactive median filter is used to further define and separate the tracers from the background, meniscus, reflection from channel sides, etc. This filter uses a basic kernel and size (i.e. 17 pixel diameter circle), and then the basic kernel can be manipulated to obtain the desired results. An image is then obtained, with a 255 gray level (white) background and 0 gray level (black) particles. Again, an inverse is performed, to get a "cleaned" picture of white particles on a black background which is necessary for the final processing. This final processing provides the tracer information for the tracking programs. It uses the "cleaned" picture as a "mask" which is overlaid on the original picture. Any connected pixels in the original 8-bit image that appear under the mask are determined to be particles, and various parameters, such as x-centroid, y-centroid, area, average gray level, shape function, etc., can be calculated. The output data can be manipulated on the monitor (for example, particles can be segregated by size or gray level) or the output stored in a file.

The images obtained with the CCD camera and EPIX frame grabbers are analyzed similarly, with one exception. They are loaded into a clean memory board in a certain position, flipped about the x and y axis, and then magnified by two. This is done to make them appear similar to the MegaVision images. The reason is twofold. First, the tracking programs and final vector presentation plots are set up for 1024 by 1024 resolution images. Since the CCD camera has a 640 by 480 resolution, these programs would perform well, but the output would appear small. A simple modification to the programs could remedy this. The most important reason to magnify by two is that the interactive image threshold and filter operations are difficult to perform with the smaller images on the high resolution monitor, and it is crucial that this step is performed correctly. The twice magnified image now has a 1280 by 960 resolution, so that some of the x-dimension data is removed (approximately 128 of the original picture's pixels). For some images this may not be acceptable, however, for the channel pictures taken with the CCD camera, little useful data was lost in the analysis.

A overlay of the ten processed images (binary and inversed) for the channel experiment 2w30am is given in Fig. 29, clearly showing the air seed at top, the interface, and seeded water flow at bottom.

The final processing of the image data occurs after the data files are transferred to the engineering mainframe computers (VAX's), using the Ethernet line connection to the laboratory PC with FTP (File Transfer Protocol) software. A program (Appendix B) takes the original data, splits it into separate air and water data files (to be discussed in a later section), checks for errors, and performs coordinate transforms, if desired. The MegaVision camera takes data at a slight tilt, probably due to a tube misalignment, and it is desired to rotate the data to the horizontal for esthetic reasons.

IV.7 Vector Tracking

It has become evident that some means to analyze images, process and track the sequential data, and produce visual and numerical output, both quickly and automatically, must be devised. We can now take 26 images (EPIX) or 10 images (MegaVision) within about 1 sec. The data quantity is enormous ($\approx$ 10MByte), and the process can be repeated in a few minutes, limited only by storage limits. The problem is that we can now take more data then we will ever have the time to *manually* analyze. The driving force behind this work has been to get a handle on that beast (information overload, which appears in most fields of study), and process the data automatically as a set of frames vs. individual frames, to make the problem more tangible.

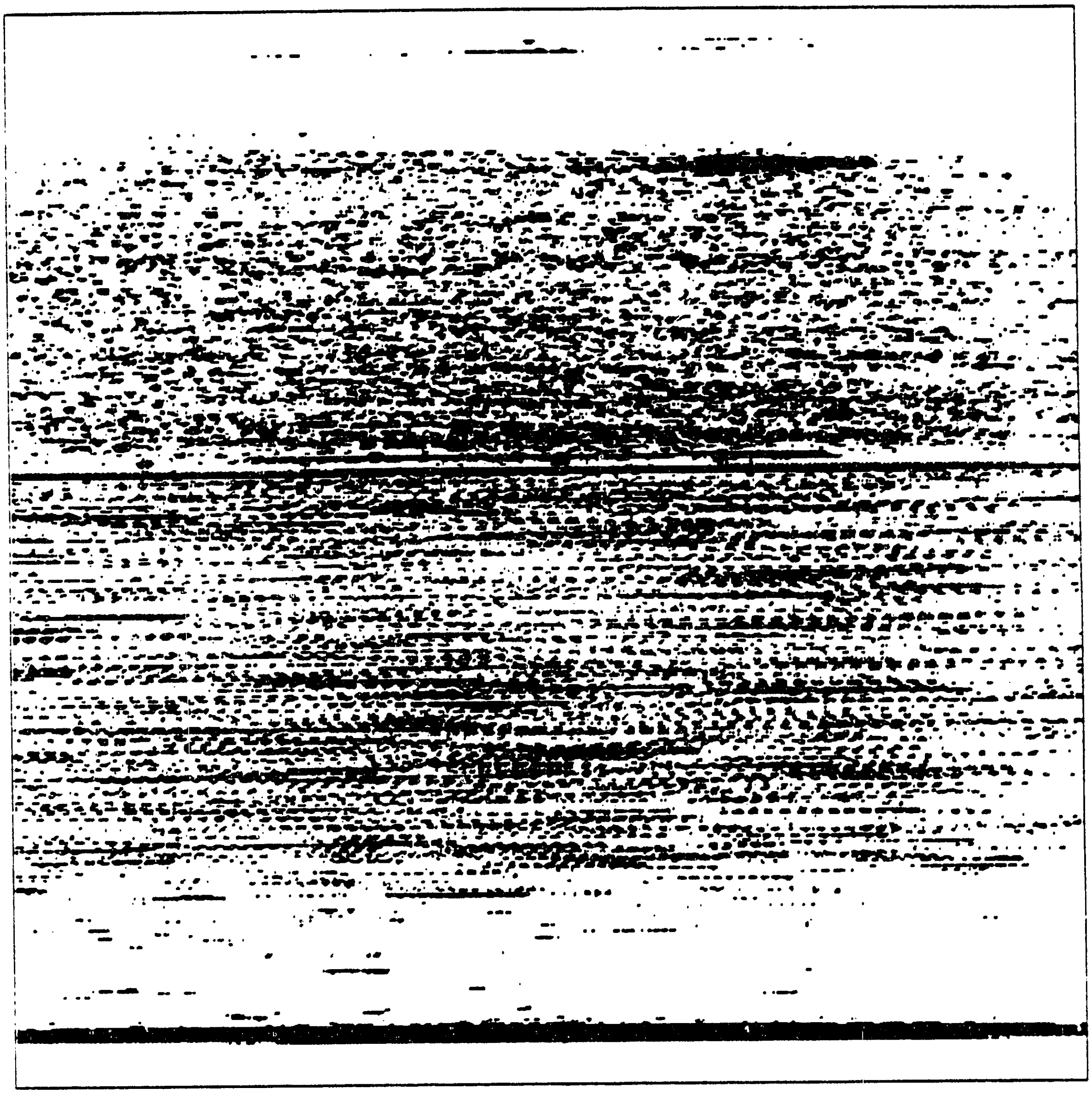

Flow direction: ————

Camera view: 94 x 94 mm

Figure 29. Binary Inverse Overlay, Set 2w30am

The first step to process data as a set has already occurred. The program mentioned in the image analysis section has separated the air and water particles (based on relative position to the known interface coordinates). The input requirements were the set name, number of files in the set, coordinates of air, interface, water, channel top or bottom, or coordinate transform, if relevant.

This data is tracked (air and water separately) by the cross-correlation tracking program (Appendix C). Again, the major input is the set name, set type (air or water), start and stop frames (for partial tracking), and the candidate and dynamic search region dimensions discussed in the tracking code chapter. The major output is a file with the best candidate vectors along with their respective correlation coefficients and pair confidence values. Each file (10 water and 10 air files for a set of 10 images) will also have a set average and standard deviation cross-correlation coefficient and pair confidence value. The program was setup on the CRAY-YMP, with typical run times varying from a few hundred cpu seconds to as much as an hour, for those images with large seed concentrations. Appendix A includes a cross-correlation data sheet for each set.

A method, discussed in the code testing chapter, has been devised to automatically "clean" vectors. This method has been further enhanced to clean a set of stratified flow vectors obtained with the tracking code. The program, AutoCleanSet (Appendix D), reads an input file with the name of the set, start and stop frames (for partial cleaning), air and water percent difference (PD) cleaning values, and boundary conditions (BC) (location and number of points for top, interface, and channel bottom, if desired).

The autocleaning is best described through example. Assume that the three BC locations have been identified. The complete uncleaned water vector file is input. The best vectors are identified (those with correlation coefficients greater than the frame average plus frame standard deviation and pair confidence values greater than frame standard deviation). This usually is about 10-20% of the total. The channel bottom zero velocity or "no-slip" BC is imposed with the addition of 32 high quality (perfect vector) zero velocity vectors at the bottom location. The Hardy-Multiquadratic equations (equations (16-18)) are used to make a full-field water flow equation. The original file is checked against the equation. Think of the PD value as a circle of some diameter centered at the arrowhead of a vector in the flow equation. For example, a 10% PD clean value would be a circle of 1 pixel radius centered at the tip of a 10 pixel long vector. If any vectors fall within the PD value, they are added to the "cleaned" file, and the process reiterates until no new vectors (or some percentage, currently set to 2%) is added. The water file is now cleaned. The water equation is extrapolated to the interface (usually a few pixels above a water vector), and 128 interface velocity BC vectors determined. It was determined the somewhat large number (128) was needed to smooth the air velocity gradient at the interface, giving more accurate shear stress results. The interface BC vectors are added to the original air file, imposing the BC that air and water velocities must be equal at the interface. The channel top "no slip" BC is added (32 vectors), and the air file cleaned. The output consisted of a separate, cleaned, air and water vector file and full-field flow equation for each frame pair (i.e. frame 1-2, frame 2-3,...) of the set.

A program was written to plot as a set the final results of the automatic cleaning process (Appendix G). Figure 30 shows the cleaned air and water vectors from frame 12-13 of set 2w30am. These pictures simulate a view from the 1024 x 1024 camera, and the size of the view frame is given. Since the channel top and bottom were visible in the view plane, they are represented, along with a line depicting the interface. The vectors are shown without magnification, and a vector scale (used for both air air and water vectors) is provided. Velocity and shear profiles along the vertical y-axis (from data taken at camera centerline, x=512 pixels) are shown. The profiles are multiplied by a factor determined so that the maximum width of any profile in a set does not exceed 200 pixels. These profiles are not draw to scale. The purpose of the profiles is to allow the experimenter to quickly perform a visual analysis of the data. Velocity profiles are reviewed to check for steady-state, fully-developed flow, and to insure the boundary conditions used in the analysis were correctly applied. The shear profile is studied near the air/water interface: for ideal flow conditions should set the boundary condition that the air shear will equal the water shear at the interface. The making of these profiles is discussed in the shear results section.

The necessity to separate air and water was determined by the BC (which was not imposed) that the air and water interfacial shear stress should be equal. Shear is equal to viscosity times velocity gradient. If viscosity is unequal at the interface (and, in this experiment, it is by two orders of magnitude due to the difference in fluid properties), then, this implies that the velocity gradients of the air and the water at the interface be discontinuous. It was first attempted to process air and water files together, but,

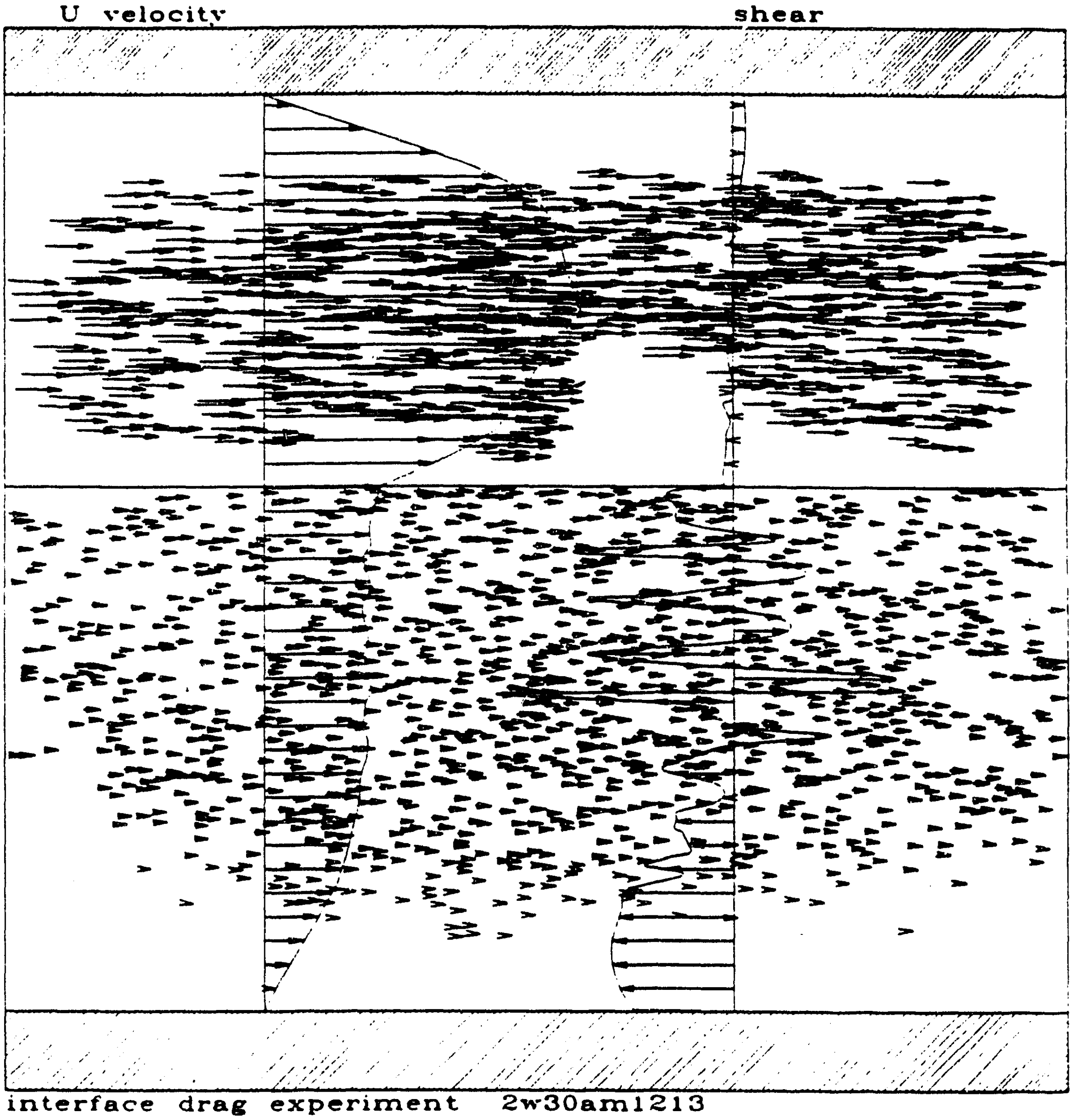

Camera view: 94 x 94 mm
Vector scale: — 50 mm/s
Velocity and shear profiles not to scale

Figure 30. Velocity and Shear, Set 2w30am, Frame 12-13

the Hardy equation which resulted provided a smooth velocity interpolation at the interface. This was because few air particles were imaged near the interface, hence, few air vectors were determined by the tracking program. The smooth interpolation was fine for the interface velocity BC, but completely unsatisfactory for the interfacial shear.

IV.8 Interface Shear Calculations and Results

Flow parameters, such as velocity, vorticity, and shear, can be calculated at any point in the flow field once the final flow-field equation is known. The shear theory, equation (20) and equation (21), is based on knowing average (bulk) air velocity and interface velocity in the flow field.

A program was written (Appendix E) to take the final air and water flow-field velocity equations, differentiate them, and produce profile data files of velocity, vorticity, and shear. Shear stress is based on temperature dependent air and water viscosity, which needs to be determined. Temperature dependent viscosity (in poise) of air can be found using Sunderland's (Anderson, 1984) correlation, which is based on air viscosity at STP conditions ($\mu_o = 1.7894 \times 10^{-04}$ at $T_o = 288.16\ K\ \frac{g}{cm\ sec}$)

$$\mu = 1.7894 \times 10^{-04}\left(\frac{T}{T_o}\right)^{1.5}\left(\frac{T_o - 110}{T - 110}\right)\ \frac{g}{cm\ sec} \tag{44}$$

Temperature dependent viscosity (in poise) of water from 0-100 C is found using CRC tables (note that $\mu_{20} = 1.0019414 \times 10^{-02}\ \frac{g}{cm\ sec}$ at $T = 20\ C$). For water temperature less than 20 C,

$$\mu = \frac{1301.0}{998.333 + 8.1855(T - 20) + 0.00585(T - 20)^2} - 3.30233\ \frac{g}{cm\ sec} \tag{45}$$

For water temperature greater than 20 C,

$$\mu = \mu_{20} \cdot 10^{\frac{1.3272(20.0-T)-0.001053(T-20)^2}{T+105.0}} \quad \frac{g}{cm\ sec} \tag{46}$$

The set profiling program uses a set name, start and stop frames, laser pulse separation time, a flag to determine the appropriate imaging system (MegaVision or EPIX) along with the image analysis magnification factor, the camera view area, temperature of air and water flow, the x position where the vertical profiles will be determined, and the channel top, interface, and bottom locations. It will then determine velocity, velocity gradient, vorticity, and shear at requested locations.

Test section average air velocity and interface velocity for frames 12-13 of set 2w30am are shown in Fig. 31 and Fig. 32. Since the data (especially the air) does not encompass the entire camera view area, data is only used for profiling and calculational purposes in the region over the average x position plus or minus the standard deviation of all the cleaned air vectors. The channel average air velocity was determined by sampling every 25th y pixel position between the interface and the channel top, and every 25th x position (typically between the 200 to 800 pixel position), or approximately 500 points. Figure 31 presents data showing a small fluctuation in average velocity of the air over a small section of the channel. The average of the air velocity data (denoted by exp average) is the parameter U_g, used in equation (20). The large standard deviation from the average is due to the parabolic nature of the air flow field.

The experimental interface velocity and air shear were determined at every pixel along the interface, over the same width as the air velocity calculation. The average

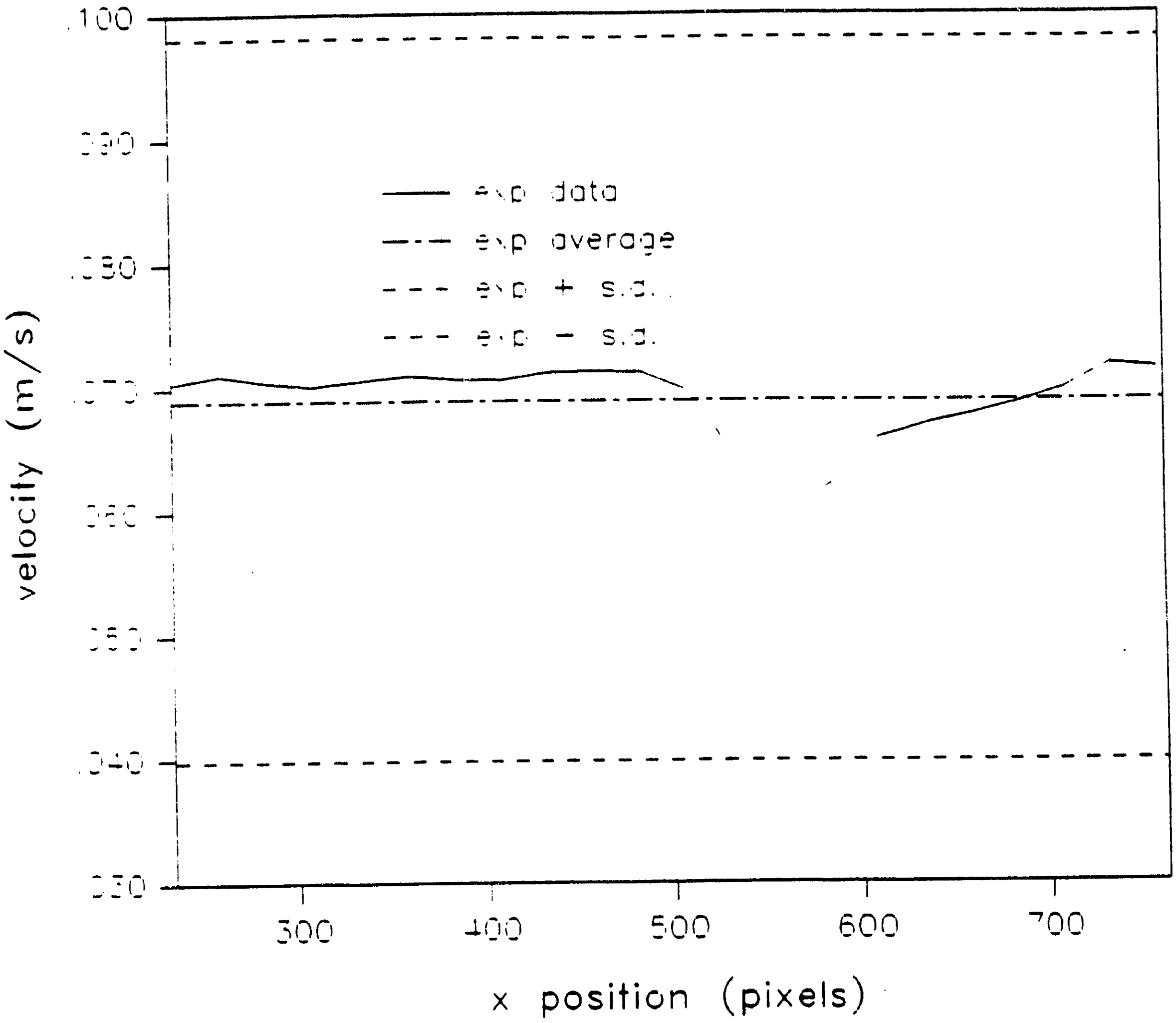

Figure 31. Average Air Velocity, Set 2w30am, Frame 12-13

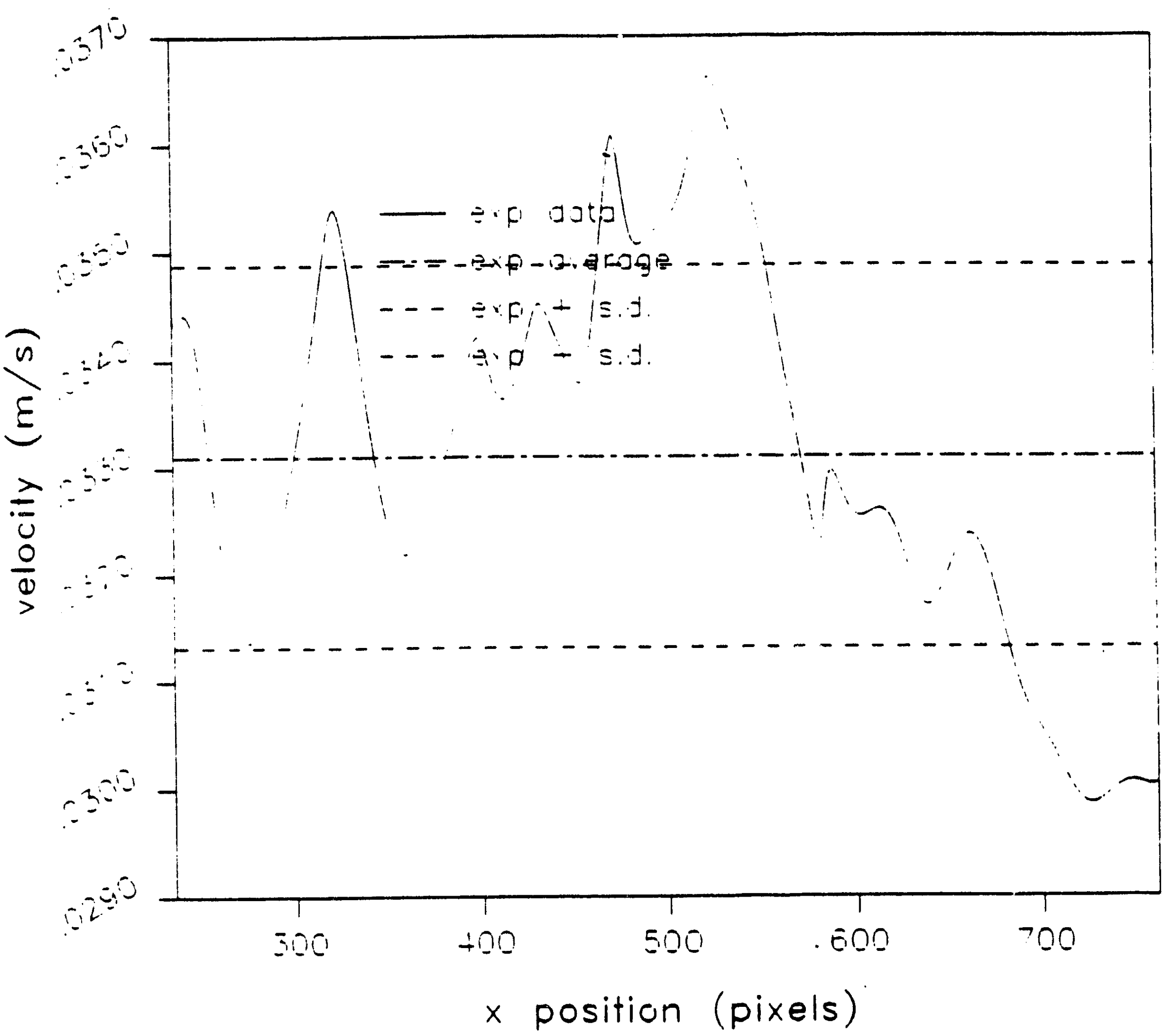

Figure 32. Interface Velocity. Set 2w30am. Frame 12-13

of the interface velocity data, shown in Fig. 32 (denoted by exp average), is the parameter U_i, used in equation (20). Air shear stress was determined using the differentiated Hardy velocity equation (between the interface and one pixel above the interface to determine the velocity gradient), and the temperature corrected air viscosity value. The interface shear for frames 12-13 of set 2w30am is shown in Fig. 33. Each figure also presents the average value, the average plus the standard deviation, and the average minus the standard deviation. In addition, Fig. 33 also presents the value of the theoretical interfacial shear stress based on experimental conditions, as calculated using equation (29).

Another program (Appendix F) was written to take the data from the profiling program, and compute the theoretical shear. Air density, used in equation (20) and equation (21), was temperature corrected using the ideal gas law

$$\rho_g = \rho_o\left(\frac{T_o}{T}\right) \tag{47}$$

where $\rho_o = 1.225\ kg\ m^3$ at $288.16\ K$. The output was a plot comparing the theory to the experimental data (with standard deviation), along with a linear least-square fit line through the theory points for the set. Figure 34 shows this plot with one data point removed (from frame 5-6, where the profile showed the the air flowing backward, see complete data in Appendix A). A file containing experimental velocity and shear data for the air and water flow, and theoretical shear calculations for each frame in the set, is shown Fig. 35. Other pertinent information for the experiment, such as camera view area and magnification, fluid properties and dimensions, and gas Reynolds number and interface fraction factor, is also presented in Fig. 35.

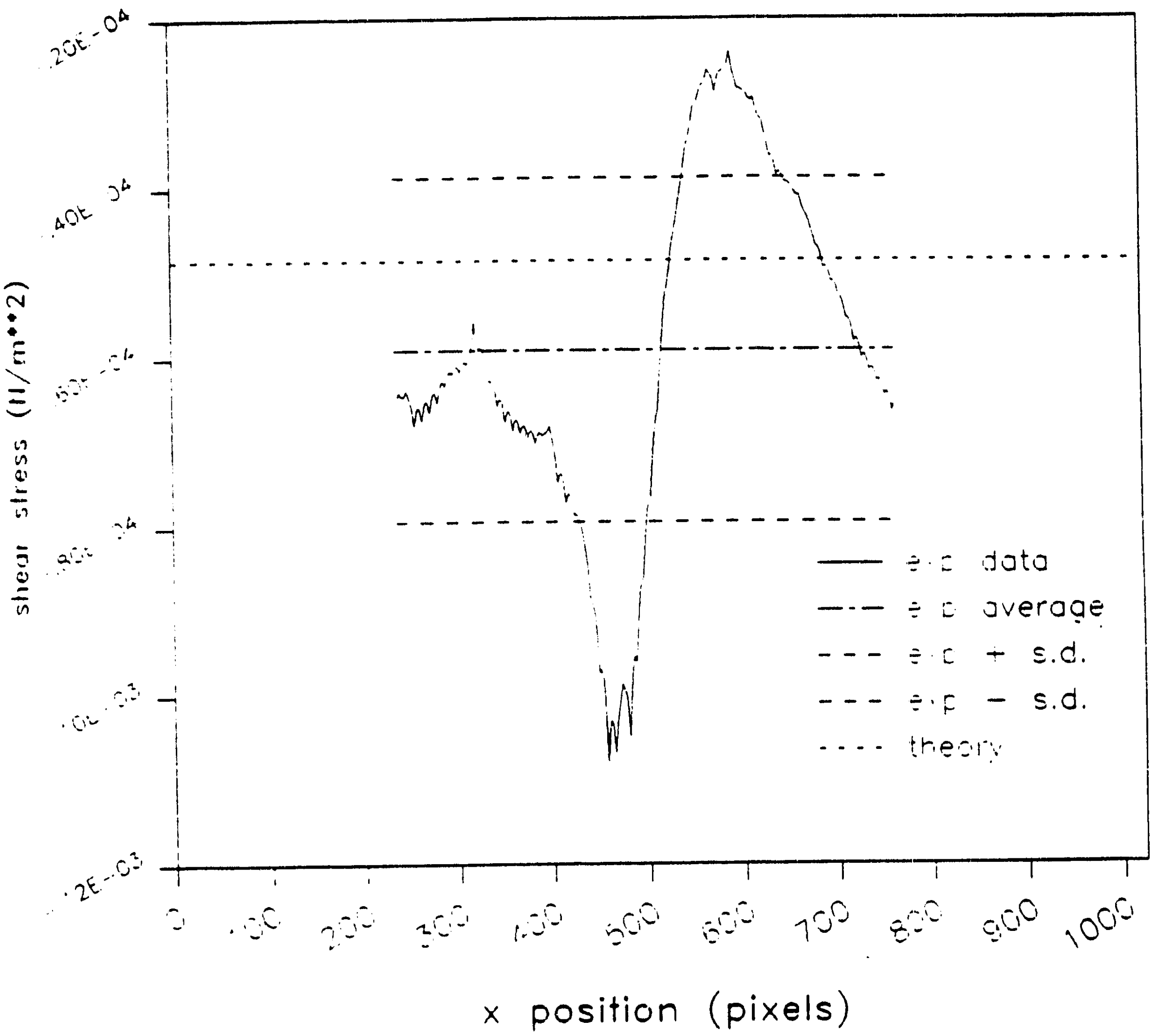

Figure 33. Interface Air Shear. Set 2w30am, Frame 12-13

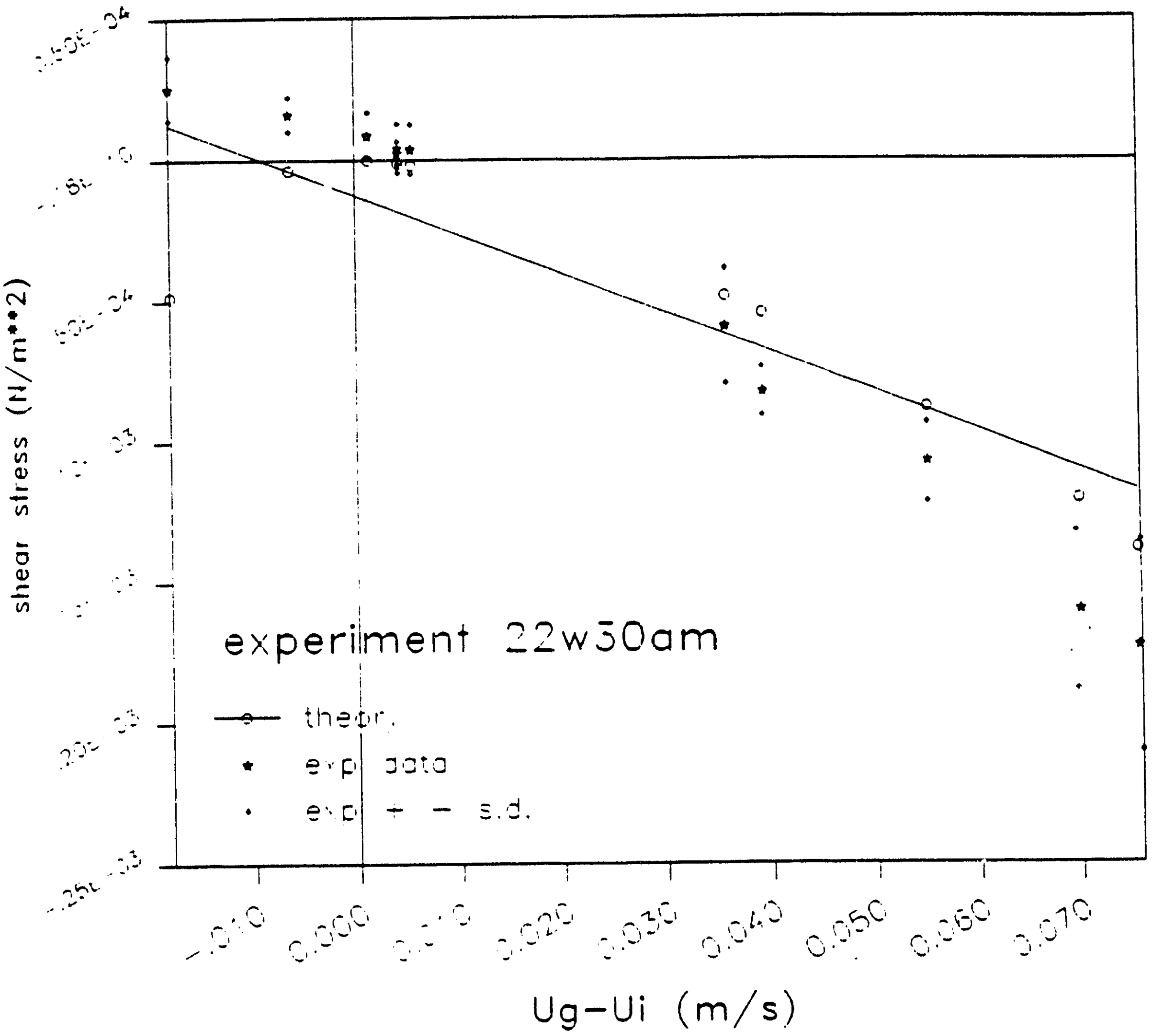

Figure 34. Shear Experiment vs. Theory Comparisons, Set 2w30am

```
Profile and Interfacial Shear Calculations for set: 2w30am
 959.0000                        TOP        of channel     (pixels)
 582.0000                        INTERFACE of channel     (pixels)
 76.00000                        BOTTOM     of channel     (pixels)
 3.696000                        Camera view height        (inches)
 2.000000                        Camera magnification factor
5.2800000E-02                    Laser pulse rep time         (sec)
 24.50000                        gas     temperature            (C)
 24.60000                        liquid temperature             (C)
 1.185943                        gas density             (kg/m**3)
1.8347882E-05                    gas viscosity             (kg/m-s)
1.5471131E-05                    gas kinematic viscosity (m**2/s)
 3.187500                        channel height            (inches)
 6.000000                        channel width             (inches)
3.4567226E-02                    gas height                     (m)
0.1524000                        gas width                      (m)
0.1524000                        interface width                (m)
0.2215344                        gas perimeter                  (m)
5.2680452E-03                    gas area                    (m**2)
5.6352608E-02                    gas hydraulic diameter         (m)
 539.9324            conversion factor from m/s to pixels/pulse

frame water U  interface U water shear air shear +/- st.dev.   air U
        m/s       m/s         N/m**2      N/m**2                  m/s
  1  2 0.258E-01  0.330E-01  -.348E-05  0.860E-05 0.812E-05  0.343E-01
  2  3 0.250E-01  0.346E-01  -.138E-03  -.822E-04 0.863E-05  0.739E-01
  3  4 0.252E-01  0.334E-01  -.198E-04  0.161E-04 0.605E-05  0.271E-01
  4  5 0.247E-01  0.323E-01  -.990E-04  -.173E-03 0.375E-04  0.108E+00
  5  6 0.243E-01  0.325E-01  -.729E-04  0.749E-04 0.180E-04  -.484E-02
  6  7 0.254E-01  0.349E-01  -.243E-04  -.107E-03 0.141E-04  0.900E-01
  7  8 0.245E-01  0.317E-01  -.351E-04  0.244E-05 0.398E-05  0.359E-01
  8  9 0.248E-01  0.322E-01  -.960E-04  0.376E-05 0.868E-05  0.377E-01
  9 10 0.259E-01  0.360E-01  -.729E-04  -.160E-03 0.282E-04  0.106E+00
 10 11 0.258E-01  0.351E-01  -.163E-03  0.254E-04 0.113E-04  0.172E-01
 11 12 0.252E-01  0.316E-01  0.776E-04  0.406E-05 0.863E-05  0.358E-01
 12 13 0.251E-01  0.331E-01  -.117E-03  -.591E-04 0.204E-04  0.689E-01

velocity (m/s) and shear (N/m**2) SET AVERAGES +/- STANDARD DEVIATION
average values along interface from (min,max)   (X =  212 -  777)
 0.252E-01 +/- 0.516E-03          U water     (bulk)
 0.334E-01 +/- 0.147E-02          U interface
 0.525E-01 +/- 0.361E-01          U air       (bulk)
 -.637E-04 +/- 0.666E-04          shear water (interface)
 -.372E-04 +/- 0.783E-04          shear air   (interface)

frame       Ug          Ui         Reg     fi    shear(thy)  shear(exp)
           m/s         m/s                        N/m**2      N/m**2
  1  2  0.343E-01  0.330E-01     125    0.128  -.128E-06   0.860E-05
  2  3  0.739E-01  0.346E-01     269    0.059  -.544E-04   -.822E-04
```

Figure 35. Profile and Interfacial Shear Calculations, Set 2w30am

```
 3  4  0.271E-01  0.334E-01   99   0.162  -.381E-05  0.161E-04
 4  5  0.108E+00  0.323E-01  393   0.041  -.138E-03  -.173E-03
 5  6  -.484E-02  0.325E-01   18  -0.908  0.750E-03  0.749E-04
 6  7  0.900E-01  0.349E-01  328   0.049  -.879E-04  -.107E-03
 7  8  0.359E-01  0.317E-01  131   0.122  -.128E-05  0.244E-05
 8  9  0.377E-01  0.322E-01  137   0.117  -.209E-05  0.376E-05
 9 10  0.106E+00  0.360E-01  386   0.041  -.120E-03  -.160E-03
10 11  0.172E-01  0.351E-01   63   0.255  -.485E-04  0.254E-04
11 12  0.358E-01  0.316E-01  130   0.123  -.128E-05  0.406E-05
12 13  0.689E-01  0.331E-01  251   0.064  -.485E-04  -.591E-04

Shear theory average +/- standard deviation 0.203E-04 +/- 0.235E-03
```

Figure 35. Continued

This process was repeated for the nine experiments. All data was processed and presented in Appendix A. For the purpose of comparison of theoretical shear to experimental shear, three sets were removed from the final results plot. Two sets, 2w5a and 2w10a, were suspect since they were obtained immediately prior to the discovery of the "melted" vacuum cleaner. Another set, 2w10am, was very unstable (average air velocity reversing direction drastically between frames). Of the six sets used in the final comparison plot, one other point (frame 2-3 of set 0w5a) was removed due to negative air flow. The six sets that were used were 0w5a, 0w10a, 1w5a, 1w5as, 1w10a, and 2w30am. The complete comparison of theoretical with experimental shear stress results, using 51 measurements, is presented in Fig. 36. This figure shows that theoretical and experimentally obtained interface shear results compare favorably.

It has been determined that two conditions can exist where theory cannot predict actual shear. If $U_g - U_i > 0$, and $U_g < 0$, than the theory will predict a sign error. It must be admitted that this condition rarely exists in most flows. This is the cause of the large difference between theory and experiment highlighted by the furthermost left point on Fig. 36.

The other condition which can easily exist in unstable flows, such as that caused by a pipe break, and will certainly cause problems for 1- or 2-dimensional codes, is the condition that flow near the interface is transient, and dissimilar from bulk flow. This condition of interface flow reversal is seen in many of the images of set 0W10A, an example is shown in Fig. 37. The experiment rightly determines a negative velocity gradient (implying positive shear) at the interface. However, since bulk air

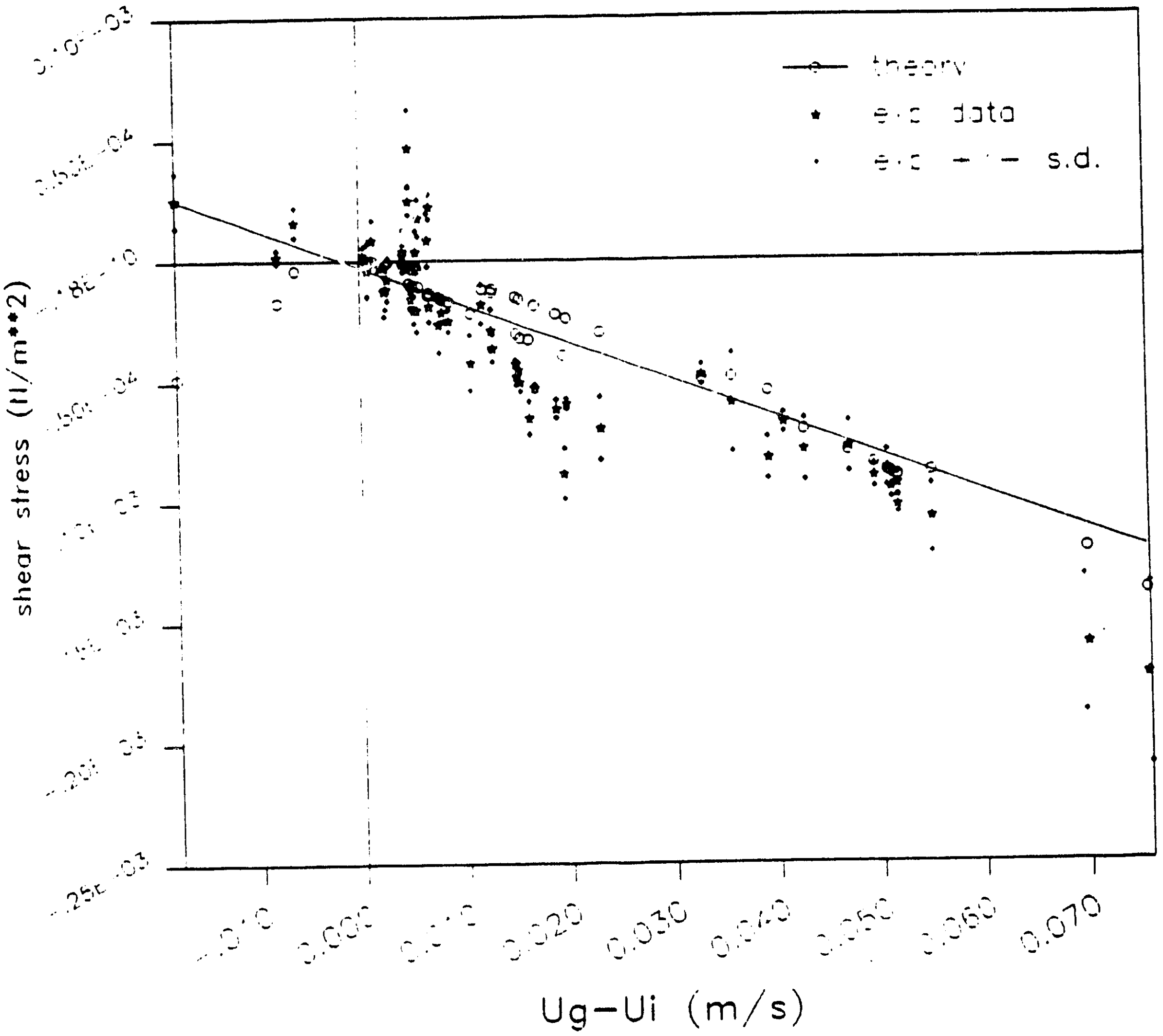

Figure 36. Shear Experiment vs. Theory Comparisons, All Sets

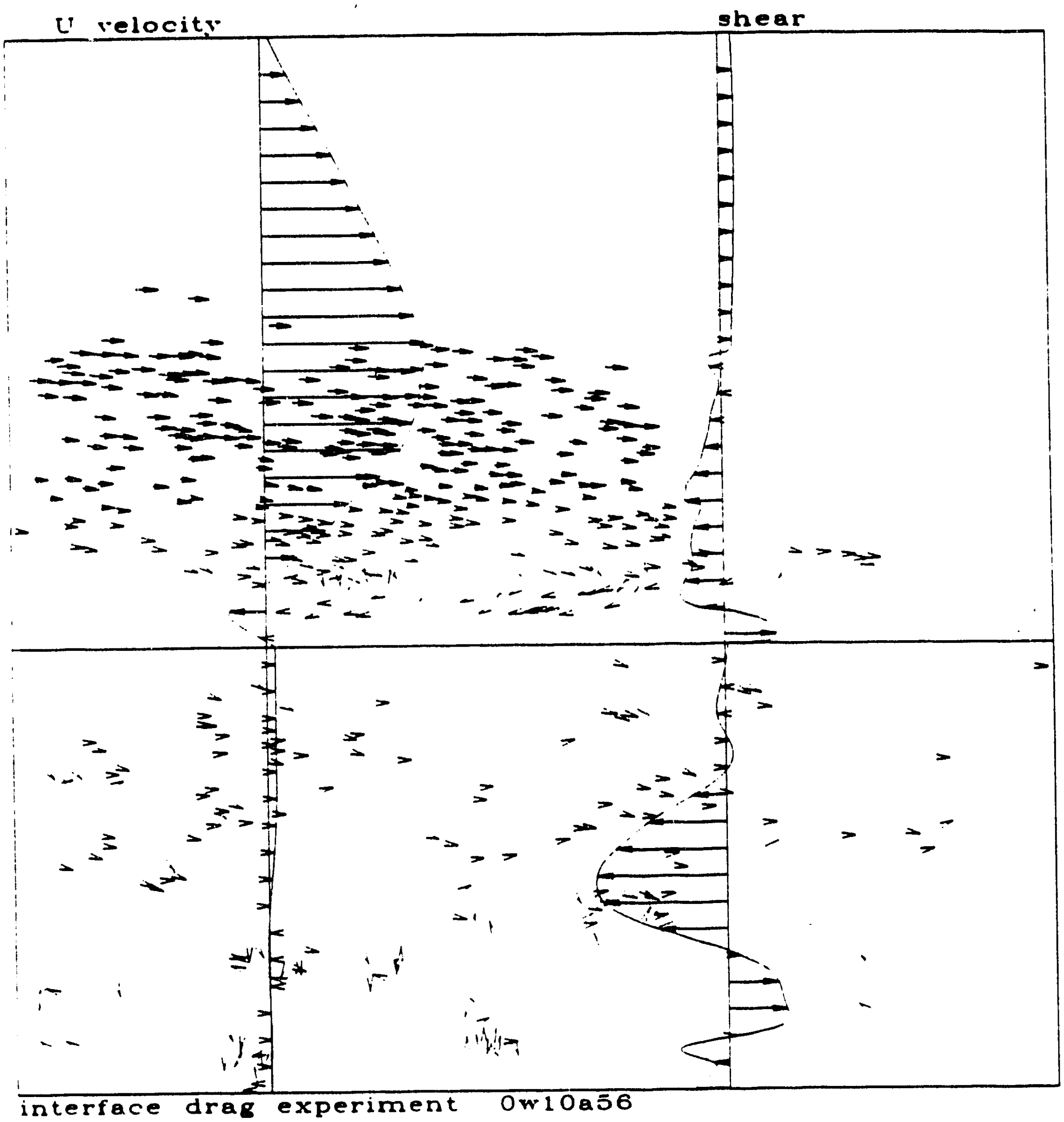

Camera view: 84 x 84 mm
Vector scale: — 20 mm/s
Velocity and shear profiles not to scale

Figure 37. Velocity and Shear. Set 0w10a. Frame 5-6

is positive, theory will predict negative shear. This phenomena causes the cluster of positive experiment shear vs. negative theoretical shear near $U_g - U_i = 0$, shown on Fig. 36.

CHAPTER V

CONCLUSION

Two methods have been described which perform tracking of seed particles in a in a two-phase flow field, using the Pulsed Laser Velocimetry method. One method tracks particles through four or more frames. The other method involves correlating groups of particles between two sequential frames. These methods have been proven to be fast and reliable.

A novel method has been proposed which eliminates tedious, undesirable, manual operator assistance in removing erroneous vectors. This method uses an iterative process involving an interpolated field produced from the most reliable vectors.

Since both of the tracking techniques presented in this paper can be performed quickly, it is recommended that experimental data be analyzed with both methods, if possible. This should be performed to verify the results.

It is felt that the largest contribution of this work has been the greatly reduced time it now takes to process image data, not only individual frames, but also complete sets of images. Much of the work has been performed with this goal in mind.

A stratified channel flow facility was used to conduct two-phase interface studies. Flow visualization data was directly digitized with high resolution cameras using PLV techniques, and analyzed with new tracking software. Direct determination of interphase drag coefficients was performed. The interfacial drag experiment clearly shows that PLV can be an investigative flow visualization instrument. This was proven by the matching of interfacial drag theory to experimentally obtained drag results. In addition, in reference to this work, PLV has dramatically shown *where* and *why* (with full-field flow visualization), certain theory based on macroscopic, space-averaged behavior, is not applicable.

PLV has proven to be an accurate, full-field, noninvasive, quantitative velocity profiling technique applicable to a wide range of flow patterns. The advent of increased speed and resolution of computer-based imaging systems has allowed the direct digitization and analysis of particle images. Though many improvements are possible in this field, the technique's development at this time may make it the preferable method for obtaining reliable velocity information about experimental, transparent, flow problems.

Recommendations for future work continue to stress the need to analyze and present data quickly and accurately. MegaVision software should be written to enable the user to enter the pertinent image analysis routines for a set of images, and walk away, without having to interactively enter each image manipulation for every image in a set.

Further, it is recommended that a "imaging" workstation be acquired, with the increased gains in interactive image manipulation and the zero cost (after overhead) of tracking and cleaning, more than offsetting the purchase cost. Computer time is money, and it took approximately 10-15 CRAY cpu hours to perform all the analysis presented here.

Speaking specifically on the PLV shear experiment, two facts are evident. Wide fluctuations are seen in air velocity, especially at very low flow. Therefore, the air side seed pump and recirculation system should be redesigned, possibly in the following manner. It is still believed that a closed loop is desired. Therefore, to achieve a closer representation to a constant pressure air supply, the tasks of pumping and recirculation should be separated. A possible suggestion would be a mixing box with an internal fan for recirculation purposes, and a separate blower for forcing the air seed mixture through the mixing box and channel.

Secondly, another means of "illuminating" the flow field must be obtained. Due to laser limitations, we can only take data in 50-300 μs and 50-150 ms time scales (or longer). This leave a large time region, 3 orders of magnitude, where we cannot study. In other words, we are forced to design an experiment to fit the equipment. This limitation could be remedied with the purchase of another laser, or some other light source, possibly a high intensity "arc" strobe. This, by far, is the most important problem which must be solved, in order to advance PLV studies at Texas A&M University.

NOMENCLATURE

A = area, number of overlapped pixels
$B1$ = number of 1-valued pixels in correlation region in frame 1
$B2$ = number of 1-valued pixels in correlation region in frame 2
BC = boundary condition
C = correlation coefficient, Blasius friction factor constant
CCT = cross-correlation tracking
D, d = diameter
f = friction factor, focal length
$f\#$ = focal length divided by camera aperature
F = force
$F1$ = binary pixel value in image frame 1
$F2$ = binary pixel value in image frame 2
g_x = gravitational acceleration in x cordinate direction
H = height of region
k = wave number
K = characteristic kinetic energy per unit volume
l = vector length
L = length of region
m = Blasius friction factor constant
M = camera magnification
MFT = multiframe tracking
N = number of vectors, number of overlapped particles
NSI = number of spots (or particles) per image
P = pressure
PD = percent difference (cleaning parameter)
R = radius, reliability index
Re = Reynold's number
S = surface, perimeter
t = time
T = temperature
u = velocity
v = velocity
V(U, V, W) = vector velocity with x, y, z components
x, y, z = rectangular spatial dimension components
X(X, Y) = image plane vector coordinate position

Symbols

δ = differential increment
Δ = increment
$\mathcal{E}$ = exposure
I = intensity of illuminating beam
$\mathcal{J}$ = intensity of particle image
λ = wavelength
μ = viscosity
ν = kinematic viscosity
Ω = solid angle
∂ = partial differential increment
π = 3.1418
ρ = density
σ = multiframe tracking parameter, Mie scattering coefficient

θ = angle

Subscripts

c = centroid

e = image nominal

g = vapor phase

i = interface, interphase, particle or frame index

j = particle or frame index

l = liquid phase

L = outlet

n = new

o = old, inlet, STP value

p = particle

r, θ = cylindrical radial and circumferential components

s = point response function

x, y, z = rectangular spatial dimension components

REFERENCES

Adrian, R.J. and Yao, C.S., 1983, "Development of Pulsed Laser Velocimetry for Measurement of Fluid Flow," Eighth Symposium on Turbulence, University of Missouri-Rolla, pp. 170-186.

Adrian, R.J., 1984, "Scattering Particle Characteristics and Their Effect on Pulsed Laser Measurements of Fluid Flow: Speckle Velocimetry vs. Particle Image Velocimetry," Applied Optics, Vol. 23, No. 11, pp. 1690-1691.

Adrian, R.J. and Yao, C., 1984, "Development of Pulsed Laser Velocimetry (PLV) for Measurement of Turbulent Flow," Proceedings of the Symposium on Turbulence, Rolla University, Missouri, pp. 170-186.

Adrian, R.J., Yao, C., 1985, "Pulsed Laser Technique Application to Liquid and Gaseous Flows and the Scattering Power of Seed Materials," Applied Optics, Vol. 24, No. 1, pp. 44-52.

Adrian, R.J., 1986, "Image Shifting Technique to Resolve Directional Ambiguity in Double-Pulsed Velocimetry," Applied Optics, Vol. 25, No. 21, p. 3855.

Adrian, R.J., 1988a, "Statistical Properties of Particle Image Velocimetry Measurements in Turbulent Flow, "Laser Anemometry in Fluid Mechanics-Vol.III, Ladoan-Instituto Superior Tecnico, Lisbon, Portugal, pp. 115-129.

Adrian, R.J., 1988b, "Double Exposure, Multiple-Field Particle Image Velocimetry for Turbulent Probability Density," Optics and Lasers in Engineering, Vol. 9, pp. 211-228.

Adrian, R.J., Offutt, P.W., Landreth, C.C., Liu, Z., and Hanratty, T.J., 1990, "Studies of Liquid Turbulence Using Double-Pulsed Particle Correlation," Proceedings of the 5th International Symposium on Application of Laser Techniques to Fluid Mechanics, July 9-12, Lisbon, Portugal, p. 15.4.

Adrian, R.J., 1991, "Particle-Imaging Techniques for Experimental Fluid Mechanics," Annual Reviews in Fluid Mechanics, Vol. 23, Annual Reviews, Inc., Palo Alto, California.

Agarwal, J.K. and Johnson, E.M., 1981, "Generating Aerosol for Laser Velocimeter Seeding," TSI Quarterly, Vol. VII, No. 3, pp. 5-12.

Agui, J.C., and Jiménez, J., 1987, "On the Performance of Particle Tracking," Journal of Fluid Mechanics," Vol. 185, pp. 447-468.

Analytis, G., Richner, M. and Aksan, S., 1987, "Qualification of Modifications of Interfacial Shear and Wall Heat Transfer of RELAP5/MOD2/36.02 During Reflooding," American Nuclear Society Winter Meeting, Nov. 15-19, Los Angeles, California, ANS Transactions, Vol. 55, pp. 705-707.

Anderson, J.D., Jr., 1984, Fundamentals of Aerodynamics, McGraw-Hill Book Company, Singapore.

Archbold, E., and Ennos, A.E., 1972, "Displacement Measurement from Double-Exposure Laser Photographs," Optica Acta, Vol. 19, No. 4, pp. 253-271.

Arnold, W., Hinsch, K., and Platen, W., 1986, "Analysis of Non-Stationary Flows by Evaluating the Fringe Visibility in Speckle Velocimetry," Flow Visualization IV, Proceedings of the Fourth International Symposium on Flow Visualization, Aug 26-29, Paris, France, pp. 127-132.

Bird, R., Stewart, W.E., and Lightfoot, E.N., 1960, Transport Phenomena, John Wiley & Sons, Inc., New York.

Braun, M.J., Canacci, V.A., and Russell, L.A., 1990, "Non-Intrusive Laser Based Computer Aided High Speed Flow Visualization in an Air Tunnel," Proceedings of the 5th International Symposium on Application of Laser Techniques to Fluid Mechanics, July 9-12, Lisbon, Portugal, p.6.1.

Burch, J.M. and Tokarski, J.M.J., 1968, "Production of Multiple Beam Fringes from Photographic Scatterers," Optica Acta, Vol. 15, No. 2, pp. 101-111.

Canaan, R.E., 1990, "Full-Field Velocity Measurements of Single and Two Phase Flows Using Digital Image Pulsed Laser Velocimetry," Master Thesis, Texas A&M University, College Station, Texas.

Chen, D.J. and Chiang, F.P., 1990, "Digital Processing of Young's Fringe in Speckle Photography," Optical Engineering, Vol. 29, No. 11, pp. 1413-1420.

Chu, C., 1987, "A New Technique to Automatically Analyze Laser Digital Images for Two-Phase Pipeline Flow," Master Thesis, University of South Carolina, Columbia, South Carolina.

Collicott, S.H. and Hesselink, L., 1986, "Anamorphic Optical Processing of Multiple-Exposure Speckle Photographs," Optical Letters, Vol. 11, No. 7, pp. 410-412.

Coupland, J.M. and Pickering, C., 1988, "Particle Image Velocimetry, Estimation of Measurement Confidence at Low Seeding Densities," Optics and Lasers in Engineering, Vol. 9, p. 201.

Coupland, J., Pickering, C., and Halliwell, N., 1988, "Particle Image Velocimetry, The Ambiguity Problem," Optical Engineering, Vol. 27, No. 3, p. 193.

Delahunte, K. and Hassan, Y., 1990, "A Full-Field Droplet Velocity Measurement of a Spray by Particle Imaging Displacement Interferometry," Proceedings, ASME Winter Annual Meeting, Session of Thermal Hydraulics of Advanced Nuclear Reactors, HTD-Vol. 150, November 25-30, Dallas, Texas, pp. 91-97.

Dudderar, T.D., Meynart, R., and Simpkins P.G., 1988, "Full-Field Laser Metrology for Fluid Velocity Measurement," Optics and Lasers in Engineering, Vol. 9, pp.163-199.

Economikos, L., 1988, "Image Processing and Analysis of Colored Particle Motions in Turbulent Flow," Ph.D. Thesis, Ohio State University, Columbus, Ohio.

Gazley, C., 1949, "Interfacial Shear and Stability in Two-Phase Flow," Ph.D. Thesis, University of Delaware, Newark, Delaware.

Grant, I. and Smith, G.H., 1988, "Modern Developments in Particle Image Velocimetry," Optics and Lasers in Engineering, Vol. 9, pp. 245-264.

Grousson, R. and Mallick, S., 1977, "Study of Flow Pattern in a Fluid by Scattered Laser Light," Applied Optics, Vol. 16, No. 9, pp. 2334-2336.

Guezennec, Y. and Kiritsis, N., 1990, "Statistical Investigation of Errors in Particle Image Velocimetry," Experiments in Fluids, Vol. 10, pp. 138-146.

Hanzevack, E. and Ju, C., 1988, "New Technique to Automatically Analyze Laser Digital Images of Two-Phase Pipeline Flow," Optical Engineering, Vol. 27, No. 7, July, p. 528.

Haralick, R. 1980, "Edge and Region Analysis for Digital Image Data," Computer Graphics and Image Processing, Vol. 12, p. 60.

Hardy, R.L., 1971, "Multiquadric Equations of Topography and Other Irregular Surfaces," Journal of Geophysics Research, Vol. 76, p. 1905.

Hassan, Y., 1987, "Assessment of a Modified Interfacial Drag Correlation in Two-Fluid Model Codes," American Nuclear Society Meeting, June 7-11, Dallas, Texas, ANS Transactions, Vol. 54, pp. 211-212.

Hassan, Y., Hild, R. and Blanchat, T., 1990, "Full-Field Velocity Imaging Technique using High-Energy Pulsed Laser Velocimetry," Proceedings SPIE/SPSE Symposium on Electronic Imaging Science and Technology, Santa Clara, CA, February 11-16, Vol. 1244, pp. 130-144.

Hassan, Y. and Blanchat, T., 1991, "Flow Velocity Measurements using Digital Image Pulsed Laser Velocimetry,"Optical Engineering, Vol. 30, No. 8, pp. 1220-1227.

Hassan, Y. and Canaan, R., 1991, "Full-Field Bubbly Flow Velocity Measurements Using a Multiframe Particle Tracking Technique,"accepted for Experiments in Fluids.

Hild, R.D., 1989, "Single Phase Flow Visualization using Digital Pulsed Laser Velocimetry,"Master Thesis, Texas A&M University, College Station, Texas.

Hueckel, M.H., 1971, "An Operator Which Locates Edges in Digitized Pictures,"Journal of the Association in Computing Machinery, Vol. 18, No. 1, pp. 113-125.

Huntley, J.M., 1986, "Speckle Photography Fringe Analysis by the Walsh Transform,"Applied Optics, Vol. 25, No. 3, pp. 382-386.

Huntley, J.M., 1989, "Speckle Photography Fringe Analysis: Assessment of Current Algorithms,"Applied Optics, Vol. 28, No. 20, pp. 4316-4322.

Kowalski, J.E., 1987, "Wall and Interfacial Shear Stress in Stratified Flow in a Horizontal Pipe,"AIChE Journal, Vol. 33, No. 2, pp. 274-281.

Lakshmanan, K., 1986, "Quantitative Computer Image Processing of Color Particle Markers in Flow Visualization,"Ph.D. Thesis, Ohio State University, Columbus, Ohio.

Landreth, C.C. and Adrian, R.J., 1988, "Measurement and Refinement of Velocity Data Using High Image Density Analysis in Particle Image Velocimetry,"Applications of Laser Anemometry to Fluid Mechanics, 4th International Symposium, Lisbon, Portugal, July 11-14, pp. 484-497.

Landreth, C.C., Adrian, R.J. and Yao, C.S., 1988, "Double Pulsed Particle Image Velocimetry with Directional Resolution for Complex Flows,"Experiments in Fluids, Vol. 6, pp. 119-128.

Langlois, W.E., 1964, Slow Viscous Flow, The Macmillan Company, New York.

Lourenco, L., 1986, "Theory and Applications of Particle Image Displacement Velocimetry,"Flow Visualization and Digital Image Processing, June 9-13, von Karman Institute for Fluid Dynamics, Lecture Series 1986-09, Florida State University, Tallahassee, Florida.

Lourenco, L. and Krothapalli, A., 1987, "The Role of Photographic Parameters in Laser Speckle or Particle Image Displacement Velocimetry,"Experiments in Fluids, Vol. 5, pp. 29-32.

Lourenco, L.M. and Krothapalli, A., 1988, "Application of PIDV to the Study of the Temporal Evolution of the Flow Past a Circular Cylinder,"Laser Anemometry in Fluid Mechanics-Vol.III, Ladoan-Instituto Superior Tecnico, Lisbon, Portugal, pp. 161-178.

Meynart, R., 1980, "Equal Velocity Fringes in a Rayleigh-Bernard Flow by a Speckle Method,"Applied Optics, Vol. 19, No. 9, pp. 1385-1386.

Meynart, R., 1982, "Digital Image Processing for Speckle Flow Velocimetry,"Review of Scientific Instruments, Vol. 53, No. 1, p. 110.

Meynart, R., 1983, "Instantaneous Velocity Field Measurements in Unsteady Gas Flow by Speckle Velocimetry,"Applied Optics, Vol. 22, No. 4, pp. 535-540.

Meynart, R., 1985, "Non-Gaussian Statistics of Speckle Noise of Young's Fringes in Speckle Velocimetry,"Applied Optics, Vol. 24, No. 10, pp. 1448-1453.

Narcowich, F.J. and Ward, J.D., 1990, "Norms of Inverses and Condition Numbers for Matrices Associated with Scattered Data,"Journal of Approximation Theory, Vol. 64, No. 1, pp. 69-94.

Oh, C.H. and Mahalingam, R., 1987, "Interface Interaction in Two-Phase Gas-Non-Newtonian Liquid Flow,"Industrial & Engineering Chemistry Research, Vol. 26, pp. 2522-2528.

Otsu, N., 1979, "A Threshold Selection Method from Gray-Level Histograms,"IEEE Transactions on Systems, Man, and Cybernetics, Vol. SMC-9, No. 1, pp. 62-66.

Putney, J., 1988, "Proposals for Improving Interphase Drag Modeling for the Bubbly and Slug Regimes in RELAP5,"Central Electricity Generating Board, Research Report RD/L 3306/R88, Surrey, United Kingdom.

Ransom, V., Wagner, R., Trapp, J., Feinauer, L., Johnson, G., Kiser, D. and Riemke, R., 1985, "Code Structure, Systems Models, and Solution Methods,"RELAP5/MOD2 Code Manual, Volume 1, Idaho Falls, Idaho.

Robinson, D.W., 1983, "Automatic Fringe Analysis with a Computer Image-Processing System,"Applied Optics, Vol. 22, No. 14, pp. 2169-2176.

Russ, K.M., 1988, "Particle Color Consideration in Flow System Image Acquisition,"Master Thesis, Ohio State University, Columbus, Ohio.

Sheng, Z., 1988. "Image Processing Technique for Determining the Velocity Field for a Fluid Flow."Master Thesis, University of Wyoming, Laramie, Wyoming.

Sinha, S.K., 1988. "Improving the Accuracy and Resolution of Particle Image or Laser Speckle Velocimetry."Experiments in Fluids, Vol. 6, pp. 67-68.

Taitel, Y. and Dukler, A.E., 1975. "A Theoretical Approach to the Lockhart-Martinelli Correlation for Stratified Flow."International Journal of Multiphase Flow, Vol. 2, pp. 591-595.

Utami, T. and Ueno, T., 1987. "Experimental Study on the Coherent Structure of Turbulent Open-Channel Flow using Visualization and Picture Processing."Journal of Fluid Mechanics, Vol 174, pp. 339-440.

Wang, H. and Kondo, S., 1990. "A Study on the Stratified Horizontal Counter-Current Two-Phase Flow."Nuclear Engineering and Design, Vol. 121, p. 45-52.

Yamamoto, F., Uemura, T., Koukawa, M., Itoh, M., and Teranishi, A., 1988. "Application of Flow Visualization and Digital Image Processing Techniques to Unsteady Viscous Diffusing Free Doublet Flow."Proceedings of the 2nd International Symposium on Fluid-Control, Measurement Mechanics, and Flow Visualization, September 5-9, Sheffield, U.K., pp. 184-188.

Yano, M. and Umeda, S., 1986. "Lag Motion Between the Tracer Particles and the Fluid in Flow Visualization."Flow Visualization IV, Proceedings of the Fourth International Symposium on Flow Visualization, Aug 26-29, Paris, France, p. 203.

2 theses
cycled
separately.
da

DATE FILMED

6/7/93